Mechanistic bases for privileged capture and unidirectional targeting of tail-anchored proteins by the Get3 ATPase

Thesis by

Un Seng Chio

In Partial Fulfillment of the Requirements for

the degree of

Doctor of Philosophy

CALIFORNIA INSTITUTE OF TECHNOLOGY

Pasadena, California

2019

(Defended December 11th, 2018)

Un Seng Chio
ORCID: 0000-0002-5295-2690

ACKNOWLEDGEMENTS

I thank all the people that have been a friend and/or have helped me in some way throughout my life. It is difficult to point out everyone individually, but I first especially thank close friends from my childhood who have stuck around to now: Joe A., Jon C., Lawrence N., Wallace T., and Alan Z. I thank additional friends from those times that I will never forget: Mo A., Cynthia C., Lorene L., Sandra M., Peggy P., Tiff S., and Jackie T. I also thank friends from Stuyvesant HS, Cornell, Caltech, and elsewhere: David C., Luna C., Wesley C., Ahloom C., Adam C., Danny G., Gokul G., Peng (Brian) H., Maggie H., Kenneth L., Alex L., Chris L., Jisung J., Kenny K., Ken K., Maggie L., Tony L., Connie L., Phan N., Gerardo S., Neiman T., Julia W., Andrew W., Ray W., Samantha W., Jane Y., Elsie Y., Hyun Gi Y., Michael Z., Mervin Z., and all members of the Stuy Sticky Fingers and Alpha Chi Sigma Tau chapter (apologies if I missed anyone! But if you know me and are actually reading this, I definitely do still remember you and I thank you, too!).

I thank my family for their love and support and raising me to be the person I am today: my grandfather for taking care of my brothers and I while our parents worked; my parents for enduring and overcoming the challenge of supporting our family in a foreign environment; my brother Henry for helping me with homework when I was young and introducing me to video games; my brother Un Soi for being a role model and an inspiration to me for almost my entire life from elementary school to college; my cousins Linda C., Melanie C., Tiffany C., Angela L., Jonathan L., and Stephanie L. for their love and friendship throughout the years; and my relatives in Macau for their love and hospitality despite how infrequently we see each other.

I thank my teachers and mentors from elementary school, middle school, high school, and college. I especially thank Jim Cocoros and Emily Moore who are exceptional math and poetry teachers, respectively, and were kind enough to write recommendation letters for me to attend college. I also thank Tom Ruttledge, Jun

(Kelly) Liu, and Ralph Obendorf, who are all excellent professors and advisors and were willing to write recommendation letters for me to attend graduate school. I thank Tom for his career advice and for being an approachable professor in the Chemistry department; I thank Kelly for her kindness as an advisor and suggesting graduate school as a possible career path; and I thank Ralph for taking me on as a student in his lab even though I was in my junior year. I also thank Helen Nivison, who teaches the Biochemistry laboratory course at Cornell; her course helped ease my transition into biochemistry research at Caltech quite a lot.

The work presented in this dissertation would not have been possible without the help and support from many people. I thank the past and present members of the Shan Lab for their advice, insights, and camaraderie these past six years: Meera Rao, Michael Rome, Hyunju Cho, Sowmya Chandrasekar, Yu-Hsien Hwang Fu, Jae Ho Lee, Shuai Wang, Fu-Cheng (George) Liang, Chien-I Yang, Alex Siegel, Hao Hsuan Hsieh, Camille McAvoy, Aileen Ariosa, Kuang Shen, Thang Nguyen, David Akopian, and Ishu Saraogi. I especially thank Mike and Meera for showing me the ropes when I first started in the lab. I thank Sowmya for being a wonderful lab manager and a central pillar of support for the lab. I also thank Hyunju for being an excellent scientist and resource, and I am grateful that she chose to also work on the GET pathway.

I thank the wonderful scientists in other labs that I have had the pleasure to meet. I especially thank SangYoon Chung and Yazan Alhadid for their help and hospitality during my many visits to the Weiss lab at UCLA for μs-ALEX measurements, as well as Antonino Ingargiola and Xavier Michalet for additional support/advice on μs-ALEX data analysis. I thank Justin Chartron for his advice on using CRISPR-Cas9 to generate yeast strains. I thank Jeeyeong (Amanda) Mock, Harry Gristick, Ku-Feng (Geoffrey) Lin, and Michelle Fry from the Clemons lab for plasmids/reagents and discussions on the GET pathway. I thank Clint Regan and Catie Blunt from the Dougherty lab for their help on using their HPLC to purify dye-CoA conjugates. I thank Shabnam Hematian for her help on using the circular

dichroism spectrometer in the Beckman Institute Laser Resource Center. I thank Jennifer Keeffe from the Björkman lab for her help on using their SEC-MALLS. I thank Vladimira Najdrova, a visiting scientist from Prague, for her time in the lab working on identifying whether the GET pathway exists in *Giardia intestinalis*.

I thank the Caltech staff for their contributions behind the scenes to allow for efficient lab work: Luz Castillo and other custodial staff, Joe Drew and Chemistry stockroom staff, Margot Hoyt, Santiago Laparra, Blanca Mariona, Alison Ross, and Agnes Tong. I thank the high school volunteers that help pour SDS-PAGE gels and maintain lab stocks: Chris, Mark, Phibi, Will, Flora, and Alex.

I thank my thesis committee for their advice and feedback over the years: Bil Clemons, the committee chair who also works on the GET pathway, André Hoelz, and Dennis Dougherty.

Last but certainly not least, I thank my advisor Shu-ou for her guidance and mentorship the past six years. This thesis would have been impossible without her. I continue to be amazed by her remarkable intuition in thinking about biochemistry and enzyme kinetics, as well as her attention to details and memory on such matters. I owe her a great deal more than just an acknowledgement, and I sincerely hope I will be able to emulate her approach to science as a postdoc and beyond. I said these words introducing her prior to a talk she gave at Caltech: “Shu-ou is actually not a normal human being, but she is actually a *super-lady* with superpowers, powers to do science,” and I fully stand by them today.

ABSTRACT

C-terminal tail-anchored membrane proteins (TAs) are targeted post-translationally to the endoplasmic reticulum (ER) in eukaryotic cells mainly through the Guided entry of tail-anchored protein (GET) pathway. Here we use biochemical and biophysical approaches to shed further mechanistic insight into how the central chaperone, the Get3 ATPase, is able to capture TA substrates in a privileged manner and provide unidirectional targeting to the ER.

Specifically, we first show in Chapter 2 that Get3 dynamically samples *open* and *closed* conformations as a "protean clamp". Binding of TA substrates induces Get3 to sample more *open* conformations that causes Get3 to dissociate from the cytosolic regulatory Get4/5 complex, hydrolyze ATP, and become primed to interact with the Get1/2 membrane receptors. Therefore, a TA substrate acts as the switch for unidirectional targeting, transitioning Get3 from a "TA-loading mode" to a "membrane targeting mode". Next, in Chapter 3, we show that a small, conserved alpha-helical lid motif, known as α8, lining the substrate binding groove is necessary for Get3 to efficiently capture TA substrates in a privileged manner over competing off-pathway chaperones.

PUBLISHED CONTENT AND CONTRIBUTIONS

[1] Rome, M. E., Chio, U. S., Rao, M., Gristick, H., and Shan, S.-O. 2014. Differential gradients of interaction affinities drive efficient targeting and recycling in the GET pathway. *Proceedings of the National Academy of Sciences U. S. A.* 111(46): E4929-E4935. doi: 10.1073/pnas.1411284111.

U. S. C. prepared reagents and performed titration measurements to determine the binding affinities between the cytosolic domains of Get1 and Get2 with Get3 under different nucleotide and substrate conditions (Figures 3 and 4) with guidance from M. E. R., analyzed the data with guidance from M. E. R., and contributed to the revision of the manuscript.

[2] Rao, M., Okreglak, V.*, Chio, U.S.*, Cho, H., Walter, P., and Shan, S.-O. 2016. Multiple selection filters ensure accurate tail-anchored membrane protein targeting. *eLife* 5: e21301. doi: 10.7554/eLife.21301. (*co-second authors)

U. S. C. designed and implemented the fluorescent labeling strategy for Get3 (Figure 5; used by M. R. for TA transfer experiments in Figure 6), performed targeting and insertion assays for Get3•TA complexes with TAs that have variant C-terminal extensions (Figure 8) and analyzed the data, and contributed to the writing and revision of the manuscript.

[3] Chio, U.S., Chung, S., Weiss, S., and Shan, S.-O. 2017. A protean clamp guides membrane targeting of tail-anchored proteins. *Proceedings of the National Academy of Sciences U. S. A.* 114(41): E8585-E8594. doi: 10.1073/pnas.1708731114.

U. S. C. designed experiments with S.-O. S., performed all biochemical experiments, analyzed all biochemical data, performed µs-ALEX measurements with S. C., analyzed µs-ALEX data with S. C. with input from S. W. and S.-O. S., and wrote the manuscript with S.-O. S.

[4] Chio, U.S., Cho, H., and Shan, S.-O. 2017. Mechanisms of Tail-Anchored Membrane Protein Targeting and Insertion. *Annual Review of Cell and Developmental Biology* 33: 417-438. doi: 10.1146/annurev-cellbio-100616-060839. (*Review*)

U. S. C. wrote the initial draft for the section entitled "The GET Pathway for Targeting of Tail-Anchored Proteins to the ER" from pages 421 to 427, prepared the initial version of Figure 2, contributed to the initial version of Figure 3, and contributed to the revision of the final manuscript.

[5] Cho, H., Chio, U.S., and Shan, S.-O. 2018. *In vitro* Assays for Targeting and Insertion of Tail-Anchored Proteins into the ER Membrane. *Current Protocols in Cell Biology* 81(1): e63. doi: 10.1002/cpcb.63.

U. S. C. wrote the initial draft for "Basic Protocol 3: Membrane Insertion of TA from Get3•TA" and contributed to the revision of the final manuscript.

[6] Chio, U.S., Chung, S., Weiss, S., and Shan, S.-O. 2019. A Chaperone Lid Ensures Efficient and Privileged Client Transfer during Tail-Anchored Protein Targeting. *Cell Reports* 26(1): 37-44.e7.

U. S. C. designed experiments with S.-O. S., performed all experiments and analyzed all data, and wrote the manuscript with S.-O. S.

TABLE OF CONTENTS

Acknowledgements iii
Abstract vi
Published Content and Contributions vii
Table of Contents ix
List of Illustrations and/or Tables x
Nomenclature xii
Chapter I: Introduction – The GET pathway for targeting of tail-anchored proteins to the endoplasmic reticulum 1
Summary of the pathway 2
Structure and function of Sgt2 5
Get4/5: a scaffold that bridges Sgt2 and Get3 6
The Get3 ATPase cycle: Nucleotide-, effector-, and substrate-induced conformational changes drive the targeting pathway 7
The Get1/2 membrane receptor complex remodels the targeting complex 10
Chapter II: A protean clamp guides membrane targeting of tail-anchored proteins 14
Introduction 15
Results 19
Discussion 48
Materials and Methods 53
Chapter III: A chaperone lid ensures efficient and privileged client transfer during tail-anchored protein targeting 62
Introduction 62
Results 67
Discussion 84
Materials and Methods 87
Bibliography 100

LIST OF ILLUSTRATIONS AND/OR TABLES

Figures		*Page*
1.1	Major steps in the yeast GET pathway. ……	4
1.2	The Get3 ATPase cycle is driven by nucleotides, effectors, and tail-anchored protein (TA) substrates. ……	8
2.1	Current model for Get3 conformations throughout the GET pathway. ……	16
2.2	Structures of *open* and *closed* Get3. ……	17
2.3	Monitoring Get3 conformational changes using µs-ALEX. ……	20
2.4	Direct observation of Get3 conformational changes using µs-ALEX. ……	22
2.5	Replicates of the FRET histograms for *apo*-Get3. ……	24
2.6	Get3 FRET histograms with ATTO 550. ……	25
2.7	Controls for dye photophysics in µs-ALEX measurements of Get3. ……	25
2.8	Controls for monomer exchange in µs-ALEX measurements of Get3. ……	26
2.9	The TA substrate induces Get3 to dynamically sample *open* conformations. ……	28
2.10	Prepared Get3•TA complexes are active in targeting and insertion into the ER. ……	30
2.11	Prepared Get3•TA complexes are kinetically stable. ……	31
2.12	Sequential *opening* of Get3 upon TA loading and Get4/5 release. ……	33
2.13	Adapted K-S tests for Get3•Get4/5 FRET histograms. ……	34
2.14	α8 is not necessary for a stable Get3•TA complex. ……	36
2.15	Interactions at the Get3 ATPase site. ……	38
2.16	Point mutations at the ATPase active site bias Get3 to more *closed* conformations. ……	39
2.17	Comparisons of FRET histograms between wild-type and mutant Get3 complexes. ……	40
2.18	Get3 active site mutants block the targeting of Get3•TA complexes. ……	42
2.19	Get3•TA targeting and insertion in the presence of AMPPNP. ……	43
2.20	The TA substrate regulates the Get3–Get4 interaction. ……	45
2.21	The TA substrate induces a rearrangement of the Get3–Get4 interaction interface. ……	46
2.22	Model for how TA-induced Get3 *opening* drives the membrane targeting of the Get3•TA complex. ……	52
2.23	Purification of wild-type and mutant Get3•TA complexes. ……	55

3.1	Current model of the GET pathway in yeast. ……	64
3.2	A conserved α8 motif lines the substrate binding groove of Get3. ……	66
3.3	Get3(Δα8) exhibits the same global structure, basal ATPase activity, and ATP-dependent binding to Get4/5 as wild-type Get3. ……	68
3.4	Get3(Δα8) displays a similar conformational distribution and undergoes conformational regulations by nucleotides, Get1, and Get4/5 similarly to wild-type Get3. ……	70
3.5	The α8 motif in Get3 is important for TA targeting to the ER. ……	72
3.6	α8 prevents promiscuous TA handoff from Get3 to off-pathway chaperones. ……	74
3.7	cpSRP43 can bind TA proteins. ……	75
3.8	Kinetic simulations of TA release from Get3(Δα8). ……	76
3.9	Additional kinetic simulations of TA release from Get3(Δα8). ……	77
3.10	TA targeting and insertion assays starting with preformed Get3•TA and Get3(Δα8)•TA complexes. ……	79
3.11	α8 and Get4/5 synergistically enable rapid TA transfer from Sgt2 to Get3. ……	80
3.12	Both α8 and Get4/5 are required for privileged TA transfer to Get3 in the GET pathway. ……	82
3.13	Independent verification that α8 is required for privileged TA transfer to Get3 in the GET pathway. ……	83
3.14	TA targeting and insertion assays starting with a preformed Sgt2•TA complex. ……	84
3.15	Model for the dual roles of α8 as a substrate conduit and as a chaperone lid in the GET pathway. ……	86

Tables *Page*

1.1	Components of the GET pathway in yeast and mammalian cells.	3
2.1	Determination of ATP content in Get3 and Get3•TA. ……	44
2.2	Summary of equilibrium binding affinities between Get4/5 and Get3 variants in different substrate and nucleotide states. ……	47
3.1	List of plasmids used in this study. ……	88
3.2	List of recombinant proteins used in this study. ……	89

NOMENCLATURE

µs-ALEX. Microsecond alternating laser excitation spectroscopy; solution-based single-molecule FRET technique that can determine E^* and S values for individual fluorescent molecules.

Acrylodan. Environmentally sensitive fluorophore.

ADP. Adenosine diphosphate.

ADP•AlF_4. Adenosine diphosphate complexed with aluminum tetrafluoride; nonhydrolyzable analog of ATP.

AMPPNP. Adenylyl-imidodiphosphate; nonhydrolyzable analog of ATP.

ATP. Adenosine triphosphate.

ATPase. ATP hydrolase; class of enzyme that catalyzes the hydrolysis of ATP to ADP and a free phosphate ion, which releases energy.

ATTO 550. ATTO dye that can act as a FRET donor for ATTO 647N.

ATTO 647N. ATTO dye that can act as a FRET acceptor for ATTO 550 or Cy3B.

BAG6. An additional protein subunit found in the mammalian scaffolding complex that bridges SGTA and TRC40 (mammalian homologs of Sgt2 and Get3, respectively).

BODIPY FL. Green fluorescence dye that can act as a FRET acceptor for coumarin or as a FRET donor for TMR.

Bos1. Tail-anchored protein; SNARE protein.

BSA. Bovine serum albumin; inert protein used as a surfactant for fluorescence experiments.

BVA. Burst variance analysis; used to determine whether heterogeneity in a FRET histogram is static or dynamic.

CaM. Calmodulin; multifunctional protein; can bind and chaperone tail-anchored proteins.

CAML. Mammalian counterpart of the Get2 membrane receptor.

CD. Cytosolic domain.

Coumarin. Blue fluorescence dye that can act as a FRET donor for BODIPY FL.

cpSRP43. ATP-independent membrane protein chaperone found in the chloroplast of green plants; can also bind and chaperone tail-anchored proteins.

CTD. C-terminal domain.

Cy3B. Cyanine dye that can act as a FRET donor for ATTO 647N.

***DS*.** Dynamic score; used to quantify the dynamics of a FRET histogram.

***E**.** Relative FRET efficiency.

ER. Endoplasmic reticulum.

FRET. Förster resonance energy transfer.

GET pathway. Guided entry of tail-anchored protein pathway; one of the main pathways responsible for the targeting and insertion of tail-anchored proteins to the endoplasmic reticulum.

Get1. One of the two protein subunits of the Get1/2 membrane receptor complex.

Get2. One of the two protein subunits of the Get1/2 membrane receptor complex.

Get3. ATPase; central chaperone of the GET pathway.

Get4. One of the two protein subunits of the Get4/5 scaffolding/regulatory complex; interacts with Get3.

Get4/5N. Get4/5 complex consisting of a truncated Get5 that only contains its N-terminal domain.

Get5. One of the two protein subunits of the Get4/5 scaffolding/regulatory complex; interacts with Sgt2.

Hsp70. Class of chaperones that are about 70 kDa in molecular weight.

K-S test. Kolmogorov-Smirnov test; nonparametric statistical test.

NMR. Nuclear magnetic resonance spectroscopy.

NTD. N-terminal domain.

PDB. Protein Data Bank.

Privileged. Having special advantages.

Protean. Ever-changing; dynamically fluctuating.

***S*.** Stoichiometry value; reports on the fraction of total fluorescence emitted from excitation at the donor excitation wavelength.

Sbh1. Tail-anchored protein; Sec61β-homolog 1; component of the Sec61 translocon.

SD. Standard deviation.

Sgt2. Cochaperone; receives TA proteins from Ssa1 and then delivers the TA protein to Get3 with assistance from the Get4/5 complex.

SNARE proteins. Proteins of a protein complex involved in vesicle fusion.

SPR. Surface plasmon resonance.

SRP. Signal recognition particle; mediates co-translational targeting of nascent membrane and secretory proteins to either the ER in eukaryotes or the plasma membrane in bacteria.

Ssa1. Highly abundant Hsp70 chaperone; mediates the initial capture of newly synthesized tail-anchored proteins from ribosomes.

TA. Tail-anchored protein.

Tail-anchored protein. Membrane protein with a single transmembrane domain at the extreme C-terminus.

TMD. Transmembrane domain.

TMR. Red fluorescence dye that can act as a FRET acceptor for BODIPY FL.

TRC35. Mammalian homolog of Get4.

TRC40. Mammalian homolog of Get3.

UBL4A. Mammalian homolog of Get5.

***WDS*.** Weighted dynamic score; dynamic score that is normalized for differences in bin population.

WRB. Mammalian homolog of Get1.

yRM. Yeast rough microsomes.

Zn^{2+}. Zinc ion.

Chapter 1

INTRODUCTION – THE GET PATHWAY FOR TARGETING OF TAIL-ANCHORED PROTEINS TO THE ENDOPLASMIC RETICULUM

Adapted from:

Chio, U.S., Cho, H., and Shan, S.-O. 2017. Mechanisms of Tail-Anchored Membrane Protein Targeting and Insertion. *Annual Review of Cell and Developmental Biology* 33: 417-438. doi: 10.1146/annurev-cellbio-100616-060839. (*Review*)

Membrane proteins account for ~35% of the proteins encoded by the genome. The proper functioning of biological membranes requires all newly synthesized membrane proteins to be localized to and inserted into the appropriate membrane destinations. The best-studied pathway for membrane protein targeting and insertion utilizes the signal recognition particle (SRP). SRP recognizes TMDs near the N-terminus of nascent proteins and delivers them to translocation machineries on the eukaryotic endoplasmic reticulum (ER) during translation; this co-translational mode of targeting effectively minimizes the aggregation of membrane proteins in the cytosol (Akopian et al. 2013).

Nevertheless, numerous membrane proteins cannot use SRP and must be targeted via post-translational pathways, the mechanisms of which are far less well-understood. A salient example is the class of tail-anchored proteins (TAs), which contain a single TMD near the C-terminus. TAs compose 3–5% of the eukaryotic membrane proteome and mediate diverse cellular processes, including protein translocation across organelle membranes, vesicular transport, apoptosis, and protein quality control (Chartron et al. 2012a, Hegde & Keenan 2011). Because the C-terminal TMDs of TAs are obscured by the ribosome during translation, it was predicted early on that these proteins would be targeted by post-translational

mechanisms (Kutay et al. 1993). In support of this hypothesis, synaptobrevin 2 (Syb2), a tail-anchored SNARE protein, can be targeted to and inserted into the ER after release from the ribosome (Kutay et al. 1995).

Much recent progress on TA biogenesis was driven by the discovery of the GET (Guided Entry of TA) pathway. The structure, dynamics, and interactions of GET components have been extensively characterized, providing the highest-resolution understanding of a TA-targeting pathway thus far.

1.1 SUMMARY OF THE PATHWAY

Early studies showed that TA insertion into the ER is ATP-dependent and requires machineries distinct from those that mediate co-translational protein targeting (Kutay et al. 1995). Subsequently, cross-linking studies in reticulocyte lysate identified a 40-kDa ATPase, TRC40, as a key targeting factor for TAs (Favaloro et al. 2008, Stefanovic & Hegde 2007). The yeast homolog of TRC40, Get3, was genetically linked to two integral membrane proteins on the ER, Get1 and Get2 (Schuldiner et al. 2005), which were shown to form the receptor complex for Get3 (Schuldiner et al. 2008). An additional protein complex, comprising Get4 and Get5, was found to participate in the pathway on the basis of the genetic interactions of Get4 and Get5 with Get1, Get2, and Get3; reduced TA targeting in get5 lysates; and the physical association of the Get4/5 complex with Get3 (Jonikas et al. 2009). Biochemical reconstitutions showed that Get4/5 facilitates TA loading onto Get3 from the upstream cochaperone Sgt2 (Wang et al. 2010) and TA proteins are first loaded onto the Hsp70 chaperone Ssa1 before transfer to Sgt2 (Cho and Shan 2018). Homologs or functional orthologs of all components of the yeast GET pathway have been identified in mammalian cells (Table 1.1) (Colombo et al. 2016; Mock et al. 2015; Vilardi et al. 2011, 2014; Xu et al. 2012; Yamamoto & Sakisaka 2012). Collectively, these works define a conserved pathway in eukaryotic cells that mediates the targeted delivery and insertion of TAs into the ER.

Cell type	Upstream cochaperone	Scaffolding complex	Cytosolic ATPase	Membrane receptors
Yeast	Sgt2	Get4/5	Get3	Get1/2
Mammal	SGTA	TRC35/UBL4A/BAG6	TRC40	WRB/CAML

Table 1.1: Components of the GET pathway in yeast and mammalian cells.

This early work, together with subsequent mechanistic studies, defined the major molecular events in the GET pathway (Figure 1.1). After a nascent TA is synthesized and released from the ribosome, it is captured by Sgt2 through transfer from the Hsp70 chaperone Ssa1 (step 1). The Get4/5 complex, via its abilities to bridge between Sgt2 and Get3 and to regulate the conformation of Get3, stimulates the transfer of TA substrate from Sgt2 to ATP-bound Get3 (step 2). The Get3•TA complex dissociates from Get4/5, and the TA substrate stimulates ATP hydrolysis on Get3 (step 3). The Get3•TA complex then engages the Get1/2 receptor complex at the ER membrane (step 4), where Get1/2 releases TA from Get3 and facilitates TA insertion into the membrane (step 5). Finally, Get3 is released from Get1 and is returned to the cytosol through binding of ATP and Get4/5 (step 6). Our understanding of the molecular mechanisms of these events prior to the work presented in this thesis is further discussed below.

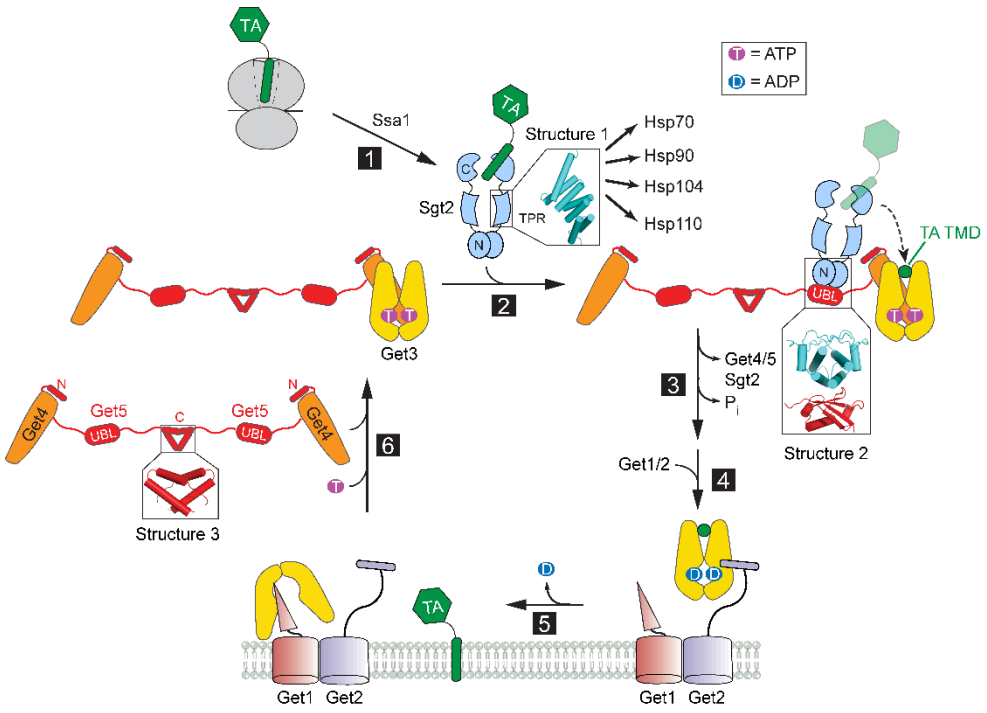

Figure 1.1: Major steps in the yeast GET pathway. (1) A nascent tail-anchored protein (TA) is captured by Sgt2 through Ssa1 after translation by the ribosome. Structure 1 (PDB 3SZ7) shows the Sgt2 tetratricopeptide repeat (TPR) domain, which binds various chaperones. (2) Sgt2 transfers the TA to Get3, a process stimulated by the Get4/5 complex. Structure 2 (PDB 2LXC) shows the N-terminal domain of Sgt2 bound to the ubiquitin-like (UBL) domain of Get5. (3) The Get3•TA complex dissociates from Get4/5, and ATP hydrolysis is activated. (4) The Get2 subunit in the Get1/2 receptor captures the Get3•TA complex. (5) Following ADP release, Get1 interacts with and disassembles the Get3•TA complex, and the TA is inserted into the membrane through an unknown mechanism. (6) ATP and Get4/5 together drive the release of Get3 from Get1, recycling Get3 for additional rounds of targeting. Structure 3 (PDB 2LNZ) shows the Get5 homodimerization domain. TMD denotes transmembrane domain.

1.2 STRUCTURE AND FUNCTION OF SGT2

The most upstream factor identified thus far in the GET pathway is the Hsp70 chaperone Ssa1, which captures TAs after their translation. Ssa1 then transfers TAs to the cochaperone Sgt2 (Cho & Shan 2018). Sgt2 contains multiple protein interaction domains: an N-terminal homodimerization domain (NTD) that binds Get5, a tetratricopeptide repeat (TPR) domain that interacts with chaperones, and a glutamine- and methionine-rich C-terminal domain (CTD) (Figure 1.1). Immunoprecipitation experiments demonstrated that the Sgt2 CTD forms the substrate-binding site that selectively captures the TMDs of ER-destined TAs (Rao et al. 2016, Wang et al. 2010). The molecular basis of this recognition is unclear but was speculated to be analogous to how the methionine-rich domain of SRP recognizes hydrophobic signal sequences in substrate proteins (Wang et al. 2010). As the individual domains of Sgt2 are connected by flexible linkers, the relative positions of these domains have not been defined. Small-angle X-ray scattering (SAXS) data suggested that the global conformation of Sgt2 is extended but likely flexible (Chartron et al. 2011), which raises possibilities of regulation by its diverse binding partners.

The Sgt2 NTD is both a homodimerization domain and interaction platform for the ubiquitin-like (UBL) domain of Get5, linking this cochaperone with the rest of the GET pathway (Chang et al. 2010, Chartron et al. 2010, Liou et al. 2007, Wang et al. 2010). Nuclear magnetic resonance (NMR) and crystallographic analyses of the *Saccharomyces cerevisiae* Sgt2 NTD bound to the Get5 UBL domain elucidated the molecular details of their interaction (Figure 1.1, Structure 2) (Chartron et al. 2012b, Simon et al. 2013, Tung et al. 2013). The Sgt2 homodimer interface is formed by a four-helix bundle, which is contributed by two N-terminal helices from each Sgt2 NTD and is stabilized by hydrophobic interactions. In contrast, the interaction of the Sgt2 NTD with the Get5 UBL domain is electrostatically driven. Conserved residues on the second helices of the Sgt2 NTD form an acidic surface that interacts with

conserved basic and hydrophobic residues on a single Get5 UBL domain via charge and shape complementarity (Figure 1.1, Structure 2). The Sgt2-Get5 interaction is stable but occurs with fast association and dissociation kinetics (Chartron et al. 2012b, Simon et al. 2013), which may allow Get4/5 to rapidly sample Sgt2 molecules.

1.3 GET4/5: A SCAFFOLD THAT BRIDGES SGT2 AND GET3

After capture by Sgt2, the TA substrate is transferred to Get3 in a Get4/5-dependent process (Wang et al. 2010). Get5 is a modular protein composed of an NTD that interacts with Get4, a UBL domain that binds the Sgt2 NTD as described above, and a CTD that mediates homodimerization (Figure 1.1, Structure 3) (Chartron et al. 2010). A minimal Get4/5N complex, formed between Get4 and the Get5 NTD, was sufficient to recognize Get3 in a specific conformation and nucleotide state (Gristick et al. 2014, 2015) and was hence subjected to extensive biochemical and structural studies. Get4 forms an α2-solenoid fold composed of 14 right-handed helical coils (Bozkurt et al. 2010, Chang et al. 2010, Chartron et al. 2010). The N-terminal helix of Get5 docks into a hydrophobic groove formed by helices α12 and α13 and the β-tongue of Get4, forming an extremely stable Get4-Get5 interface (Chang et al. 2010, Chartron et al. 2010). On the other side of the Get4/5N complex, the N-terminal helices of Get4 provide a combination of acidic and hydrophobic residues to mediate interaction with Get3 (further discussed in the section titled The Get3 ATPase Cycle, below).

Multiple groups have reconstituted Get4/5-mediated stimulation of TA transfer from Sgt2 to Get3 (Mateja et al. 2015, Rao et al. 2016, Wang et al. 2010). Nevertheless, the precise mechanism(s) underlying the stimulatory effect of Get4/5 is not completely understood. By bringing Sgt2 and Get3 into close proximity, Get4/5 could enable a facile route for relay of a TA substrate while minimizing cytosolic exposure of the substrate TMD (Figure 1.1). In support of this model, the TA is protected from external traps during the transfer, and mutations disrupting the Sgt2-

Get5 interaction resulted in significantly less TA transfer and less insertion-competent Get3•TA complexes (Mateja et al. 2015, Shao et al. 2017). As discussed below in the section titled The Get3 ATPase Cycle, the Get4/5 complex also regulates the conformation of the Get3 ATPase, which could further promote substrate capture by Get3. It is also plausible that Get5 induces rearrangements in Sgt2 that facilitate TA release. The relative contributions of these mechanisms to the substrate handover event remain to be defined.

The Get5 CTD forms a stable dimer interface mediated by hydrophobic interactions (Chartron et al. 2012c). SAXS data also showed that Get4 and Get5 form an elongated heterotetramer (2:2) spanning 240 Å (see architecture of the heterotetrameric complete Get4/5 complex in Figure 1.1) (Chartron et al. 2010). Nevertheless, the functional relevance of Get5 homodimerization is unclear. The residues that mediate Get5 homodimerization are not conserved in its mammalian homolog. Furthermore, there appears to be an intriguing asymmetry in the Get4/5 complex such that only one copy of Get4 in this heterotetramer binds Get3 at physiological protein concentrations (Gristick et al. 2015, Mateja et al. 2015). The mechanism of this asymmetric interaction and the evolutionary relevance of the Get5 homodimerization domain remain to be determined.

1.4 THE GET3 ATPASE CYCLE: NUCLEOTIDE-, EFFECTOR-, AND SUBSTRATE-INDUCED CONFORMATIONAL CHANGES DRIVE THE TARGETING PATHWAY

Central to the GET pathway is the ATPase Get3, which uses its ATPase cycle to capture and deliver TAs to the ER membrane (Favaloro et al. 2010, Stefanovic & Hegde 2007). Early crystallographic work showed that Get3 undergoes ATP-dependent rearrangements that can be coupled to substrate binding (Figure 1.2, step 1). Get3 is an obligate homodimer bridged by a tightly coordinated Zn^{2+} ion. Each Get3 subunit contains a nucleotide hydrolase domain structurally and functionally coupled to a helical domain. *Apo*-Get3 crystallizes in an *open* conformation, in which the two helical domains are apart (Figure 1.2, Structure 1). In contrast, non-

hydrolyzable ATP analogs induce readjustments at the dimer interface that bring the helical domains closer to one another (Figure 1.2, Structure 2) (Bozkurt et al. 2009, Hu et al. 2009, Mateja et al. 2009, Suloway et al. 2009). Importantly, *closing* of Get3 brings together conserved hydrophobic residues in the helical domains to form a hydrophobic groove that provides the binding site for the TA TMD (Mateja et al. 2015). Nevertheless, Get3 has been observed in a variety of conformations that differ in the degree of *opening* or *closing*, suggesting the presence of more than two defined states. Furthermore, molecular dynamics simulations suggest that Get3 dynamically samples multiple conformations (*wide-open*, *open*, *semi-open*, *semi-closed*, and *closed*) in different nucleotide states (Wereszczynski & McCammon 2012). The number of conformational states in Get3 and how they are regulated by nucleotides remain to be defined.

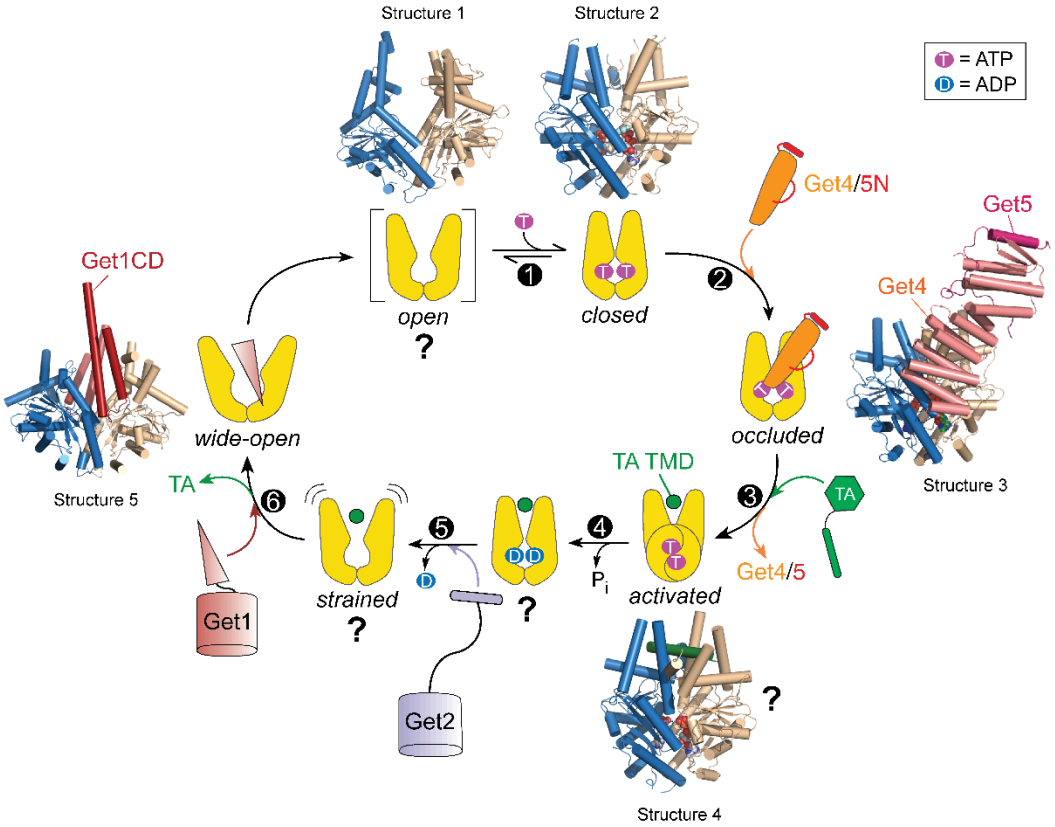

Figure 1.2: The Get3 ATPase cycle is driven by nucleotides, effectors, and tail-anchored protein (TA) substrates. Structure 1 shows *apo*-Get3 in an *open* conformation (PDB 3H84), although whether this species exists *in vivo* is unclear. (1) ATP binding induces Get3 into a *closed* conformation (Structure 2; PDB 2WOJ). (2) Get4/5 preferentially binds *closed* Get3 and inhibits its ATPase activity, generating an *occluded* state (Structure 3; PDB 4PWX). (3) TA binding induces Get3 into an *activated* state, and Get3 dissociates from Get4/5. The crystal structure of Get3 bound with a transmembrane domain (TMD) peptide is shown in Structure 4 (PDB 4XTR), although the structural basis for the TA-induced activation of Get3 is unclear. (4) *Activated* Get3 hydrolyzes ATP, and the ADP-bound Get3•TA complex can bind Get2. (5) ADP release induces additional rearrangements in the Get3•TA complex, which enable it to interact with Get1. (6) The strong preference of Get1 for a *wide-open* Get3 (Structure 5; PDB 3SJB) drives the release of TA from Get3. CD denotes cytosolic domain. The two subunits in the Get3 homodimer are in blue and tan in all structures.

Indeed, subsequent biochemical, enzymatic, and structural analyses uncovered additional conformational states in Get3 that are regulated by the TA substrate and other GET components. A major regulator is the Get4/5 complex. Pulldown (Chartron et al. 2010, Gristick et al. 2014) and fluorescence (Rome et al. 2014) studies showed that Get4 preferentially binds ATP-bound Get3, and reciprocally, Get4/5 stabilizes ATP binding to Get3 (Rome et al. 2013). As ATP stabilizes *closed* Get3, the synergy between ATP and Get4/5 in binding Get3 strongly suggests that Get4/5 also stabilizes Get3 in a *closed* conformation. In contrast, Get4/5 inhibits the ability of Get3 to hydrolyze ATP (Rome et al. 2013), suggesting that the global *closing* of Get3 can be uncoupled from catalytic activation at the ATPase site. This Get4/5-induced new state of Get3, termed *occluded*, was visualized crystallographically using Get4/5N bound to a hydrolysis-deficient mutant of Get3, Get3 (D57V), loaded with ATP (Gristick et al. 2014). A single Get4 molecule bridges the Get3 dimer interface and interacts with both subunits of Get3 (Figure 1.2,

Structure 3). The interaction with one Get3 subunit consists of both electrostatic and hydrophobic contacts, generating an anchoring interface for high-affinity binding of Get4/5 to ATP-bound Get3 (Gristick et al. 2014). Additional residues in Get4 establish a regulatory interface with the other Get3 subunit, at which a putative salt bridge between Get3 K69 and Get4 D74 is critical for ATPase inhibition (Gristick et al. 2014). Together, these results show that Get4/5 primes Get3 into the optimal conformation and nucleotide state for capturing the TA substrate.

In contrast to Get4/5, a TA substrate induces a rapid round of ATP hydrolysis on Get3 (Rome et al. 2013). This observation led to the proposal that the TA substrate induces Get3 into an *activated* conformation and leads to the ATP hydrolysis event after TA loading on Get3 (Figure 1.2, steps 3 and 4). Upon TA loading, the interaction of Get3 with Get4/5 is weakened at least tenfold in the presence of ATP, and the interaction becomes undetectable with a nucleotide-free Get3•TA complex (Rome et al. 2014). These findings suggest that the TA substrate also helps drive the dissociation of Get3 from Get4/5. Finally, the TA substrate significantly slows nucleotide exchange on Get3. Compared to free Get3, ADP release from the Get3•TA complex is 200-fold slower, and ATP rebinding to the Get3•TA complex is 10,000-fold slower and rate limited by a conformational change at physiological ATP concentrations (Rome et al. 2013). Slower nucleotide exchange provides extended time windows of ~14 and ~12 s for Get3•TA complexes in the ADP-bound and nucleotide-free states, respectively, during which these complexes can interact with the Get1/2 receptor complex (see the section titled The Get1/2 Membrane Receptor Complex Remodels the Targeting Complex, below).

1.5 THE GET1/2 MEMBRANE RECEPTOR COMPLEX REMODELS THE TARGETING COMPLEX

Get1/2 provides the receptor complex for the Get3•TA complex at the ER membrane (Schuldiner et al. 2008). Biochemical reconstitution with proteoliposomes validated that these two proteins (and their mammalian homologs) are necessary and

sufficient for TA targeting and insertion (Mariappan et al. 2011, Vilardi et al. 2014, Wang et al. 2011, Yamamoto & Sakisaka 2012). Both Get1 and Get2 contain three predicted TMDs via which they assemble into a complex (Mariappan et al. 2011, Wang et al. 2014). Both proteins also contain large cytosolic domains (CDs) (the N-terminal CD in Get2 and the TM1-TM2 loop in Get1) that interact with Get3. Get2CD contains two amphiphilic helices connected by a glycine linker, and helix α1 electrostatically contacts one of the subunits in the Get3 dimer via conserved basic residues in the ^{14}RERR motif (Mariappan et al. 2011, Stefer et al. 2011, Wang et al. 2011). Whereas the Get2CD co-crystallized with *closed,* nucleotide-bound Get3 (Mariappan et al. 2011, Stefer et al. 2011), the Get1CD co-crystallized with *apo*-Get3 in the most *open* conformation observed thus far (Figure 1.2, Structure 5). The Get1CD consists of two helices that form a coiled coil, which inserts like a wedge into the Get3 dimer interface and contacts both Get3 subunits in the dimer (Kubota et al. 2012, Mariappan et al. 2011, Stefer et al. 2011). Contacts with one Get3 subunit occur at its nucleotide-binding domain, where an extensive interface is formed by both aromatic and charged residues. Contacts with the other Get3 subunit are smaller and involve helix α4 in its helical domain. Finally, Get1 and Get2 share overlapping interaction surfaces, notably the ^{303}DELYED motif on helix α11, on Get3 (Mariappan et al. 2011, Stefer et al. 2011). Both receptor subunits also share overlapping binding sites on Get3 with Get4/5 (Gristick et al. 2014). Thus, these upstream and downstream GET proteins compete for interaction with Get3 during the targeting cycle.

These structural data, together with the following observations, strongly suggest that the Get3•TA complex is first captured by Get2 and then transferred to Get1. Get2 contains a >100-amino-acid linker that connects its Get3-binding helices to its TMDs, which may allow Get2 to search for Get3•TA complexes further away from the ER. Surface plasmon resonance (SPR) and fluorescence analyses show that the Get2CD can bind Get3 and Get3•TA complexes in nucleotide-bound states, whereas the Get1CD binds only the nucleotide-free Get3•TA complex and strongly

prefers *apo*-Get3 in which the TA-binding groove is disrupted (Mariappan et al. 2011, Rome et al. 2014, Stefer et al. 2011). Finally, high concentrations of the Get1CD can displace TA from Get3, whereas the Get2CD cannot (Mariappan et al. 2011, Wang et al. 2011). Together, these results support a model in which the Get3•TA complex bound with ADP is initially recruited to the membrane by Get2; upon ADP release, the Get1CD initiates interaction with and remodels the Get3•TA complex, leading to the release of TA from Get3 and to its insertion into the ER membrane (Figure 1.1, steps 4 and 5, and Figure 1.2, steps 5 and 6).

These data also predict that a stable complex between the Get1CD and *apo*-Get3 accumulates at the ER membrane at the end of the targeting cycle (Figure 1.1, end of step 5). The tip of Get1 remodels both switch I and switch II loops at the Get3 ATPase site, inducing these loops into a conformation incompatible with nucleotide binding (Kubota et al. 2012, Mariappan et al. 2011, Stefer et al. 2011). Consistent with the structures, SPR and fluorescence measurements showed that ATP and the Get1CD strongly antagonize one another for binding to Get3 (Kubota et al. 2012, Mariappan et al. 2011, Rome et al. 2014, Stefer et al. 2011). Furthermore, addition of ATP accelerated the release of Get3 from the Get1CD and vice versa, suggesting a release mechanism involving active displacement (Kubota et al. 2012, Rome et al. 2014). Finally, with full-length Get1/2 proteoliposomes or ER microsomes, Get4/5 was also needed to promote the facile release of Get3 from the membrane (Rome et al. 2014). Thus, the recycling of Get3 in the GET pathway is an elaborate event driven by both ATP and Get4/5 (Figure 1.1, step 6).

Despite extensive progress, multiple questions remain for the GET pathway. First, the structural basis for the TA-induced changes in Get3 activity is unclear. Although a co-crystal structure of Get3 (D57N) bound to a TMD peptide (Mateja et al. 2015) is available, the conformation of Get3 in this structure is similar to the conformations in the Get3·Get4/5 complex and in ADP•AlF_4-bound Get3. The structure, dynamics, and mechanism of regulation of the Get3•TA complex remain to be elucidated at the molecular level (Figure 1.2, question marks) and are the

subjects of the work presented in Chapters 2 and 3 of this thesis. In addition, the structures of important intermediates in the pathway, such as Get2 and/or Get1 bound to the Get3•TA complex, are still unavailable. Whether Get2 acts passively to bring the Get3•TA complex to Get1 or plays a more active role is unclear and remains to be determined.

Chapter 2

A PROTEAN CLAMP GUIDES MEMBRANE TARGETING OF TAIL-ANCHORED PROTEINS

Adapted from:

Chio, U.S., Chung, S., Weiss, S., and Shan, S.-O. 2017. A protean clamp guides membrane targeting of tail-anchored proteins. *Proceedings of the National Academy of Sciences U. S. A.* 114(41): E8585-E8594. doi: 10.1073/pnas.1708731114.

Proper localization of proteins to target membranes is a fundamental cellular process. How the nature and dynamics of the targeting complex help guide substrate proteins to the target membrane is not understood for most pathways. In this chapter, we address this question for the conserved ATPase Get3, which targets the essential class of tail-anchored proteins (TAs) to the endoplasmic reticulum (ER). Single-molecule fluorescence spectroscopy showed that, contrary to previous models of a static *closed* Get3•TA complex, Get3 samples *open* conformations on the sub-millisecond timescale upon TA binding, generating a fluctuating "protean clamp" that stably traps the substrate. Point mutations at the ATPase site bias Get3 toward *closed* conformations, uncouple TA binding from induced Get3•Get4/5 disassembly, and inhibit the ER targeting of the Get3•TA complex. These results demonstrate an essential role of substrate-induced Get3 dynamics in driving TA targeting to the membrane, and reveal a tightly coupled channel of communication between the TA-binding site, ATPase site, and effector interaction surfaces of Get3. Our results provide a precedent for large-scale dynamics in a substrate-bound chaperone, which provides an effective mechanism to retain substrate proteins with high affinity while also generating functional switches to drive vectorial cellular processes.

2.1 INTRODUCTION

Over 35% of proteins need to be localized to the correct cellular destinations after their initial synthesis in the cytosol. These protein-targeting processes are essential for the establishment and maintenance of compartmentalization in all cells and pose complex mechanistic challenges to targeting machineries. To minimize improper exposure of substrate proteins in the cytosol, targeting factors must bind substrate proteins with high stability. This requirement is especially stringent during the targeting of integral membrane proteins, whose high aggregation propensity in the cytosol and other aqueous cellular environments demands that targeting factors also serve as effective chaperones to protect substrates from aggregation. Further, to minimize futile cycling of targeting factors, loading of substrates on the targeting factor must be tightly coupled to their delivery to membrane receptor sites. Finally, once at the target membrane, the targeting machinery must readily switch to a low-affinity state to release substrate proteins to receptor complexes, translocases, or the phospholipid bilayer. With a few exceptions (Akopian et al. 2013, Tsirigotaki et al. 2017), the nature and dynamics of protein targeting complexes and how their biophysical properties help meet these complex functional demands are not well understood, especially for post-translational protein targeting pathways.

The targeting of tail-anchored proteins (TAs) provides an excellent system to address these questions. TAs, defined by a single transmembrane domain (TMD) near the C terminus, comprise up to 5% of the eukaryotic membrane proteome and mediate diverse key cellular functions, including protein translocation across multiple organelle membranes, vesicular fusion, protein quality control, and apoptosis (Borgese & Fasana 2011). In eukaryotic cells, TAs are targeted to the endoplasmic reticulum (ER) by the conserved guided entry of tail-anchored protein (GET) pathway, in which the Get3 ATPase captures TAs with help of the cytosolic Get4/5 complex and then delivers TAs to the Get1/2 receptor complex at the ER membrane (Chartron et al. 2012a, Denic et al. 2013, Hegde & Keenan 2011). During

the targeting cycle, Get3 undergoes extensive changes in conformation and activity in response to nucleotides, effector proteins, and the TA substrate (Figure 2.1). In the cytosol, ATP binding drives the Get3 homodimer from an *open* conformation, in which the helical domains of the two Get3 subunits are apart, to a *closed* conformation in which the helical domains are close together (Bozkurt et al. 2009, Mateja et al. 2009) (Figure 2.2). *Closed* ^{ATP}•Get3 is preferentially bound by the Get4/5 complex (Gristick et al. 2014, Rome et al. 2014), which bridges between Get3 and the upstream cochaperone Sgt2 and stimulates TA transfer from Sgt2 onto Get3 (Mateja et al. 2015, Rao et al. 2016, Wang et al. 2011). After dissociation from Get4/5, the Get3•TA complex hydrolyzes ATP and interacts with the Get1/2 membrane receptors (Rome et al. 2013, 2014). Get1 drives Get3 into an *open* conformation, enabling TA release and insertion into the membrane (Kubota et al. 2012, Mariappan et al. 2011, Stefer et al. 2011, Wang et al. 2011). (See Chapter 1 for a more detailed review)

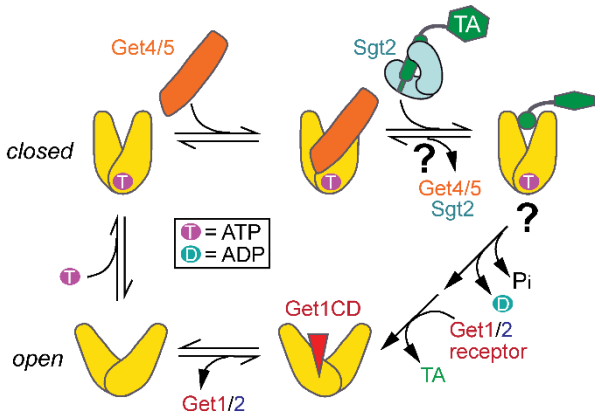

Figure 2.1: Current model for Get3 conformations throughout the GET pathway. Question marks ("?") highlight unresolved questions.

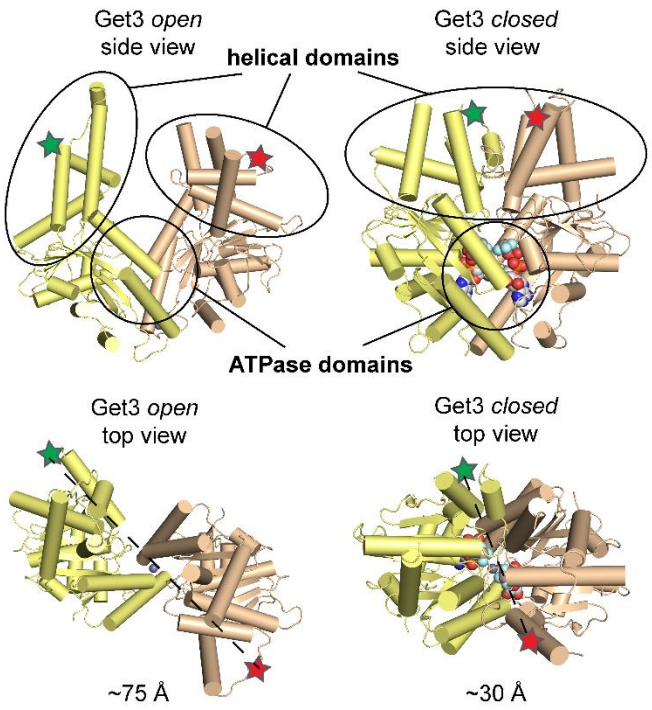

Figure 2.2: Structures of *open* and *closed* Get3. Approximate positions of donor and acceptor dyes (green and red stars, respectively) in the structures of *open* Get3 (left; PDB 3H84) and *closed* Get3 (right; PDB 2WOJ). The bound ADP•AlF_4^- in *closed* Get3 is in space-fill.

Despite these advances, the conformation and dynamics of the Get3•TA complex during targeting remain an outstanding question (Chartron et al. 2012a, Denic et al. 2013, Shan 2016). Crystallographic analyses showed that Get3 "*closing*" generates a contiguous hydrophobic groove in its helical domains (Bozkurt et al. 2009, Mateja et al. 2009), which provides a binding site for the TMD of TA substrates. The co-crystal structure of Get3 bound with a TA-TMD (Mateja et al. 2015) also shows a *closed* Get3 similar to that in the ^{ATP}•Get3•Get4/5 complex (Gristick et al. 2014). It was proposed that *closed* Get3 stably binds TA substrates and protects the TMD from exposure to the cytosol (Mateja et al. 2009, 2015). However, an exclusively *closed* Get3•TA complex poses a fundamental dilemma for targeting (Figure 2.1, "?"). Based on thermodynamic coupling, if both Get4/5 and TA prefer *closed* Get3, TA loading would strengthen the Get3–Get4/5 interaction. In

contrast, multiple downstream events in the pathway require Get3 to dissociate from Get4/5 after TA loading. These include the interaction of Get3 with Get1/2, whose binding sites on Get3 overlap with Get4/5 (Gristick et al. 2014, Kubota et al. 2012, Mariappan et al. 2011, Rome et al. 2014, Stefer et al. 2011), and ATP hydrolysis by Get3, which is inhibited by Get4/5 (Rome et al. 2013). These considerations predict that substrate-loaded Get3 must adopt conformation(s) that are different from the highly *closed* structures observed previously. Indeed, biochemical studies showed that a TA substrate destabilizes the interaction of Get3 with Get4/5 and activates the Get3 ATPase activity (Rome et al. 2013, 2014), implying that the substrate induces Get3 into distinct conformational state(s).

The GET pathway provides a salient example of the complex functional demands on the targeting machinery during a targeting cycle, as well as the conceptual and experimental challenges in understanding how these demands are met. The model of an exclusively *closed* Get3•TA complex also exemplifies the typical view of targeting complexes as static structures, wherein substrates fit into well-defined grooves or pockets in conformationally *closed* targeting factors or chaperones. Recent NMR studies began to challenge this view, demonstrating that client proteins populate a dynamic ensemble of conformational states and transit between multiple short-lived interaction sites when bound to chaperones such as Skp, SurA, and Spy during trafficking through the bacterial periplasm (Burmann et al. 2013, He et al. 2016, Thoma et al. 2015). Nevertheless, the nature and dynamics of the targeting factors/chaperones in these complexes, and how these properties help guide substrate proteins to the target membrane, have not been addressed.

To address these questions, we studied the conformation and dynamics of Get3 using single-molecule spectroscopy with microsecond time resolution. These analyses show that, contrary to previous models, the TA substrate destabilizes a *closed* Get3 and induces the ATPase to sample *open* conformations on the sub-millisecond timescale. Biochemical analyses demonstrate that these changes in the TA-binding domain are transmitted via the ATPase active site to drive the

dissociation of Get3 from Get4/5, and are essential for the targeting of TA substrates to the Get1/2 receptors at the ER membrane. These results provide a unifying model to explain how the TA substrate drives the switch of Get3 from a substrate-loading mode to a membrane-targeting mode. Moreover, they demonstrate how rapid protein motions allow a targeting factor/chaperone to stably retain its substrate protein while undergoing changes in structure and function to vectorially drive a cellular pathway.

2.2 RESULTS

Diffusion-based single-molecule spectroscopy detects global structure and dynamics of Get3

To measure the global conformational changes of Get3, we used diffusion-based single-molecule Förster resonance energy transfer (FRET) between donor (Cy3B) and acceptor (ATTO 647N) dyes site-specifically incorporated in the two subunits of the Get3 dimer (Figure 2.2). Fluorophores were incorporated at a nonconserved loop in the Get3 helical domain, and labeling does not affect the activity of Get3 (Rao et al. 2016). We used confocal microscopy with alternating laser excitation with microsecond time resolution (μs-ALEX) to detect and quantify the fluorescence of single molecules transiting through a femtoliter-scale observation volume, and extracted relative FRET efficiencies (E^*) for individual molecules (Kapanidis et al. 2005) (Figure 2.3). The distances between the dye pair are estimated to be ~75 Å and ~30 Å in *open* and *closed* Get3, respectively (Figure 2.2). Thus, a significant difference in FRET between the *open* and *closed* conformations of Get3 is expected for this dye pair, allowing us to monitor transitions along these states.

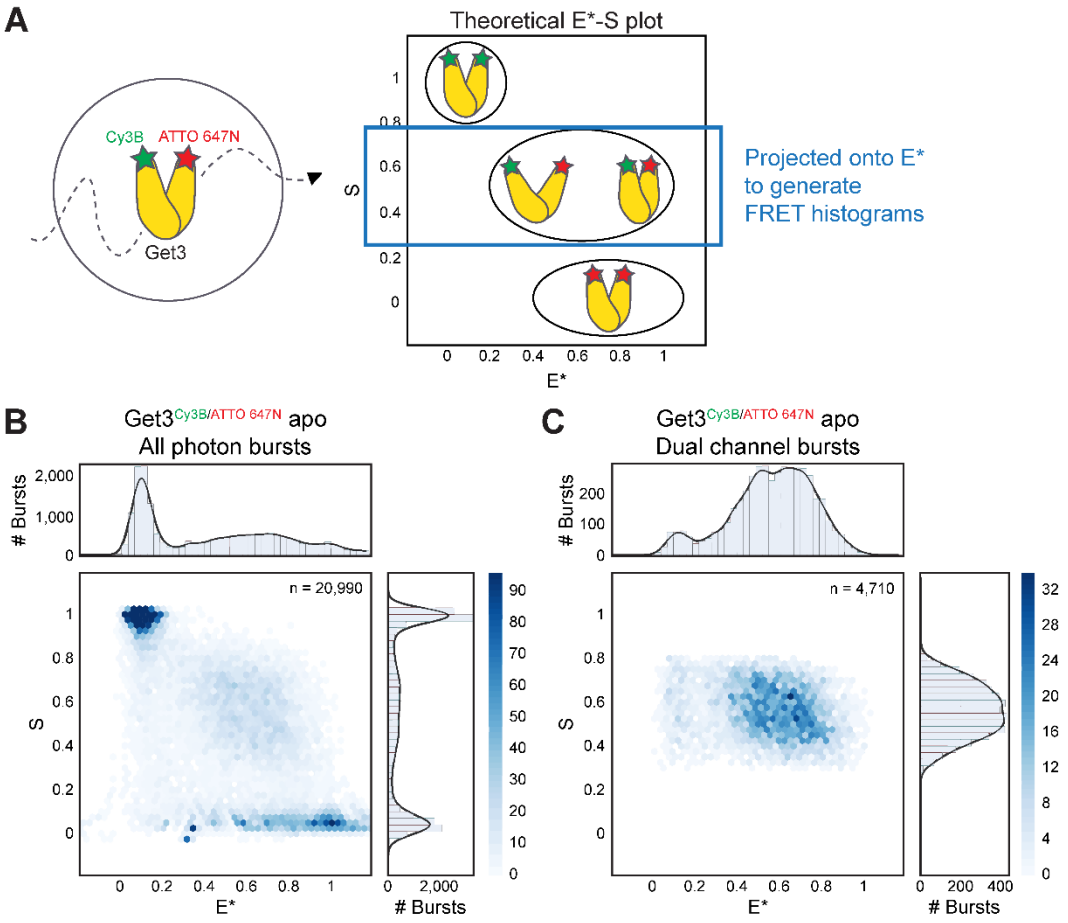

Figure 2.3: Monitoring Get3 conformational changes using µs-ALEX. (A) Schematic depiction of the µs-ALEX method. Donor and acceptor dyes labeled on Get3 were alternatively excited as they diffused through a confocal volume. Both the donor-to-acceptor *S* and relative *E** were determined for individual Get3 molecules, allowing for optical purification of doubly labeled Get3 (*S* ~ 0.5; cyan bracket) and differentiation of Get3 conformations displaying different *E** values. FRET histograms were obtained by 1D projection of 2D *E**-*S* histograms onto the *E** axis after isolating doubly-labeled Get3. (B) Representative *E**-*S* histogram of stochastically double-labeled *apo*-Get3 showing both single- and doubly-labeled Get3 populations. (C) Representative *E**-*S* plot of *apo*-Get3 after a dual-channel burst search to isolate doubly-labeled Get3.

We first used μs-ALEX to visualize the conformations of Get3 under well-established conditions. *Apo*-Get3 displayed a broad FRET distribution, with *E** maxima ranging from 0.5–0.7 (Figure 2.4 and reproducibility of data in Figure 2.5). The distribution for ADP-bound Get3 was also broad but peaked at higher FRET (Figure 2.4B). When Get3 was bound to the non-hydrolyzable ATP analog adenosine 5′-(β,γ-imido)triphosphate (AMPPNP), the FRET distribution was narrower and peaked at an *E** of ~0.8 (Figure 2.4C). In contrast, the cytosolic domain of Get1 (Get1CD) shifted the distribution to lower FRET (peak *E** of ~0.3; Figure 2.4D). These data agree with previous work showing that ATP induces Get3 to *closed* conformations (Bozkurt et al. 2009, Mateja et al. 2009), whereas Get1CD induces the *open* state of Get3 (Kubota et al. 2012, Mariappan et al. 2011, Stefer et al. 2011). To exclude photophysical artifacts, we repeated these measurements using another FRET pair, ATTO 550 and ATTO 647N, which yielded the same nucleotide and Get1CD-induced changes in FRET distributions (Figure 2.6). In addition, the presence of various ligands and interaction partners did not affect the dye photophysics in a way that would alter the FRET distributions (Figure 2.7). We also confirmed that Get3 dimers do not exchange subunits during measurements (Figure 2.8). Thus, our labeling strategy coupled with μs-ALEX can monitor the conformational transitions of Get3.

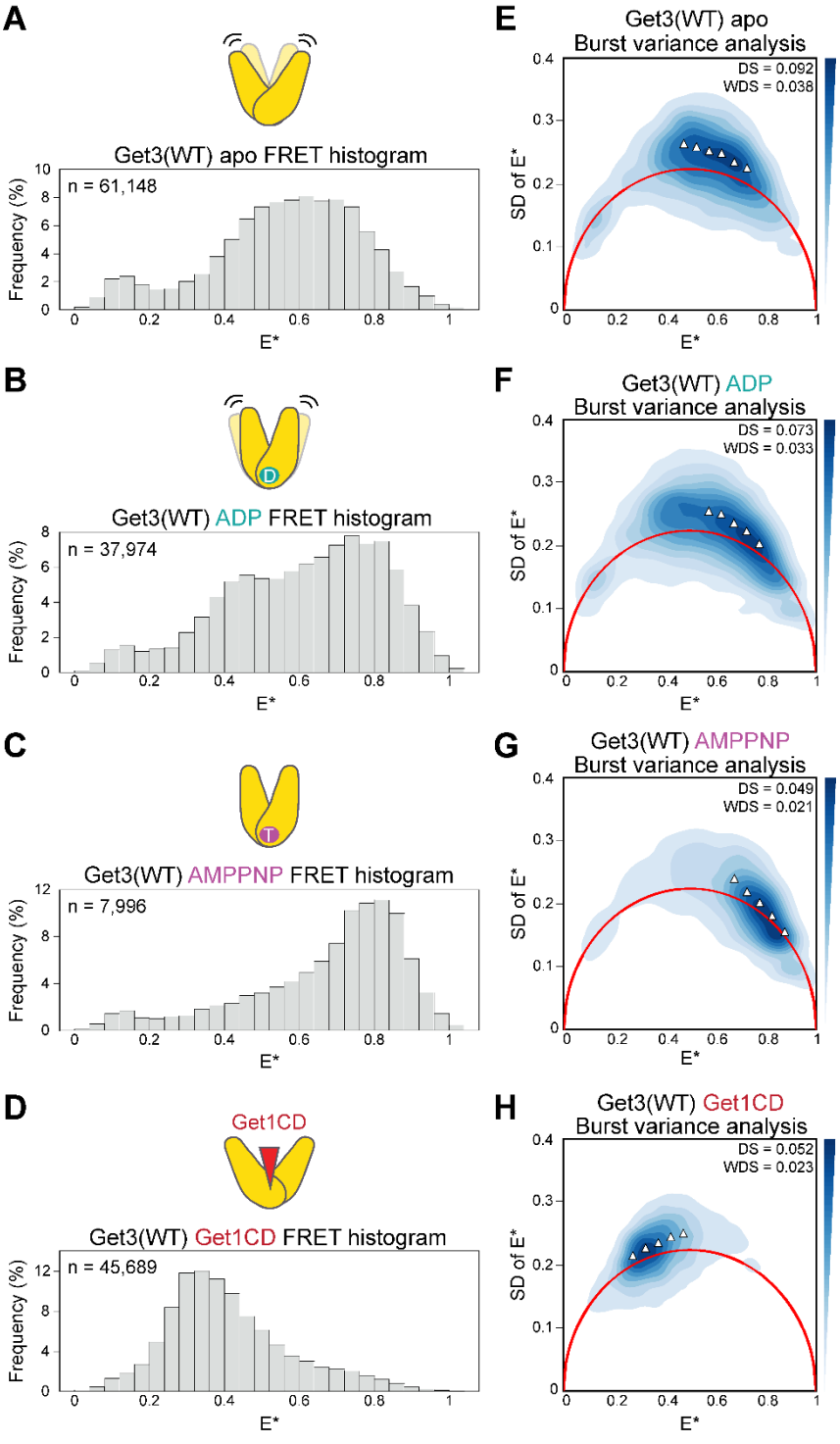
A
Get3(WT) apo FRET histogram
n = 61,148
Frequency (%)
E*
B
Get3(WT) ADP FRET histogram
n = 37,974
Frequency (%)
E*
C
Get3(WT) AMPPNP FRET histogram
n = 7,996
Frequency (%)
E*
D
Get1CD
Get3(WT) Get1CD FRET histogram
n = 45,689
Frequency (%)
E*
E
Get3(WT) apo
Burst variance analysis
DS = 0.092
WDS = 0.038
SD of E*
E*
F
Get3(WT) ADP
Burst variance analysis
DS = 0.073
WDS = 0.033
SD of E*
E*
G
Get3(WT) AMPPNP
Burst variance analysis
DS = 0.049
WDS = 0.021
SD of E*
E*
H
Get3(WT) Get1CD
Burst variance analysis
DS = 0.052
WDS = 0.023
SD of E*
E*

Figure 2.4: Direct observation of Get3 conformational changes using µs-ALEX. (A–D) FRET histograms for Get3 in *apo*-, ADP-, AMPPNP-, and Get1CD-bound states, respectively. Lighter shaded molecules depict alternative conformations sampled by Get3. The letter "n" denotes the number of observed doubly-labeled Get3 used to generate each FRET histogram. (E–H) BVAs for *apo*-, ADP-, AMPPNP-, and Get1CD-bound Get3, respectively. The red curves indicate the expected SD for shot-noise-limited E^* (static limit). Triangles denote the mean SD for individual FRET bins used to calculate the dynamic score (*DS*) and weighted dynamic score (*WDS*) (see Chapter 2.4, µs-ALEX data analysis).

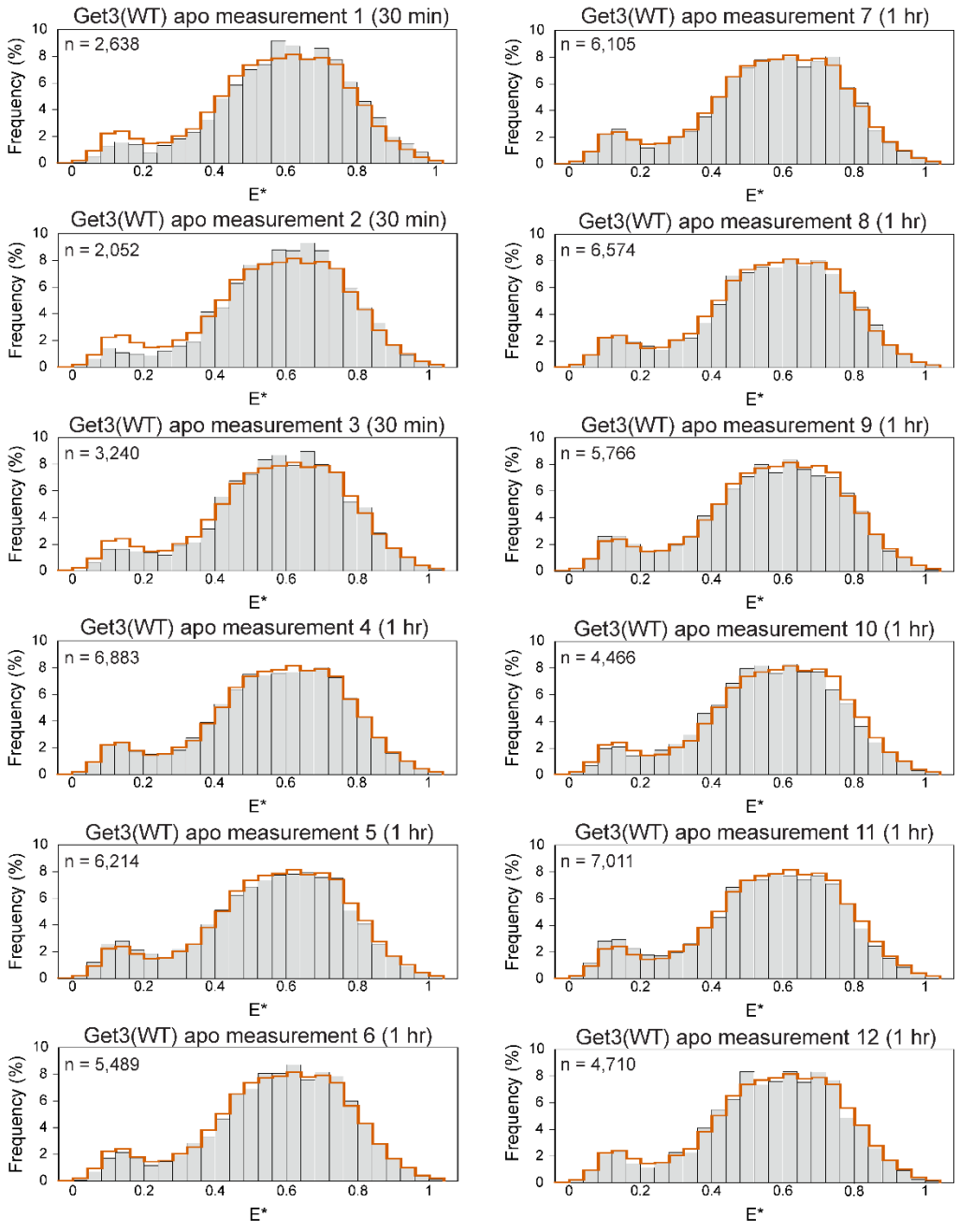

Figure 2.5: Replicates of the FRET histograms for *apo*-Get3. The orange outline shows the histogram generated by combining all of the data.

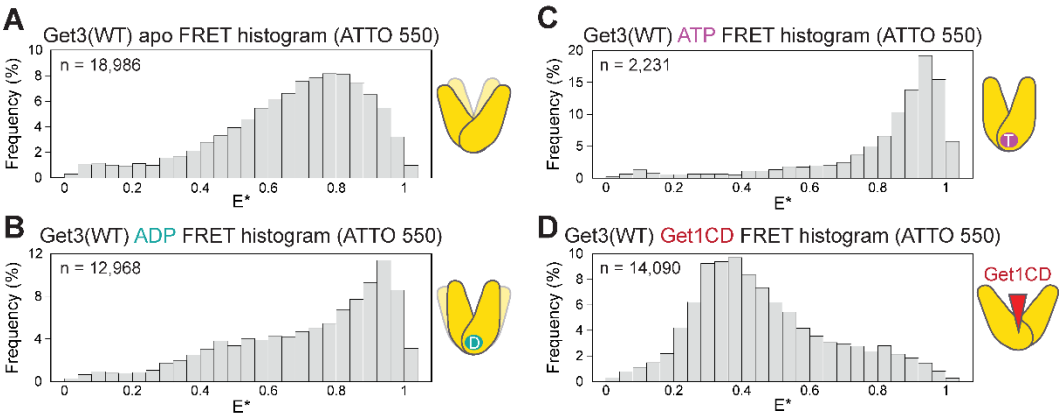

Figure 2.6: Get3 FRET histograms with ATTO 550. (A–D) FRET histograms of Get3 in the *apo*-, ADP-, ATP-, and Get1CD-bound states, respectively, for Get3 doubly-labeled with ATTO 550 and ATTO 647N. All of the FRET histograms are shifted to higher *E** compared with Cy3B- and ATTO 647N-labeled Get3, as expected from the longer Förster radius of the ATTO 550-ATTO 647N pair. Nevertheless, the ligand-induced changes in the FRET histogram follow the same trends as those measured with the Cy3B-ATTO 647N pair. The letter "n" denotes the number of observed doubly-labeled molecules used to generate each FRET histogram.

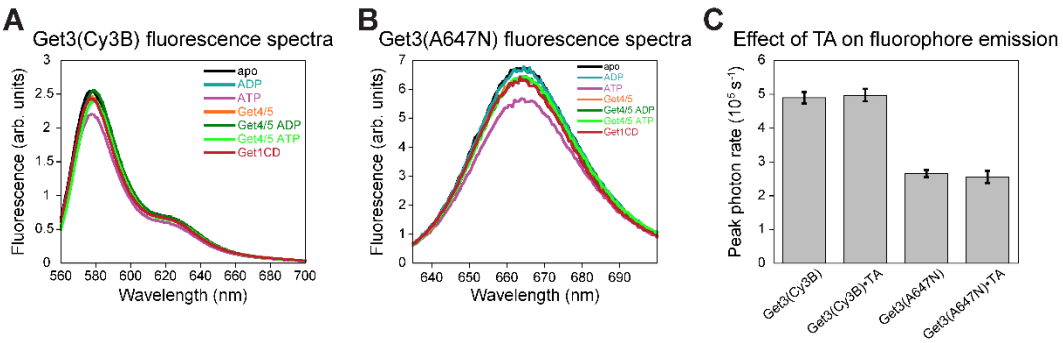

Figure 2.7: Controls for dye photophysics in µs-ALEX measurements of Get3. (A and B) Effects of ligands on the steady-state fluorescence spectra of Cy3B-labeled Get3 and ATTO 647N-labeled Get3, respectively, measured using a Fluorolog 3-22 spectrofluorometer. Saturating amounts of each interaction partner (2 mM ATP, 4 mM ADP, 10 µM Get1CD, 4 µM Get4/5) were used. Most interaction partners did not significantly affect Cy3B or ATTO 647N fluorescence. ATP modestly reduced

the fluorescence for both Cy3B and ATTO 647N, which should not significantly affect calculated FRET. arb., arbitrary. (C) TA substrate did not significantly affect the peak photon rate for both Cy3B and ATTO 647N, determined using the µs-ALEX setup for singly-labeled Get3. This suggests that the TA substrate does not affect the photophysics of the FRET pair on Get3.

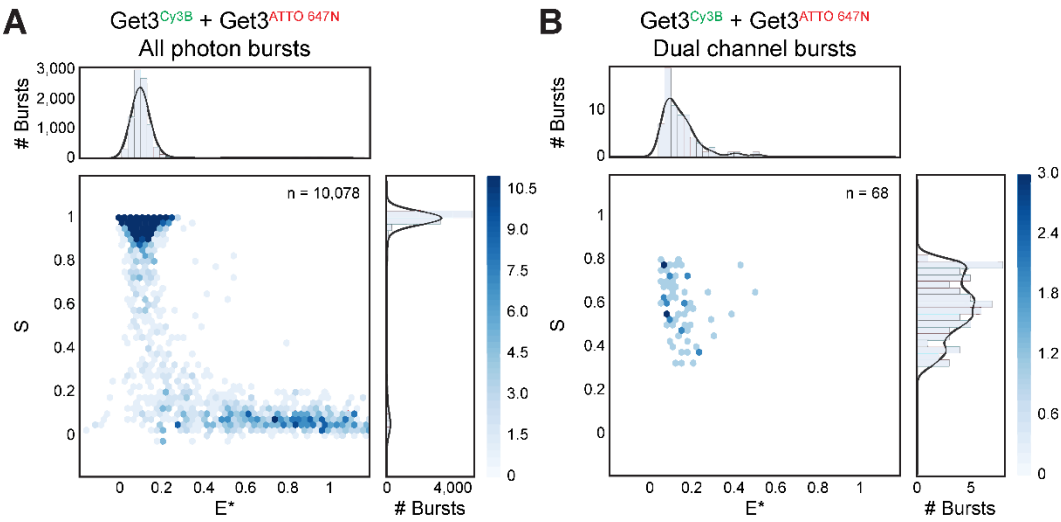

Figure 2.8: Controls for monomer exchange in µs-ALEX measurements of Get3. (A and B) Representative *E**-*S* plots for a mixture of donor-only and acceptor-only labeled Get3 before (A) and after (B) a dual-channel burst search. The absence of substantial colocalization of the donor and acceptor fluorophores indicates no significant exchange of Get3 subunits on our experimental timescale.

The FRET distributions of Get3 are broad, suggesting conformational heterogeneity. To distinguish whether this arises from the coexistence of multiple static structures or from dynamic conformational sampling, we performed burst variance analysis (BVA), which detects dynamics by comparing the SD of *E** over time with the SD expected from shot noise (Torella et al. 2011). If the FRET distribution arises solely from static species, the SD is limited by shot noise and would lie on the static limit curve (Figure 2.4 E–H, red lines). In contrast, if multiple conformations interconvert on the sub-millisecond or faster timescale, the observed

SD would be higher than the static limit. *Apo*- and ADP-bound Get3 displayed substantially higher SDs than the static limit, especially for molecules that exhibit intermediate *E** values (Figure 2.4 E and F). In contrast, the SDs for AMPPNP- and Get1CD-bound Get3 are close to the static limit, especially for molecules at the peak *E** values (Figure 2.4 G and H). Thus, *apo*-Get3 and ADP-bound Get3 sample a range of conformations on the sub-millisecond timescale, as suggested by molecular dynamics simulations (Wereszczynski & McCammon 2012), and the peak *E** values of 0.4–0.6 exhibited by *apo*-Get3 arise from conformational averaging between states with higher and lower FRET. Further, different interaction partners lock Get3 into distinct and more defined conformations.

The TA substrate induces Get3 to dynamically open

To determine the conformation of Get3 when bound to the TA substrate, we assembled Get3•TA complexes by *in vitro* translation of Bos1, a model GET substrate (Rao et al. 2016), in *Escherichia coli* lysate in the presence of Get3 and affinity-purified Get3•TA complexes via the 3xStrep-tag on Bos1 (Rao et al. 2016) (Figure 2.9A). Get3•TA complexes generated by this procedure were kinetically stable and highly efficient in TA targeting and insertion into the ER membrane (Rao et al. 2016) (Figures 2.10 and 2.11). In μs-ALEX measurements, ^{AMPPNP}•Get3•TA displayed a broader FRET distribution shifted toward lower *E** values compared with ^{AMPPNP}•Get3 (Figure 2.9B). The distributions shifted further to lower FRET and peaked at *E** values of ~0.55–0.6 with ^{ADP}•Get3•TA and Get3•TA (Figure 2.9 C and D). In addition, BVA showed that, in contrast to ^{AMPPNP}•Get3, Get3•TA complexes exhibiting intermediate *E** values displayed higher SD than the static limit in all nucleotide states (Figure 2.9 E–G). These observations indicate that Get3 also becomes more dynamic upon TA binding, and the observed *E** values of 0.4–0.6 result from averaging of Get3•TA complexes that interconvert between lower (<0.4) and higher (>0.6) FRET states on the sub-millisecond or faster timescale. Thus, contrary to the highly *closed* Get3•TA structure observed crystallographically

(Mateja et al. 2015), the TA substrate induces Get3 to dynamically sample *open* conformations.

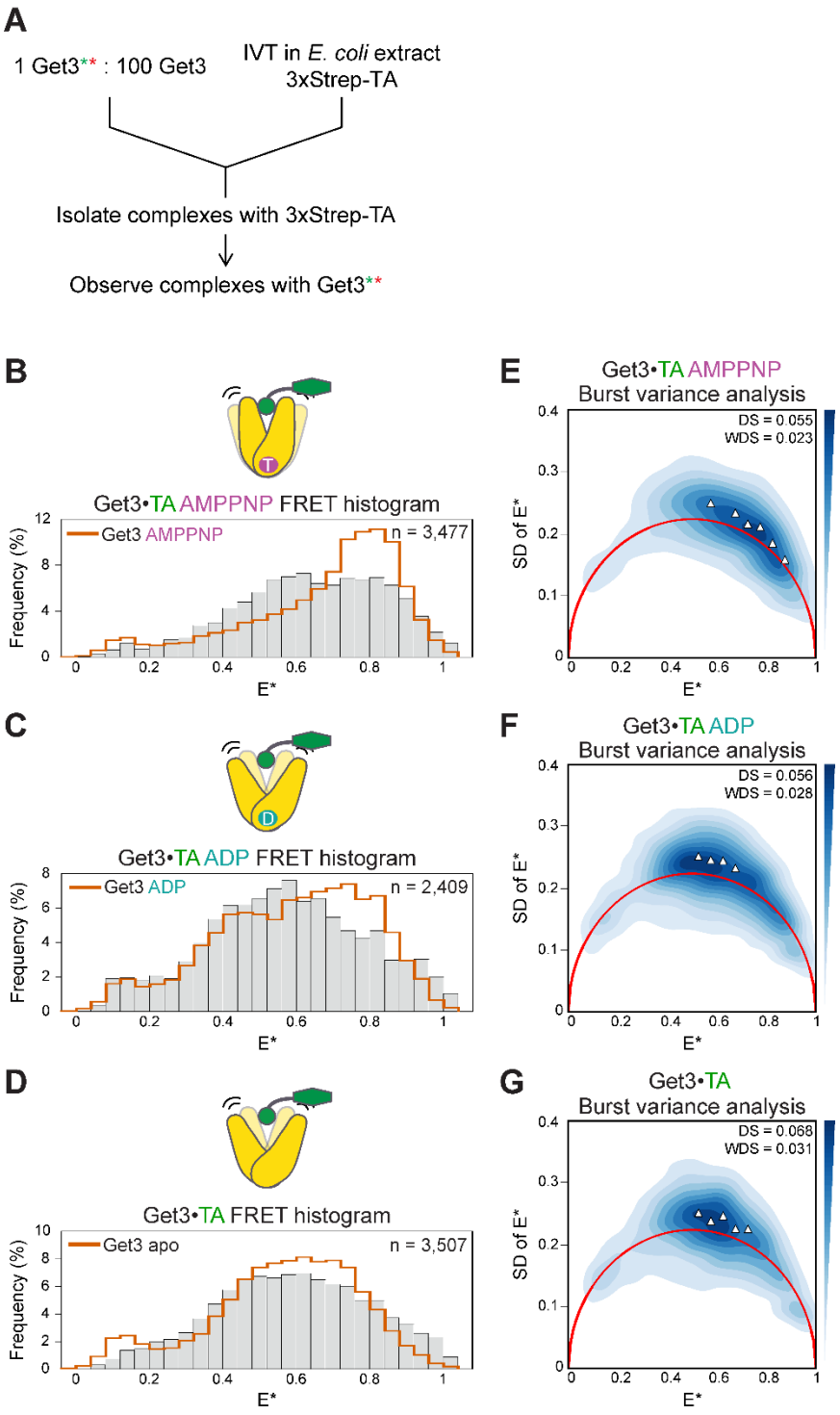

Figure 2.9: The TA substrate induces Get3 to dynamically sample *open* conformations. (A) Scheme for generation and purification of Get3•TA complexes for μs-ALEX experiments. Green and red asterisks denote donor and acceptor dyes labeled on Get3. A 100-fold excess of unlabeled Get3 was included to ensure that, statistically, intradimer FRET of Get3 was measured even in cases of potential Get3 tetramerization (Bozkurt et al. 2009, Rome et al. 2013, 2014). Experimental details are provided in Chapter 2.4. IVT, *in vitro* translation. (B–D) FRET histograms of Get3•TA complexes in AMPPNP-bound, ADP-bound, and nucleotide-free states, respectively. The outlines depict the FRET histograms of Get3 in the same nucleotide state without TA substrate and are shown for comparison; "n" denotes the number of observed doubly-labeled Get3 used to generate each FRET histogram. (E–G) BVAs of Get3•TA in AMPPNP-bound, ADP-bound, and nucleotide-free states, respectively. The red curves represent the SD expected for shot-noise-limited E^*. Triangles denote the mean SD for individual FRET bins used to calculate the dynamic score (*DS*) and weighted dynamic score (*WDS*).

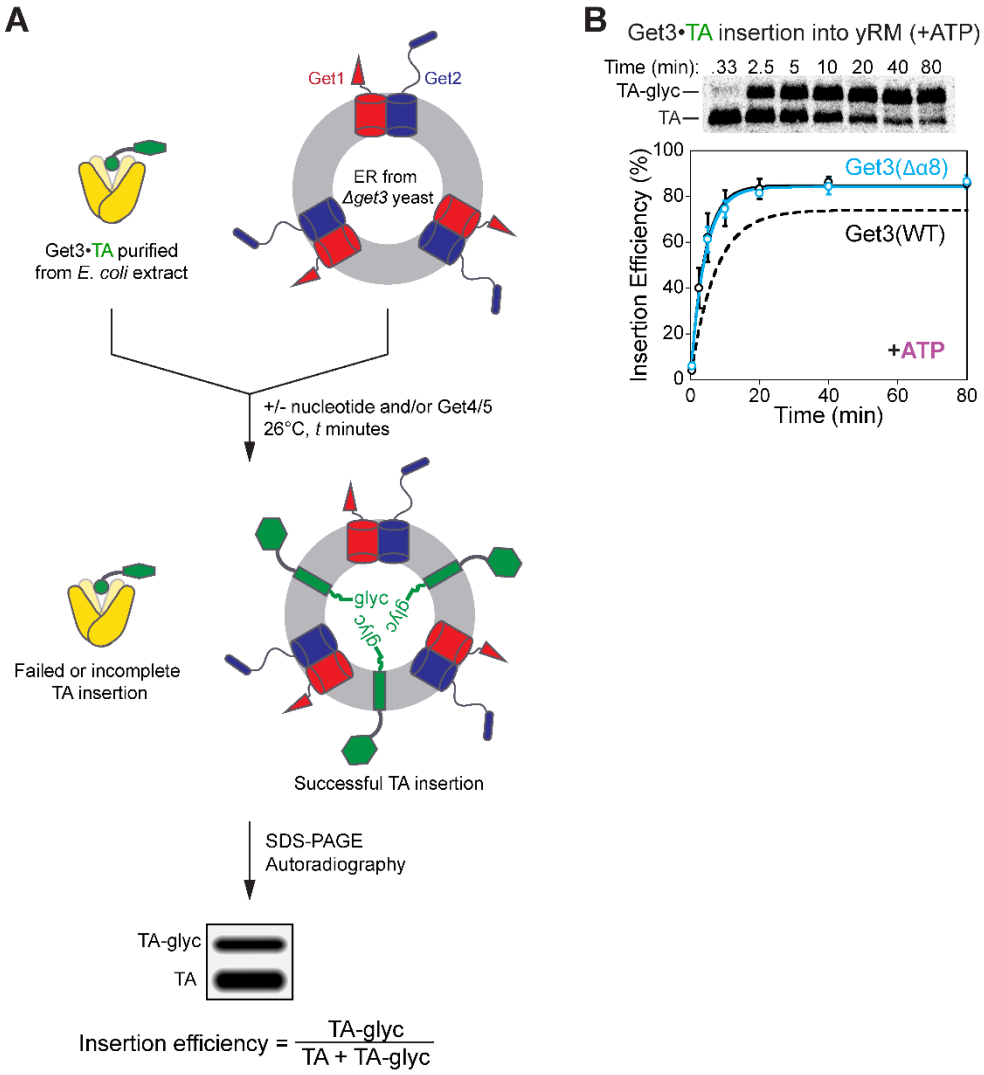

Figure 2.10: Prepared Get3•TA complexes are active in targeting and insertion into the ER. (A) Scheme of the TA targeting and insertion assay. Purified Get3•TA was presented to the ER from *Δget3* yeast with or without nucleotide and/or Get4/5. Successful TA insertion results in glycosylation (glyc) of its C-terminal opsin tag, which can be visualized as a molecular weight shift after SDS-PAGE. (B) Representative SDS-PAGE autoradiograph (top) and its quantification (bottom) for the time courses of Get3•TA targeting and insertion shown for wild-type Get3 (black solid line) and mutant Get3(Δα8) (cyan) (see Figure 2.14). The dotted curve depicts the insertion efficiency for Get3•TA generated with Sgt2 and Get4/5 included during translation as described previously (Rao et al. 2016), and shows that the inclusion of

Sgt2 and Get4/5 is not necessary for generation of a functional Get3•TA complex. glyc, glycosylated; yRM, yeast rough microsome.

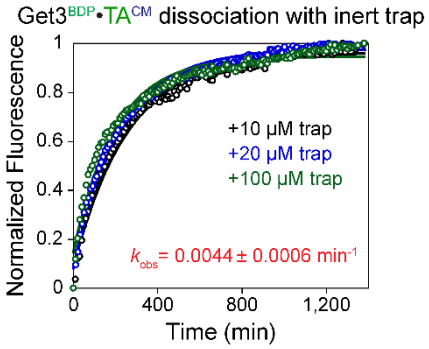

Figure 2.11: Prepared Get3•TA complexes are kinetically stable. Purified $Get3^{BDP}$•TA^{CM} (Rao et al. 2016) was presented to indicated concentrations of a TA trap, intein-cpSRP43 (Liang et al. 2016), and TA dissociation from Get3 was monitored through loss of FRET. The observed rate of TA dissociation is independent of trap concentration, indicating that intein-cpSRP43 acts as a passive trap to measure the intrinsic rate of Get3•TA spontaneous dissociation. The reported $k_{dissociation}$ value represents mean ± SD from the three measurements.

The Get3•TA complex was crystallized using a synthetic antibody (sAB), which binds at similar surfaces on Get3 as does Get4/5 (Mateja et al. 2015); it also specifically recognizes ATP-bound Get3, as does Get4/5 (Gristick et al. 2014, Mateja et al. 2015, Rome et al. 2014). Thus, a potential explanation for the difference between the crystallographic and single-molecule FRET data is that Get4/5 stabilizes a more *closed* conformation of Get3•TA, and this effect was mimicked by the sAB. We therefore tested the effect of Get4/5 on Get3 conformation using μs-ALEX. With *apo*-Get3, to which Get4/5 binds at a different surface than ^{ATP}•Get3 (Gristick et al. 2015), Get4/5 did not significantly change the FRET histogram (Figure 2.12A and Figure 2.13). With ^{ADP}•Get3, which is distributed between low and high FRET states, Get4/5 shifted the distribution to predominantly high E* values (Figure 2.12B and Figure 2.13). With ^{AMPPNP}•Get3, which is already *closed*, Get4/5 induced a modest

but statistically significant shift of the FRET distribution to a distinct high-FRET state (Figure 2.12C and Figure 2.13). These results agree well with previous work showing that Get4/5 preferentially binds *closed* Get3 (Gristick et al. 2014, Rome et al. 2014). Importantly, binding of Get4/5 also shifted the distribution of ^{ATP}•Get3•TA to higher E* (Figure 2.12D, bars vs. orange outline). Compared with the FRET distribution of ^{AMPPNP}•Get3•Get4/5 before TA loading, the distribution after TA loading peaked at the same E* value but was substantially broader (Figure 2.12D, bars vs. teal outline). Thus, Get4/5 also biases Get3•TA to more *closed* conformations. Moreover, these data illustrate sequential changes in the conformation and dynamics of Get3 during the targeting pathway (Figure 2.12E): Starting with a static, *closed* ^{AMPPNP}•Get3•Get4/5 complex (black), TA loading induces conformational "breathing" of Get3 (light orange); upon dissociation from Get4/5, Get3 more frequently samples *open* conformations (teal) that become more dominant after ATP hydrolysis (dark orange).

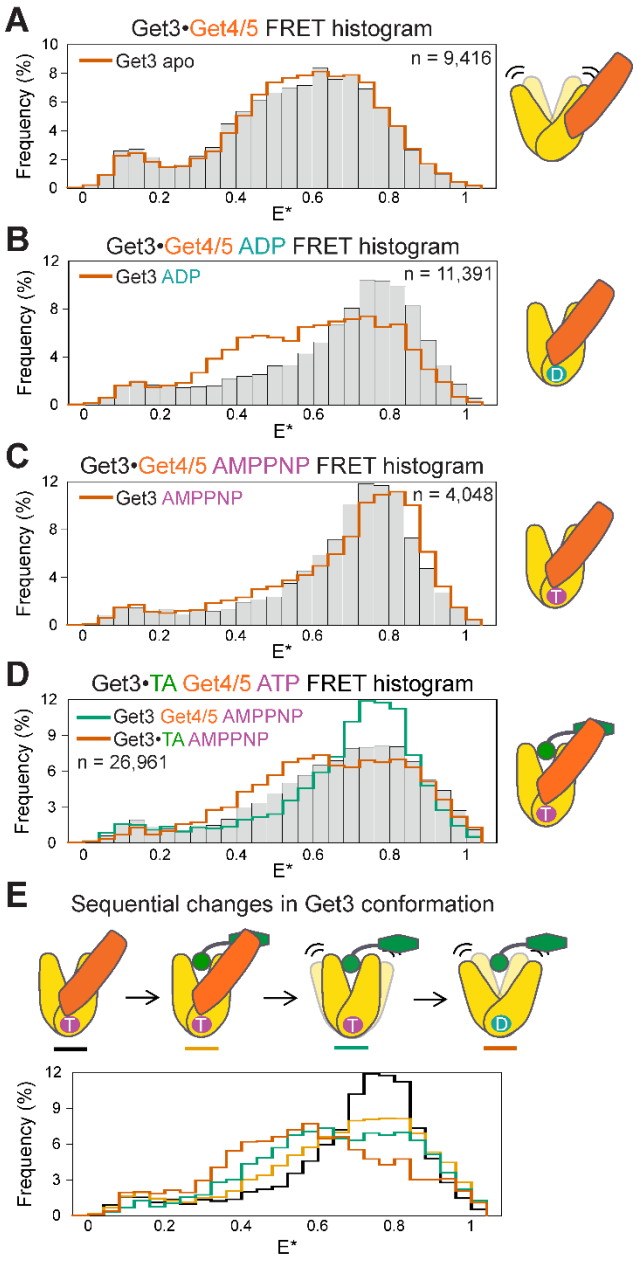

Figure 2.12: Sequential *opening* of Get3 upon TA loading and Get4/5 release. (A–C) Effects of Get4/5 on the FRET histograms of *apo*-, ADP-, and AMPPNP-bound Get3, respectively. (D) FRET histogram of Get3•TA bound with Get4/5 and ATP. The complex was generated by supplementing Get4/5 and excess ATP throughout the preparation to capture the conformation of the physiological initial loading complex (see Chapter 2.4). Since Get4/5 inhibits ATP hydrolysis (Rome et

al. 2013) and excess ATP is used, ATP turnover has no significant effect on the results. (E) Comparisons of FRET histograms of Get3 at different stages of the GET pathway. In A–D, the outlines depict the FRET histograms of indicated Get3 complexes and are shown for comparison, and "n" denotes the number of observed doubly-labeled Get3 used to generate each FRET histogram.

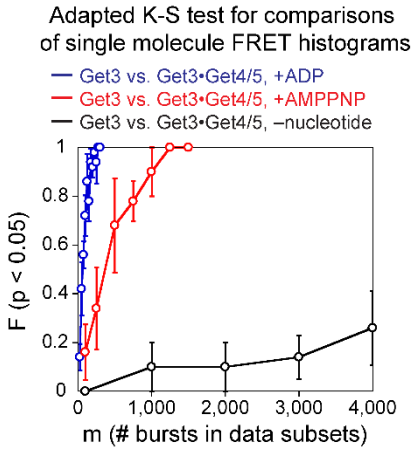

Figure 2.13: Adapted K-S tests for Get3•Get4/5 FRET histograms. Adapted K-S test to evaluate the significance of the differences between the FRET histograms of the indicated samples (see Chapter 2.4). The F ($p < 0.05$) values at each sample size m denote the fraction of 10 K-S tests from randomly selected subsets of data that yielded a statistically significant difference ($p < 0.05$), and were reported as mean ± SD, with $n = 5$. Histograms for which the F ($p < 0.05$) value rises slowly with m are considered similar (black line). Histograms for which the F ($p < 0.05$) value rises quickly with m are interpreted as significantly different (blue and red lines).

TA is stably bound by the dynamically fluctuating Get3

The dynamic *opening* of the Get3•TA complex is unexpected, as crystallographic analyses suggested that in *open* Get3, the hydrophobic groove for TMD binding becomes discontiguous (Mateja et al. 2009, Suloway et al. 2009). Intriguingly, our recent (Rao et al. 2016) and current measurements showed that Get3•TA complexes exhibit high kinetic stability: using a membrane protein

chaperone, cpSRP43 (Jaru-Ampornpan et al. 2010, Liang et al. 2016), as an inert TA trap, the timescale for spontaneous dissociation of Bos1 from Get3 was measured to be ~4 h (Figure 2.11). The lower limit for the lifetime of other Get3•TA complexes was 35–60 min (Rao et al. 2016). Thus, TAs are stably bound to Get3 despite the large-scale conformational fluctuations of Get3.

The simplest modification of the current model to explain these observations is that a 15-aa sequence termed helix α8, which was unresolved in most Get3 structures and proposed to form a lid over the TA-binding groove (Mateja et al. 2009, 2015), could prevent the escape of TA substrates during *opening*. Nevertheless, a structure of *apo*-Get3 [Protein Data Bank (PDB) ID code 3A36], in which α8 was resolved (Yamagata et al. 2010), suggests that the dimensions of α8 are unlikely to be sufficient to completely shield the helical domains and block TA escape in *open* Get3 (Figure 2.14A, α8 highlighted in cyan). To experimentally test the importance of α8, we replaced the conserved hydrophobic residues (^{199}PMLNSFM) in this sequence with a GS linker (GGSGGGS) to generate mutant Get3(Δα8). Get3•TA complexes assembled with mutant Get3(Δα8) could be purified as a stable complex (Figure 2.14B) and are fully functional in TA targeting and insertion into the ER membrane (Figure 2.10B, cyan curve). These results show that shielding by α8 is insufficient to explain the high stability of the Get3•TA complex if the current model of Get3–TA interaction were the only possible interaction mode. Following the principle of thermodynamic coupling, the observation of TA-induced Get3 *opening* further predicts that the TA substrate can explore alternative modes for interacting with a more *open* Get3 that are energetically more favorable than the established interaction mode observed with *closed* Get3 (Figure 2.14C). The implications of these observations are elaborated on in the Discussion section.

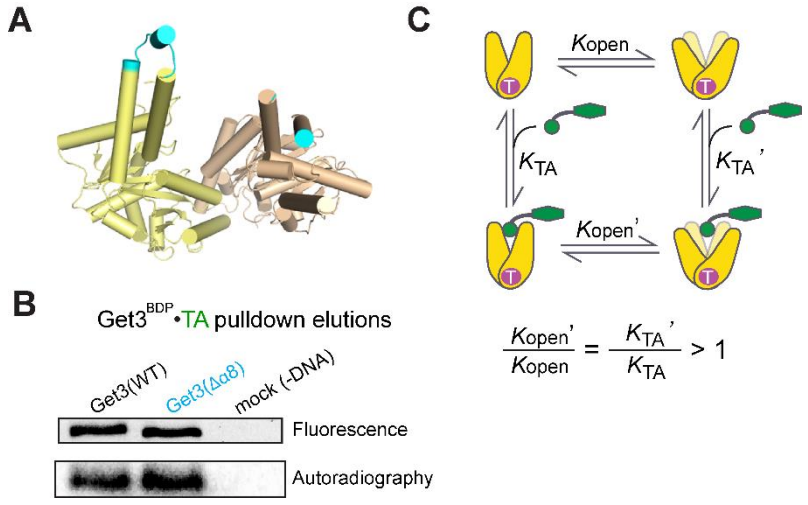

Figure 2.14: α8 is not necessary for a stable Get3•TA complex. (A) Structure of *apo*-Get3 (PDB 3A36) highlighting helix α8 (cyan) that is resolved in one of the Get3 subunits (yellow). The residues preceding and following α8 are highlighted in cyan in the other Get3 subunit (wheat). (B) Visualization of purified Get3•TA complexes, assembled with wild-type Get3 or mutant Get3(Δα8), by in-gel fluorescence (for Get3) and autoradiography (for TA). (C) Thermodynamic cycle showing the coupling of the TA-binding equilibrium (denoted by K_{TA} and K_{TA}' for *closed* and *open* Get3, respectively) to the conformational equilibrium of Get3 *opening* (denoted by K_{open} and K_{open}' for free and TA-loaded Get3, respectively).

TA-induced Get3 opening drives membrane targeting

At the junction of the Get3 helical and ATPase domains is a network of residues that interact across the dimer interface and contribute catalytic interactions with ATP (Bozkurt et al. 2009, Mateja et al. 2009, Suloway et al. 2009, Yamagata et al. 2010) (Figure 2.15A), raising the possibility that disruption of this network would interfere with the ability of Get3 to undergo regulated conformational changes. We tested two mutations in this network, D57N and E251A, which cause severe yeast growth defects under stress conditions (Mateja et al. 2009, Suloway et al. 2009). Both mutants bind ATP tightly but displayed ~100-fold slower ATPase activity than wild-

type Get3 (Mateja et al. 2009) (Figure 2.15 B–E). Surprisingly, μs-ALEX measurements showed that these mutations bias Get3 toward *closed* conformations under different conditions. Get3(E251A) is more *closed* than Get3(WT) when bound with nucleotides (Figure 2.16 A–D), whereas Get3(D57N) is more *closed* than Get3(WT) in apo- and Get1CD-bound states (Figure 2.16 G–J). In the Get3•TA complex, the FRET distributions of mutant Get3(D57N) were shifted to higher E* with and without ATP and Get4/5 present (Figure 2.16 K and L), whereas only the FRET distribution of free Get3(E251A)•TA was shifted (Figure 2.16 E and F). Although the mutational effects on the FRET distributions of Get3•TA were modest, the changes are systematic compared with variations between replicates of data and are statistically significant (Figures 2.5 and 2.17). The different effects of the two mutations on the FRET distributions of Get3•TA also agreed well with biochemical analyses of these mutants described later (see Figures 2.20 and 2.21). Thus, point mutations at the Get3 catalytic site alter the conformation and regulation of its helical domains.

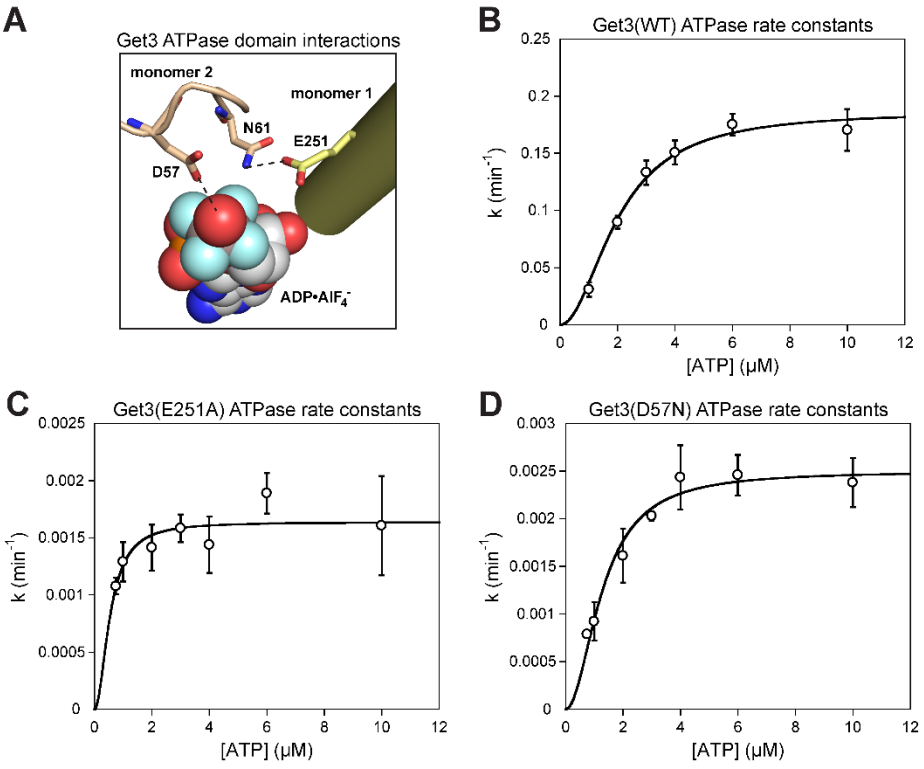

E

Get3 variant	K_M (μM)	k_{cat} (min^{-1})
Get3(WT)	4.1 ± 0.4	0.18 ± 0.01
Get3(E251A)	0.30 ± 0.07	0.0016 ± 0.0003
Get3(D57N)	1.7 ± 0.2	0.0025 ± 0.0002

Figure 2.15: Interactions at the Get3 ATPase site. (A) Network of interacting residues at the catalytic site across the Get3 dimer interface. Get3-D57 is positioned near the γ-phosphate and coordinates the nucleophilic water. Get3-N61 forms a salt bridge with Get3-E251 from the opposing Get3 monomer (PDB 2WOJ). ADP•AlF_4^- is shown in space-fill. (B–D) ATP concentration dependences of observed ATP hydrolysis rate constants for wild-type Get3 and the mutants Get3(E251A) and Get3(D57N), respectively. (E) Summary of K_M and k_{cat} values for wild-type and mutant Get3's derived from the data in B–D. All values are reported as mean ± SD ($n \geq 2$). Get3(E251A) and Get3(D57N) retain high-affinity ATP binding but are defective in ATP hydrolysis.

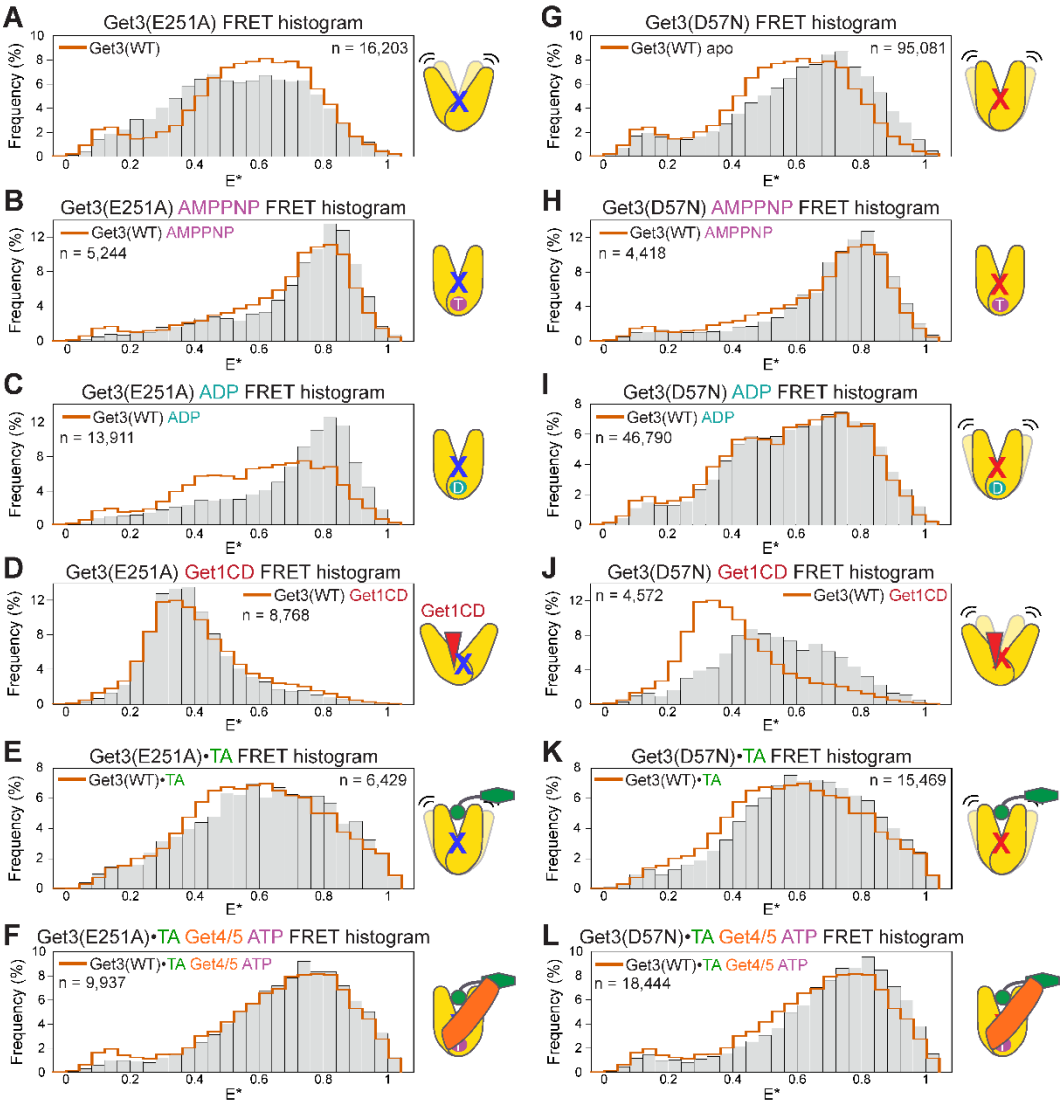

Figure 2.16: Point mutations at the ATPase active site bias Get3 to more *closed* conformations. (A–D) FRET histograms of Get3(E251A) in *apo*-, AMPPNP-, ADP-, and Get1CD-bound states, respectively. (E and F) FRET histograms of Get3(E251A)•TA without (E) or with (F) Get4/5 and ATP bound. (G–J) FRET histograms of Get3(D57N) in apo- and AMPPNP-, ADP-, and Get1CD-bound states, respectively. (K and L) FRET histograms of Get3(D57N)•TA without (K) and with (L) Get4/5 and ATP bound. In all histograms, the orange outlines depict the FRET histograms of wild-type Get3 under the same conditions, and "n" denotes the number of observed doubly-labeled molecules used to generate each FRET histogram.

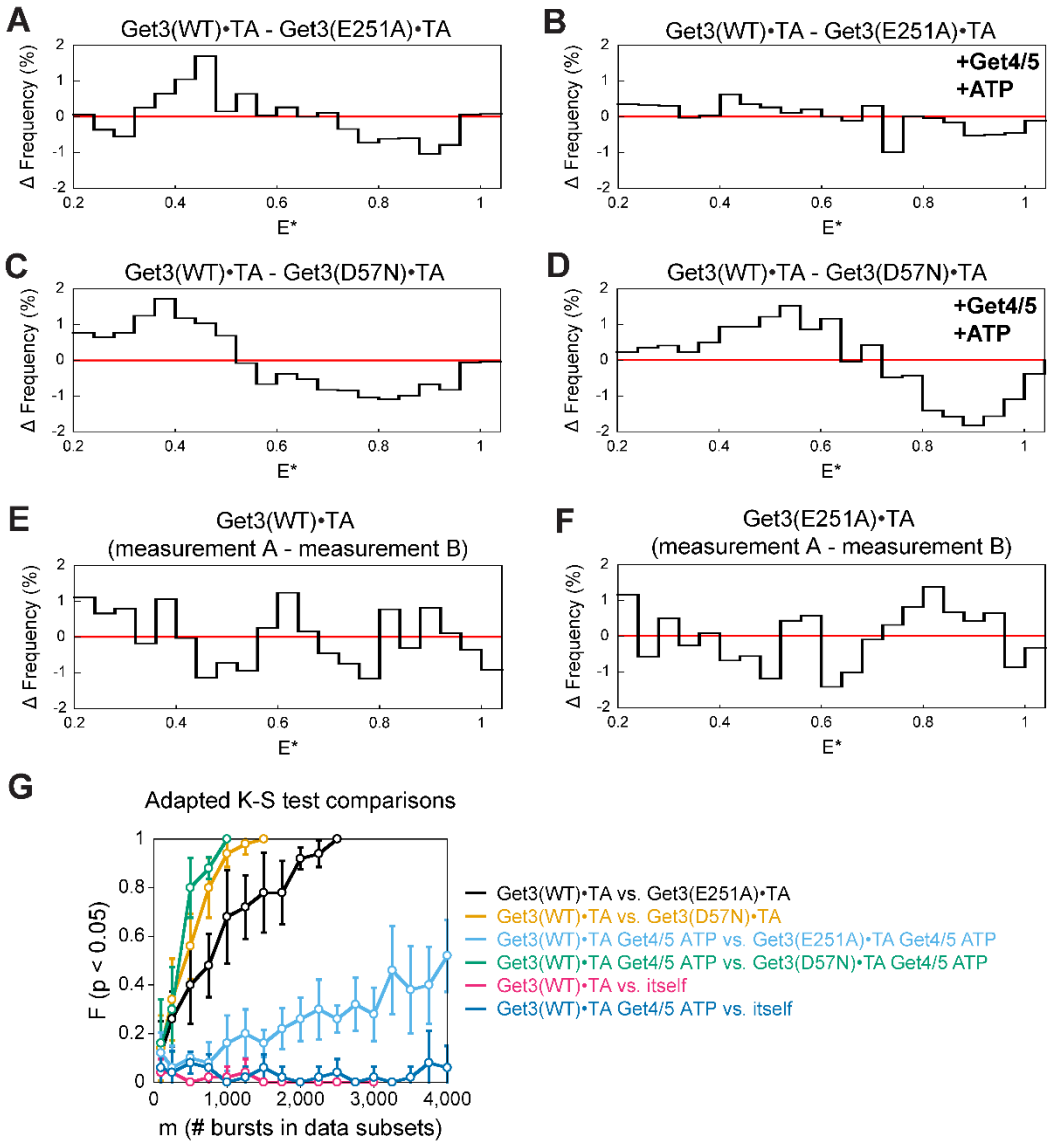

Figure 2.17: Comparisons of FRET histograms between wild-type and mutant Get3 complexes. (A–D) Differences between FRET histograms of indicated wild-type and mutant Get3 complexes. (E and F) Differences between replicates of µs-ALEX measurements for Get3•TA and Get3(E251A)•TA samples. The differences in the FRET histograms shown in A, C, and D between wild-type and mutant Get3 are systematic. In comparison, the differences in the FRET histograms between replicates of data shown in E and F are randomly distributed across E*, and the difference in the FRET histograms shown in B is smaller and more random. (G) Adapted K-S tests to evaluate the significance of the differences between the FRET

histograms of the indicated samples (see Figure 2.13, Chapter 2.4). Adapted K-S tests for molecules from the same sample usually result in $p > 0.05$ regardless of m (pink and dark blue lines), and serve as negative controls for the absence of a significant difference. Histograms for which the F ($p < 0.05$) value rises slowly with m are considered similar (light blue line). Histograms for which the F ($p < 0.05$) value rises quickly with m are interpreted as significantly different (black, orange, and green lines).

To assess if the conformational bias in Get3(D57N) and Get3(E251A) disrupts Get3 function, we tested the activities of these mutants in mediating TA targeting and insertion into the ER membrane. Without Get4/5 present, Get3(D57N)•TA and Get3(E251A)•TA were up to threefold and fivefold slower, respectively, than wild-type Get3•TA in targeting and insertion (Figure 2.18 A, C, and E). However, physiological amounts of Get4/5 (Ghaemmaghami et al. 2003) nearly abolished TA insertion with both mutants, without substantially affecting TA insertion by wild-type Get3 (Figure 2.18 B, D, and F). These mutational defects were observed regardless of the nucleotide state of Get3•TA complexes (Figure 2.18 A–F); the slower phase of the insertion reactions with *apo*-Get3 was due to the nucleotide requirement for recycling Get3 from the ER membrane during multiple rounds of TA targeting (Mariappan et al. 2011, Rome et al. 2014, Wang et al. 2011). Together, these results show that TA-induced Get3 *opening* is essential for membrane targeting of the Get3•TA complex under conditions that mimic the physiological situation, where the Get1/2 receptor and Get4/5 complex must compete for binding to Get3.

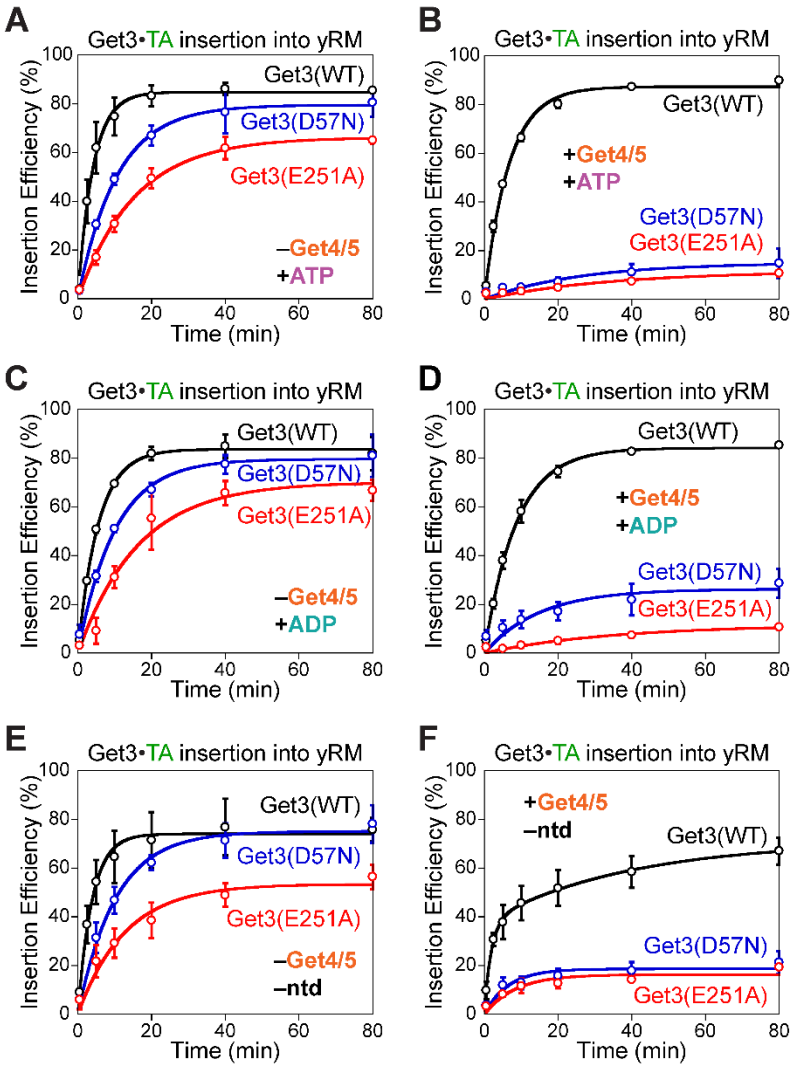

Figure 2.18: Get3 active site mutants block the targeting of Get3•TA complexes. Time courses for targeting and insertion of wild-type and mutant Get3•TA complexes in the absence (A, C, and E) and presence (B, D, and F) of 0.5 μM Get4/5. The nucleotides used in the insertion reactions are as follows: 2 mM ATP in A and B, 2 mM ADP in C and D, and no nucleotides in E and F. All experiments were repeated on different days ($n \geq 2$) and are plotted as mean ± SD. yRM, yeast rough microsome.

The following data indicate that the effects of these Get3 mutants did not arise solely from the failure to hydrolyze ATP, but rather from defects in undergoing TA-induced conformational changes. Even with AMPPNP bound, targeting and insertion

from wild-type Get3•TA was efficient (compare black lines in Figure 2.19 vs. Figure 2.18A); thus, ATP hydrolysis per se is not required for membrane targeting (Bozkurt et al. 2009). Wild-type ^{AMPPNP}•Get3•TA also tolerated the presence of Get4/5 and allowed TA insertion (Figure 2.19, purple), albeit three- to five-fold more slowly than the reaction of ^{ATP}•Get3•TA with Get4/5 present (Figure 2.18B, black). Thus, ATP hydrolysis contributes three- to five-fold, but is not obligatory for the exchange of Get4/5 with Get1/2 on the Get3•TA complex. Further, the ATP occupancy of Get3(D57N)•TA and Get3(E251A)•TA complexes was measured to be 39% and 5.8%, respectively (Table 2.1); even if only the ADP- or nucleotide-free targeting complexes were active, these ATP occupancies predict that the two mutants would retain 61% and 94%, respectively, of the targeting activity of wild-type Get3, which were insufficient to explain their targeting defects. Finally, the Get4/5-specific targeting defect of both Get3 mutants was observed regardless of the added nucleotide (Figure 2.18 A–F). Assuming the simplest model in which the observed insertion occurs from the fraction of Get3•TA complexes that acquired a targeting-competent conformation, the biochemical data suggested that the defect of mutant Get3(E251A)•TA in attaining the active conformation was ~70-fold after ATP hydrolysis [Figure 2.18D, comparing the time required for 11% insertion with ^{ADP}•Get3•TA vs. ^{ADP}•Get3(E251A)•TA]. These results underscore the essential role of TA-induced Get3 conformational change in driving membrane targeting.

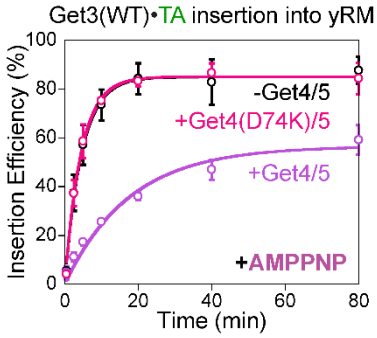

Figure 2.19: Get3•TA targeting and insertion in the presence of AMPPNP. Time courses for targeting and insertion of wild-type ^{AMPPNP}•Get3•TA with and without Get4/5 or mutant Get4(D74K)/5 (see Figure 2.21) present. All experiments were

repeated on different days ($n \geq 2$) and are plotted as mean ± SD. yRM, yeast rough microsome.

Get3 complex (1 μM)	[ATP] (nM)
Get3(WT)	0.53 ± 0.2
Get3(D57N)	8.7 ± 3
Get3(E251A)	0.86 ± 0.5
Get3(WT)•TA	6.8 ± 4
Get3(D57N)•TA	390 ± 40
Get3(E251A)•TA	58 ± 10

Table 2.1: Determination of ATP content in Get3 and Get3•TA. A luminescence-based ATP detection kit was used to determine the ATP concentrations for different Get3 and Get3•TA samples at 1 μM. Get3(D57N) shows higher nucleotide retention compared with Get3(E251A) and Get3(WT). All values are reported as mean ± SD, with $n = 3$.

The Get3 active site couples the TA-binding site to the Get3-effector interaction surface

The Get4/5-specific targeting defects of Get3(D57N) and Get3(E251A) suggest that these mutants fail to dissociate from Get4/5 after TA loading, and thus block the subsequent interaction of Get3 with the Get1/2 receptor complex at the ER membrane. To test this hypothesis, we measured the Get3–Get4/5 interaction using an established assay based on the fluorescence enhancement of acrylodan labeled at Get4(S48C/C177T) upon Get3 binding (Rome et al. 2014). Equilibrium titrations showed that while wild-type Get3•TA bound Get4/5 much more weakly than ^{ATP}•Get3, as observed previously (Rome et al. 2014), mutant Get3(D57N)•TA and Get3(E251A)•TA retained high-affinity binding to Get4/5 (Figure 2.20 and Table 2.2). Thus, small defects in Get3 *opening* (Figure 2.16 E, F, K, and L) could severely block the TA-induced disassembly of the Get3•Get4/5 complex.

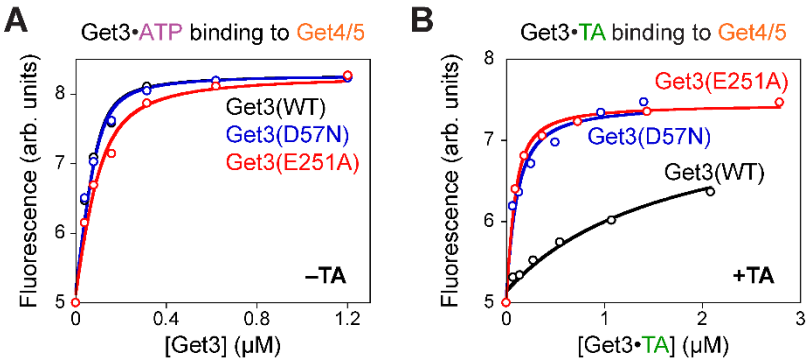

Figure 2.20: The TA substrate regulates the Get3–Get4 interaction. (A and B) Representative equilibrium titrations to measure the binding of Get4/5 to wild-type and mutant Get3 in the ATP-bound (A) and TA-bound (B) states. arb., arbitrary.

How do TAs induce the dissociation of Get3 from Get4/5? Structural work showed that Get4 contacts ATP-bound Get3 at two interfaces: an anchoring interface, which enables stable binding, and a regulatory interface, which regulates Get3's ATPase activity (Gristick et al. 2014) (Figure 2.21A). We introduced the Get4(D74K) mutation that disrupts the salt bridge between Get4-D74 and Get3-K69 at the regulatory interface (Gristick et al. 2014) (Figure 2.21B). The affinity of Get3 for wild-type Get4/5 relative to mutant Get4(D74K)/5 provides a measure for the energetic contribution of this salt bridge to Get3-Get4/5 binding. While the Get4(D74K) mutation weakened the binding to ^{ATP}•Get3 fivefold (Gristick et al. 2014), the mutational effect was >20-fold with ^{AMPPNP}•Get3•TA and then became negligible with Get3•TA (Figure 2.21C, black bars and Table 2.2). These results illustrate sequential changes at the Get3–Get4 regulatory interface, where the Get3(K69)-Get4(D74) salt bridge is ancillary before TA binding, becomes stronger upon TA loading, and then dissolves after nucleotide hydrolysis and release from Get3•TA.

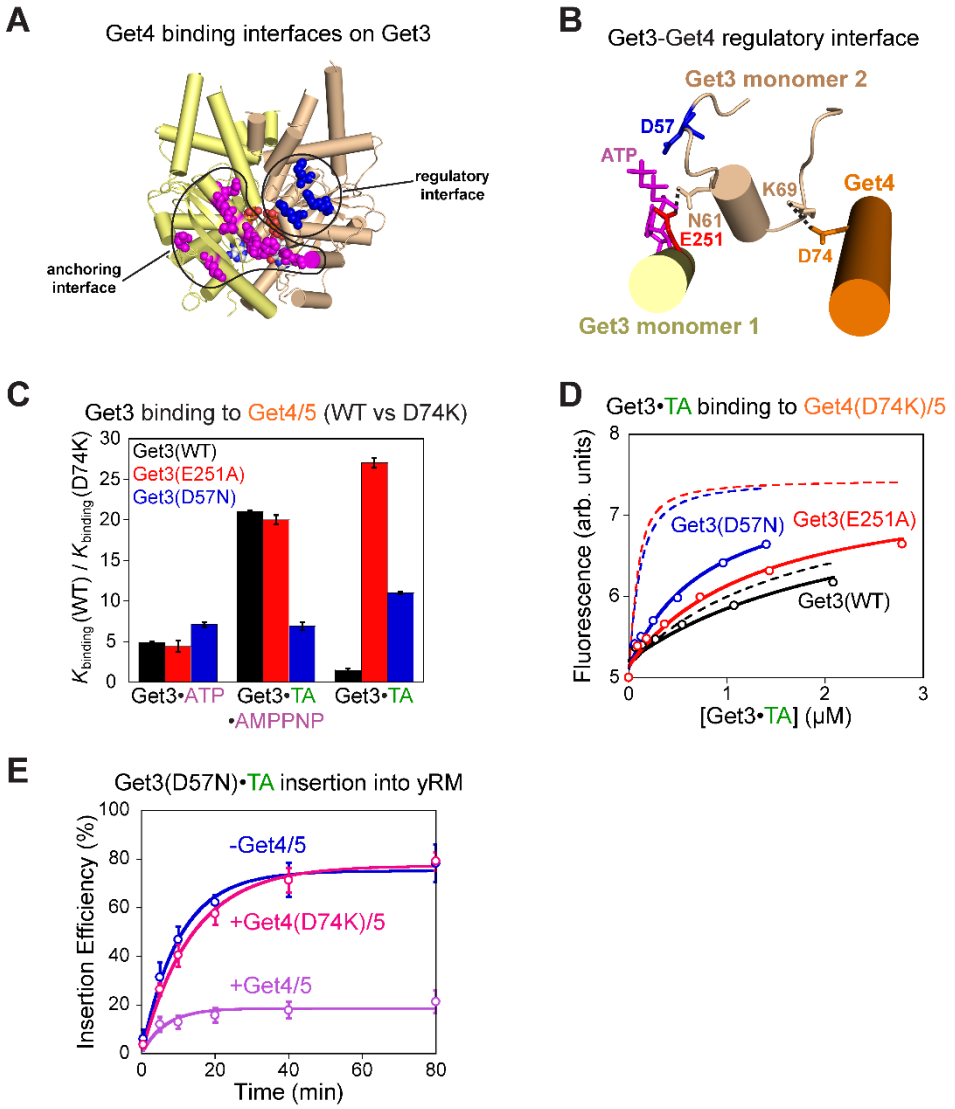

Figure 2.21: The TA substrate induces a rearrangement of the Get3–Get4 interaction interface. (A) Get3 interacts with Get4 via two interfaces: an anchoring interface (magenta spheres, which highlight residues whose mutations reduce the affinity between ATP-bound Get3 and Get4/5) and a regulatory interface (blue spheres, which highlight conserved residues that may contact Get4/5) (Gristick et al. 2014). (B) Get3-K69 forms a putative salt bridge (dotted line) with Get4-D74 at the regulatory interface (PDB 4PWX). Mutation of Get3-K69 or Get4-D74 did not substantially reduce Get3-Get4/5 binding but disrupted the ability of Get4/5 to regulate ATP hydrolysis by Get3 (Gristick et al. 2014). (C) Summary of the effects

of the Get4(D74K) mutation on the binding affinity of Get4/5 for wild-type and mutant Get3 ($K_{binding} = 1/K_d$) in the indicated complexes. Data are from Table 2.2 are reported as mean ± propagated error, with $n \geq 2$. (D) Representative equilibrium titrations to measure the binding of Get4(D74K)/5 to wild-type and mutant Get3•TA complexes. Dashed lines are the binding curves of wild-type Get4/5 to the corresponding Get3 variant (from Figure 2.20B) and are shown for comparison. (E) Time courses for targeting and insertion of Get3(D57N)•TA in the presence of ATP and indicated Get4/5 variants ($n = 2$).

Get4/5 construct	Get3 complex	Nucleotide	K_d (μM)
wild-type	wild-type	ATP	0.016 ± 0.002
	D57N	ATP	0.017 ± 0.003
	E251A	ATP	0.032 ± 0.008
	wild-type•Sbh1	none added	1.5 ± 0.2
	D57N•Sbh1	none added	0.072 ± 0.006
	E251A•Sbh1	none added	0.062 ± 0.03
	wild-type•Sbh1	AMPPNP	0.017 ± 0.004
	D57N•Sbh1	AMPPNP	0.060 ± 0.001
	E251A•Sbh1	AMPPNP	0.035 ± 0.007
D74K	wild-type	ATP	0.075 ± 0.002
	D57N	ATP	0.12 ± 0.04
	E251A	ATP	0.14 ± 0.09
	wild-type•Sbh1	none added	2.2 ± 0.3
	D57N•Sbh1	none added	0.78 ± 0.08
	E251A•Sbh1	none added	1.8 ± 0.8
	wild-type•Sbh1	AMPPNP	0.35 ± 0.01
	D57N•Sbh1	AMPPNP	0.42 ± 0.2
	E251A•Sbh1	AMPPNP	0.70 ± 0.4

Table 2.2: Summary of equilibrium binding affinities between Get4/5 and Get3 variants in different substrate and nucleotide states. All values are reported as mean ± SD ($n \geq 2$).

Importantly, while the TA substrate failed to weaken the binding of Get3(D57N) and Get3(E251A) with wild-type Get4/5 (Figure 2.20B), it did with mutant Get4(D74K)/5 (Figure 2.21D), suggesting that the Get3 active site mutants exert their effects by blocking changes at the Get3–Get4 regulatory interface. Analysis of the mutational effects of Get4(D74K) on the Get3 active site mutants further showed that Get3(E251A) is primarily defective in removing the Get3-Get4 contact at the regulatory interface after nucleotide hydrolysis and release, while Get3(D57N) is defective in rearranging this interface both before and after ATP hydrolysis (Figure 2.21C, red and blue bars and Table 2.2). These data agreed well with the different effects of these mutations on the FRET distributions of Get3•TA and ^{ATP}•Get3•TA (Figure 2.16 E and F vs. K and L), and together they showed that the catalytic residues at the Get3 active site provide key functional links between the TA-binding site and the Get4/5 interaction surface of Get3. Finally, the Get4(D74K) mutation abolished the inhibitory effect of Get4/5 on the targeting of Get3(D57N)•TA (Figure 2.21E) and wild-type ^{AMPPNP}•Get3•TA (Figure 2.19), indicating that the TA-induced rearrangements at the Get3–Get4 regulatory interface directly impact targeting efficiency.

2.3 DISCUSSION

Across all organisms, targeting complexes guide nascent proteins to diverse cellular destinations. These complexes must bind substrate proteins with high overall stability, while also readily switching structure and function to drive these vectorial processes. In this work, single-molecule fluorescence spectroscopy coupled with biochemical analyses provides a unifying model to explain how these complex demands are met during TA targeting by the Get3 ATPase. In contrast to previous models, TA loading destablizes a static, *closed* Get3•TA complex and induces Get3 to rapidly sample *open* conformations, and TA substrates are stably trapped in the rapidly fluctuating Get3. Point mutations at the ATPase active site bias Get3 toward *closed* conformations, uncouple TA binding from substrate-induced Get3•Get4/5

disassembly, and inhibit the targeting of the Get3•TA complex to the ER membrane. These data demonstrate how the substrate-induced dynamic *opening* of Get3 provides a dual mechanism that allows the targeting complex to both retain substrates with high affinity and drive the exchange of Get3's interaction partners required for the ER targeting of TAs.

The substrate-induced *opening* of Get3 is unexpected, given the large and contiguous hydrophobic groove in *closed* Get3 that appears highly conducive to TA binding (Bozkurt et al. 2009, Mateja et al. 2009, 2015) as well as the high kinetic stability of Get3•TA complexes (Rao et al. 2016) (Figure 2.11). The TA-induced *opening* of Get3 further suggests that the TA substrate explores alternative sites and conformations for interacting with Get3 besides the previously observed docking of the TA-TMD at the well-defined hydrophobic groove in *closed* Get3, and that, collectively, these alternative Get3–TA interaction modes are energetically more favorable than the established mode. In analogy to membrane protein substrates bound to the Skp and SurA chaperones (Burmann et al. 2013, Thoma et al. 2015), it is plausible that TA substrates sample multiple transient interaction sites during Get3 *opening*, and TAs could be retained because interaction with alternative sites in Get3 is more favorable than with solvent. This model would explain, in part, the weak electron density for TA-TMDs in previous Get3•TA structures (Mateja et al. 2015). Alternatively, or in addition, the rapid conformational fluctuations of Get3 could enable its *reclosing* to kinetically outcompete potential TA dissociation from the targeting complex during Get3 *opening*. Potential tetramerization of Get3 upon TA binding (Bozkurt et al. 2009, Rome et al. 2013) could provide another mechanism to retain substrate in a more *open* Get3; as a recent study did not detect stable tetrameric Get3•TA complexes and showed that dimeric Get3•TA is active in mediating TA insertion (Mateja et al. 2015), the precise roles of Get3 tetramerization remain to be determined. Finally, increased conformational entropy in these more dynamic models could contribute to the overall stability of the targeting complex. Regardless of the specific mechanism of substrate retention, our results collectively show that

substrate proteins can be stably bound to a targeting factor/chaperone while the latter undergoes large-scale fluctuations between *open* and *closed* states.

The targeting pathway demands extensive changes in the activities of Get3 before and after substrate loading. Before TA binding, Get3 must be ATP-bound and tightly bound to Get4/5, whereas after TA loading, Get3 must hydrolyze ATP and detach from Get4/5 so that it can instead interact with the Get1/2 receptors at the ER membrane. The results from this and previous work (Gristick et al. 2014, Rome et al. 2013, 2014) demonstrate that nucleotide, together with the Get4/5 complex, is responsible for inducing a highly *closed* conformation of Get3. Although these results provide an attractive mechanism to explain how Get3 efficiently captures TA substrates at early stages of the pathway, they fail to explain the functional switches of Get3 required for the targeting phase of the pathway. The substrate-induced *opening* of Get3 provides an attractive mechanism to drive this functional switch, and thus resolves this dilemma.

Experimentally, the important role of substrate-induced Get3 *opening* is demonstrated by the D57N and E251A mutations at the Get3 ATPase site, both of which bias Get3 toward *closed* conformations. These mutants uncouple TA binding from TA-induced changes in Get3's biochemical activities, including dissociation from Get4/5 and efficient targeting of TA substrates to the ER membrane. Although the targeting defect of Get3(D57N) was previously attributed to failed ATP hydrolysis (Mariappan et al. 2011, Mateja et al. 2009, Wang et al. 2011), complete analysis of the targeting reaction in all nucleotide states, including the non-hydrolyzable ATP analog AMPPNP, showed that the targeting defects of Get3 active site mutants are largely conformational in origin (Figure 2.22, step 5). The majority of the defects of Get3(D57N) and Get3(E251A) can be attributed to their failures to undergo TA-induced dissociation from Get4/5, which competes with the Get1/2 receptors for binding Get3. In addition, the three- to six-fold defects of these mutants in ER targeting in the absence of Get4/5 suggest that TA-induced Get3 *opening* facilitates the binding and remodeling of the targeting complex by Get1/2. By

combining these mutants with disruptions at the Get3–Get4 regulatory interface, we further demonstrate sequential TA-induced adjustments at the Get3–Get4 interaction surface that drive their disassembly, and how Get3 active site mutations disrupt this relay of signal. Together, these data reveal a tightly coupled channel of communication between the TA-binding site, ATPase catalytic site, and effector interaction surfaces on Get3.

Collectively, our results illustrate how substrate-induced dynamic *opening* switches Get3 from a TA-loading mode to a targeting mode, thus initiating downstream steps in the GET pathway (Figure 2.22). At early stages, ATP and Get4/5 lock Get3 into an *occluded* conformation, in which Get3 is *closed* and ATPase-inhibited (Gristick et al. 2014, Rome et al. 2013), and thus primed for TA capture (step 1). The *closed* Get3•TA-TMD structure, obtained with mutant Get3(D57N) and a sAB mimicking the interaction sites and biochemical activities of Get4/5 (Mateja et al. 2015), likely represents the initial ^{ATP}•Get3•TA•Get4/5 complex. TA loading destabilizes this static structure and induces Get3 to undergo rapid conformational fluctuations to explore the more *open* state (step 2). These changes in the TA-binding domain are transmitted via the Get3 catalytic site to induce rearrangements at the Get3–Get4 interface, shifting stabilizing interactions from the anchoring interface to the regulatory interface (step 2). At this stage, spontaneous Get4/5 dissociation from Get3 (step 3), which is rapid despite the high stability of the complex (Rome et al. 2014), allows Get3•TA to further *open* and enables TA-induced ATPase activation (step 4). *Opening* of Get3 becomes more extensive after ATP hydrolysis (step 5), rendering the dissociation of Get4/5 irreversible and priming Get3 for interaction with the Get1/2 receptors instead (step 6). In addition, dynamic *opening* of the Get3•TA complex could provide a facile pathway for its remodeling by the Get1/2 receptor complex, facilitating TA release and insertion into the ER membrane (step 6); this may explain the modest but still significant defects of the Get3 active site mutants in TA insertion in the absence of Get4/5. Importantly, while Get1 was primarily responsible for *opening* Get3 in most

previous models (Kubota et al. 2012, Mariappan et al. 2011, Stefer et al. 2011, Wang et al. 2011), our findings show that the TA substrate itself initiates this *opening* to vectorially drive late stages of the targeting cycle.

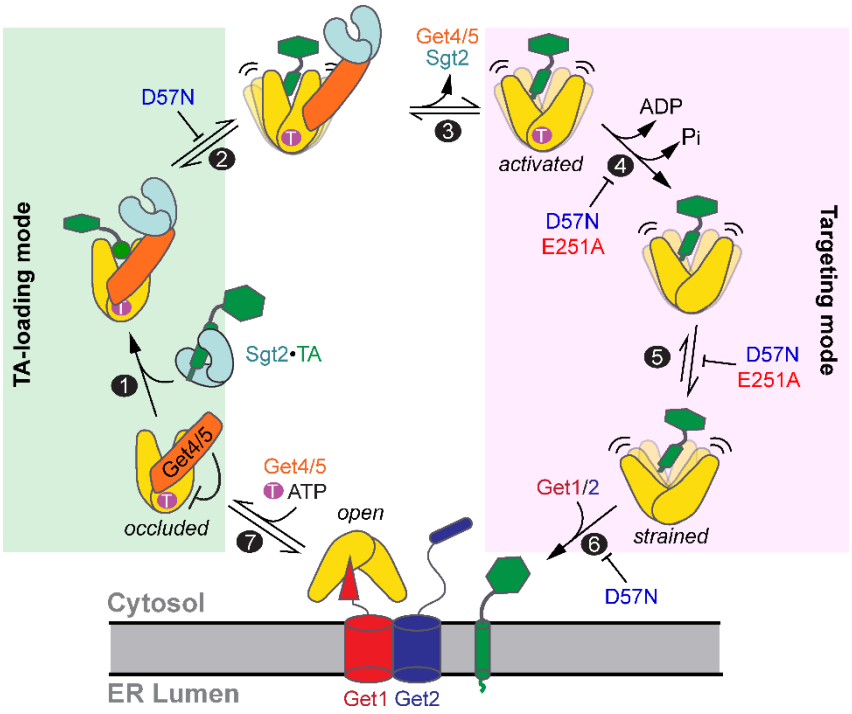

Figure 2.22: Model for how TA-induced Get3 *opening* drives the membrane targeting of the Get3•TA complex. Step 1: ^{ATP}•Get3 is bound to Get4/5, which induces Get3 to a *closed, occluded* conformation that inhibits ATP hydrolysis. TA is transferred from Sgt2 to Get3 in the Sgt2•Get4/5•Get3•TA complex, in which Get4/5 bridges Sgt2 and Get3. Step 2: TA loading induces Get3 to sample more *open* conformations, with concomitant adjustment at the Get3•Get4/5 interface that causes the regulatory interface to become the predominant stabilizing interaction. Step 3: Get4/5 spontaneously and reversibly dissociates from the conformationally adjusted Get3•TA complex. Step 4: TA induces Get3 to rapidly hydrolyze ATP after Get4/5 dissociation. Step 5: After ATP hydrolysis, Get3•TA becomes more *open*, attaining a *strained* conformation that prevents rebinding of Get4/5. Step 6: The *strained* Get3•TA complex is primed for targeting to and remodeling by the Get1/2 receptors at the ER membrane. Step 7: Get1/2 facilitates TA disassembly from Get3 and TA

insertion into the membrane. Binding of ATP and Get4/5 releases Get3 from the membrane receptors, recycling it for additional rounds of targeting. The inhibition marks denote steps inhibited by the E251A and D57N mutations, with inhibition of step 5 being responsible for the majority of defects of these mutants on the overall targeting reaction under physiological conditions.

Current models of substrate interactions with targeting factors and molecular chaperones often fall into the category of lock-and-key mechanisms, in which substrate proteins fit into pre-organized, well-structured grooves or pockets in the substrate-binding domain (Ferbitz et al. 2004, Janda et al. 2010, Keenan et al. 1998, Merz et al. 2008, Xu et al. 1997). Although these mechanisms provide excellent explanations for how substrate proteins are captured, they also generate thermodynamic sinks that inhibit subsequent steps in the pathway, analogous to the situation described for Get3 (Shan 2016). Our observations provide a precedent for a distinct class of models, in which rapid conformational fluctuations of a targeting factor/chaperone generate a "protean trap" that can retain substrates with high stability, and the dynamic nature of the complex enables functional switches to guide progression of the pathway. Analogous protean traps may provide an effective mechanism in other targeting factors, chaperones, and transporters that need to retain substrates with high affinity, while driving vectorial pathways that require distinct functions to be switched "on" and "off" in a sequential and coordinated manner.

2.4 MATERIALS AND METHODS

Plasmids

Plasmids for recombinant expression of Get3, Get4/5, Get1CD, and a superactive mutant of the cpSRP43 chaperone (intein-cpSRP43) and for *in vitro* translation of 3xStrep-SUMOnc-Bos1-opsin have been described (Liang et al. 2016, Rao et al. 2016, Rome et al. 2013, 2014). DNA encoding 2xStrep-Sbh1 was in the pACYCDuet-1 vector. Plasmids encoding mutant proteins were generated using

QuikChange site-directed mutagenesis (Stratagene) or FastCloning (Li et al. 2011), and were confirmed with DNA sequencing (Laragen).

Biochemical reagents

Get3, Get4/5, Get1CD, and intein-cpSRP43 were expressed and purified as described (Liang et al. 2016, Rao et al. 2016, Rome et al. 2013, 2014). *E. coli* S30 lysate and T7 RNA polymerase were prepared as described (Rao et al. 2016, Saraogi et al. 2011). Microsomes were prepared from Δget3 yeast cells as described (Rome et al. 2013, Rothblatt & Meyer 1986, Schuldiner et al. 2008).

Get3•TA complexes for μs-ALEX and insertion assays were generated as described (Rao et al. 2016) with modifications. For μs-ALEX, the model TA 3xStrep-Bos1-opsin (Rao et al. 2016) was *in vitro*-translated in *E. coli* S30 lysate for 2 hr at 30°C in the presence of 2 μM Get3 (1:100 double-labeled to unlabeled), with or without 2 μM Sgt2 and 2 μM Get4/5 present. Complexes containing 3xStrep-tagged TA were purified using Strep-Tactin Sepharose (IBA Life Sciences) as described (Rao et al. 2016). Omission of Sgt2 and Get4/5 in this procedure does not change the targeting and insertion activity of Get3•TA (Figure 2.10B). To characterize the effects of Get4/5 and ATP on Get3•TA conformation (Figures 2.12D and 2.16 F and L), 0.5 μM Get4/5 and 2 mM ATP were present throughout the purification, and excess Get4/5 and ATP were supplemented to the purified complex. $Get3^{BDP}$•TA^{CM} complexes used in Fig. S4B were generated as described (Rao et al. 2016).

Recombinant Get3•Sbh1 complexes were purified as described (Mateja et al. 2015) with modifications. Untagged Get3 and 2xStrep-Sbh1 were coexpressed in One Shot BL21 Star (DE3) (Invitrogen) for 6 hr at 26°C after induction with 0.1 mM isopropyl β-D-1-thiogalactopyranoside at OD_{600} ~ 0.8. Cells were disrupted by sonication in lysis buffer [50 mM Tris·HCl (pH 7.6), 300 mM NaCl, 5 mM β-mercaptoethanol, protease inhibitors]. Complexes containing 2xStrep-Sbh1 were purified using Strep-Tactin Sepharose followed by Superdex 200 10/300 GL (GE

Healthcare) in GET buffer [50 mM KHEPES (pH 7.4), 150 mM KOAc, 5 mM Mg(OAc)2, 1 mM DTT, 10% glycerol] (Figure 2.23).

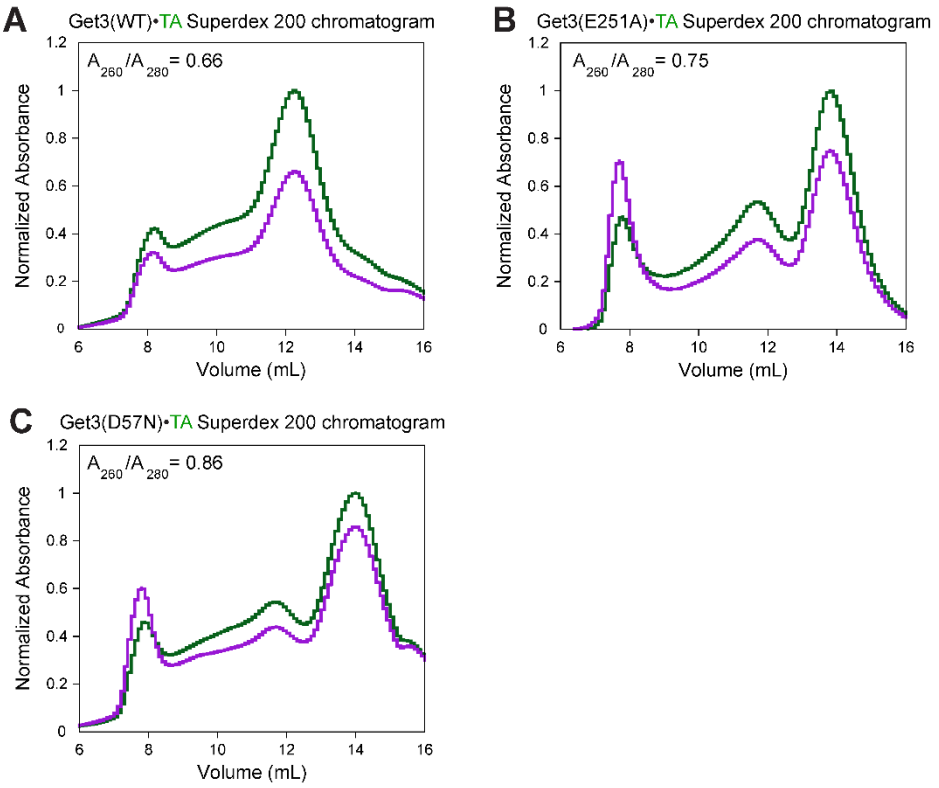

Figure 2.23: Purification of wild-type and mutant Get3•TA complexes. (A–C) Gel filtration chromatograms for recombinantly expressed and purified Get3•2xStrep-Sbh1 complexes made with Get3(WT), Get3(E251A), and Get3(D57N), respectively. Green and purple lines denote A_{280} and A_{260} readings, respectively, normalized to the peak A_{280} value. Fractions corresponding to the dominant peak were collected for each complex. The difference in elution volumes of recombinant wild-type and mutant Get3•TA has been noted previously (Mateja et al. 2015). Get3(D57N)•TA displays a higher ratio of A_{280} to A_{260} compared with Get3(WT)•TA and Get3(E251A)•TA, consistent with the higher ATP retention in this mutant complex determined in Table 2.1.

Fluorescence labeling

We have described a strategy to site-specifically label Get3 at a ybbR tag inserted between residues 110 and 111 via Sfp-catalyzed incorporation of dye-CoA conjugates; ybbR insertion and fluorescence labeling do not perturb Get3 function (Rao et al. 2016). Using this strategy, we stochastically double-labeled Get3 dimers with a 1:1 ratio of CoA-conjugated Cy3B-maleimide (GE Healthcare) or ATTO 550-maleimide (ATTO-TEC) and CoA-conjugated ATTO 647N-maleimide (ATTO-TEC) at the α4-α5 loop. Donor- or acceptor-only Get3's were generated by labeling with one of the dyes. CoA-conjugated BODIPY FL-maleimide (Thermo Fisher Scientific) was used to generate the $Get3^{BDP}$ used in Figure 2.11. Get4(C177T/S48C)/5 and Get4(C177T/S48C/D74K)/5 were labeled with acrylodan as described (Rome et al. 2014).

Biochemical assays

50 µL TA targeting and insertion reactions were initiated by adding 10 µL of *Δget3* microsomes to purified Get3•TA complexes in which [^{35}S]-methionine–labeled TA was normalized to 40,000 dpm. 2 mM nucleotide and/or 0.5 µM Get4/5 was included where indicated. Reactions were incubated at 26°C; at indicated time points, 6 µL samples were removed and quenched by addition of 2×SDS buffer and flash-freezing in liquid nitrogen. Samples were analyzed by SDS-PAGE and autoradiography.

Equilibrium-binding measurements between Get3 and acrylodan-labeled Get4/5 were performed as described (Rome et al. 2014). $Get3^{BDP}$•TA^{CM} dissociation experiments were performed as described (Rao et al. 2016), except that indicated concentrations of intein-cpSRP43 were used as a chase instead of unlabeled Get3 (which we found to modestly accelerate TA dissociation). Multi-site, multi-turnover ATPase rate constants for Get3 were measured as described (Rome et al. 2013). The ATP concentrations in Get3 and Get3•TA samples were quantified using a

luminescent ATP detection assay kit (ab113849; Abcam) per the manufacturer's instructions.

µs-ALEX measurements

All proteins were ultracentrifuged in a TLA 100 rotor (Beckman Coulter) at 100,000 rpm for 1 hr at 4°C to remove aggregates before all measurements. Get3 samples were diluted to ~100 pM in GET buffer containing 0.3 mg/mL BSA and indicated interaction partners. Based on previously determined K_d values (Rome et al. 2013, 2014), saturating amounts of each interaction partner (2 mM AMPPNP, 4 mM ADP, 10 µM Get1CD, 4 µM Get4/5) were used to ensure that all observed Get3 molecules were ligand-bound. Samples were placed in a closed chamber made by sandwiching a perforated silicone sheet (Grace Bio-Labs) with two coverslips to prevent evaporation. Data were collected over 30–60 min using an ALEX–fluorescence-aided molecule sorting setup (Kapanidis et al. 2004) with two single-photon Avalanche photodiodes (PerkinElmer) and 532-nm and 638-nm continuous wave lasers (Coherent) operating at 135 µW and 80 µW, respectively.

µs-ALEX data analysis

All single molecule FRET (smFRET) data analyses, including burst search, burst selection, and BVA, were performed using FRETBursts, a Python-based open-source burst analysis toolkit for confocal smFRET (Ingargiola et al. 2016). A dual-channel burst search (Nir et al. 2006) was performed to isolate the photon streams from species containing FRET pairs versus background noise and species containing donor or acceptor only. Each burst was identified as a minimum of 10 consecutive detected photons with a photon count rate at least 15-fold higher than the background photon count rate during both donor and acceptor excitation periods. Since the background rate can fluctuate within a measurement, the background rate was computed for every 50 second interval according to maximum likelihood fitting of the interphoton delay distribution. The identified bursts were further selected

according to the following criteria: (i) $n_{DD} + n_{DA} \geq 25$ and (ii) $n_{AA} \geq 25$, where n_{DD} is the number of photons detected from donor during donor excitation, n_{DA} is the number of photons detected from acceptor during donor excitation, and n_{AA} is the number of photons detected from acceptor during acceptor excitation.

The relative *E** and stoichiometry (*S*) for each burst were calculated using the following equations:

$$E^* = \frac{n_{DA}}{n_{DD} + n_{DA}}, \qquad [2.1]$$

$$S = \frac{n_{DD} + n_{DA}}{n_{DD} + n_{DA} + n_{AA}}, \qquad [2.2]$$

*E** corresponds to actual FRET efficiency if three conditions are met: (*i*) no donor fluorescence leaks into the acceptor detection channel (*lk* = 0), (*ii*) no acceptor is directly excited by the donor excitation laser (*dir* = 0), and (*iii*) the quantum yields and detection efficiencies for donor and acceptor are the same (γ = 1) (Lee et al. 2005). Although these conditions are not met in most cases, the contributions of *lk*, *dir*, and γ to the actual FRET efficiency are constant as long as the same optical setup and FRET pair are used throughout all measurements. Importantly, we did not observe significant changes in the quantum yields of donor and acceptor dyes depending on local environments (Figure 2.7). Therefore, conformational changes in Get3 that change the actual FRET efficiency will also change the *E** value, and the trend of the changes with different binding partners will be the same. FRET histograms were obtained by 1D projection of 2D *E**-*S* plots onto the *E** axis after dual-channel burst search.

To determine the statistical significance of the differences between FRET histograms, we adapted the nonparametric two-sample Kolmogorov–Smirnov (K-S) test (Feller 1948, Young 1977). As noted earlier, the K-S test tends to be overly sensitive to data with a large sample size, and we found the same to be true if this test was applied without modification to single-molecule data; moreover, it is important

to distinguish between statistical versus biological significance of the difference between histograms for different sets of data, which contain intrinsic variability from instrument, sample preparation, and other factors (Cox et al. 1988, Lampariello 2000). To obtain more reliable comparisons, we regenerated FRET histograms from randomly selected subsets (with sample size *m*) of the complete data for each experimental condition and performed the K-S test. Ten repetitions of this process generated a statistical significance score, defined as the fraction of comparisons that gave $p < 0.05$, for each value of *m*. This process was repeated five more times for each value of m and for data subsets with different *m* values, and the dependence of the statistical significance on sample size was plotted. Molecules with $E^* < 0.3$ were excluded from the histograms in this analysis, as the low FRET bursts could arise from photophysical artifacts and were not interpreted in this study. As shown in Figures 2.13 and 2.17G, the statistical significance of the difference remains low even at high *m* (> 4,000) for histograms that are the same or similar, whereas the statistical significance of the difference increases rapidly with increasing *m* for histograms that are different.

BVA was performed to investigate sub-millisecond dynamics of Get3 as described (Torella et al. 2011). Equation 2.3 was used to compute the static limit, defined as the expected SD of a FRET distribution due to photon statistics (shot noise) for a given *E**:

$$\sigma_{E^*} = \sqrt{\frac{E^*(1-E^*)}{n}}, \qquad [2.3]$$

where $n = n_{DD} + n_{DA}$. The observed mean FRET SD (SD of *E**) for each molecule was computed using Equation 2.4:

$$SD\ of\ E^* = \sqrt{\frac{1}{M}\sum_{i=1}^{M}(e_i^* - E^*)^2}, \qquad [2.4]$$

in which e^* and E^* are relative FRET efficiencies (calculated from Equation 2.1) of a subburst (a subset of each burst that contains a constant number of consecutive photons) and a burst, respectively, and M is the number of subbursts in the burst. A subburst size ($n_{sub} = n_{sub,DD} + n_{sub,DA}$) of five was used in this study.

To quantitatively represent the dynamics of molecules from the BVA, we calculated a dynamic score (*DS*) for each sample as follows. To reduce error that could arise from individual bursts, which contain a small number of subbursts, we first binned bursts along the E^* axis into 20 bins with a bin width of 0.05. All of the subbursts within bursts in each bin were then used to calculate the mean FRET SD for each bin (SD_{E^*}) using Equation 2.5 (Torella et al. 2011):

$$SD_{E^*} = \sqrt{\sum_{\substack{i\ where \\ L \le E_i^* < U}} \sum_{j=1}^{M_i} \left[\frac{e_{ij}^* - \mu}{\sum M_i}\right]}, \qquad [2.5]$$

where $\mu = \sum_{\substack{i\ where \\ L \le E_i^* < U}} \sum_{j=1}^{M_i} \left[\frac{e_{ij}^*}{\sum M_i}\right]$, L is the lower bound ($E^* - 0.025$) of the bin, U is the upper bound ($E^* + 0.025$) of the bin, M_i is the number of subbursts in the ith burst, and e_{ij}^* is the relative FRET efficiency of the jth subburst in the ith burst. The *DS* was calculated using Equation 2.6 (Torella et al. 2011):

$$DS = \sqrt{\sum_{SD_{E^*} - SD_{E^*,static} > 0} \left(SD_{E^*} - SD_{E^*,static}\right)^2}, \qquad [2.6]$$

where $SD_{E^*,static}$ is the SD_{E^*} of simulated static molecules using the Monte Carlo method. To ensure that the score reports on the dynamics of the majority of the molecules in a given sample, only bins with ≥ 8% of the total number of bursts in the entire FRET histogram were used to calculate *DS*, and the SD_{E^*} values for each of these bins are denoted with triangles in BVA plots. To take into account the different

numbers of bursts in each bin, we also computed a weighted dynamic score (*WDS*) to weight bins according to their size using Equation 2.7:

$$WDS = \sqrt{\sum_{SD_{E^*} - SD_{E^*,static} > 0} \left(\frac{N_{E^*}}{\sum N_{E^*}}\right) \times \left(SD_{E^*} - SD_{E^*,static}\right)^2}, \qquad [2.7]$$

where N_{E^*} is the number of bursts in each bin.

Chapter 3

A CHAPERONE LID ENSURES EFFICIENT AND PRIVILEGED CLIENT TRANSFER DURING TAIL-ANCHORED PROTEIN TARGETING

Adapted from:

Chio, U.S., Chung, S., Weiss, S., and Shan, S.-O. 2019. A Chaperone Lid Ensures Efficient and Privileged Client Transfer during Tail-Anchored Protein Targeting. *Cell Reports* 26(1): 37-44.e7. doi: 10.1016/j.celrep.2018.12.035.

Molecular chaperones play key roles in maintaining cellular proteostasis. In addition to preventing client aggregation, chaperones often relay substrates within a network while preventing off-pathway chaperones from accessing the substrate. Here we show that a conserved lid motif lining the substrate-binding groove of the Get3 ATPase enables these important functions during the targeted delivery of tail-anchored membrane proteins (TAs) to the endoplasmic reticulum. The lid prevents promiscuous TA handoff to off-pathway chaperones, and more importantly, it cooperates with the Get4/5 scaffolding complex to enable rapid and privileged TA transfer from the upstream co-chaperone Sgt2 to Get3. These findings provide a molecular mechanism by which chaperones maintain the pathway specificity of client proteins in the crowded cytosolic environment.

3.1 INTRODUCTION

Protein homeostasis requires the proper folding, assembly, and localization of proteins inside a cell. Molecular chaperones play key roles in maintaining protein homeostasis by protecting their client proteins from off-pathway interactions and guiding the folding or localization of client proteins (Kim et al. 2013). Newly synthesized membrane proteins, which comprise up to 30% of the proteins encoded in the genome, are particularly challenging clients for chaperones due to the high

aggregation propensity of hydrophobic transmembrane domains (TMDs) in the cytosol, where membrane proteins are initially synthesized. In addition, TMDs are often degenerate in sequence, amino acid composition, and secondary structure propensity, making them susceptible to promiscuous interactions with off-pathway chaperones. Therefore, chaperones that engage integral membrane proteins not only need to effectively capture and shield client proteins from solvent, but also ensure that substrates remain on-pathway en route to the target membrane. Although recent advances defined the substrate binding domains and client interactions for a variety of membrane protein chaperones (Burmann et al. 2013, Huang et al. 2016, Liang et al. 2016, Thoma et al., 2015), how these chaperones ensure the pathway specificity of substrates remains poorly understood.

Here we address this question in the conserved Guided Entry of Tail-anchored protein (GET) pathway, which mediates the targeted delivery of tail-anchored membrane proteins (TAs) to the endoplasmic reticulum (ER) in eukaryotic cells (Figure 3.1) (see Chapter 1). At the center of this pathway is the ATPase Get3 (or mammalian TRC40) (Stefanovic and Hegde, 2007), which captures TAs from the upstream co-chaperone Sgt2 (or mammalian SGTA) (Wang et al. 2010). The Sgt2-to-Get3 TA transfer is facilitated by ATP and the scaffolding complex Get4/5, which together pre-organize Get3 into a *closed* and ATPase-inhibited conformation optimal for TA capture (Gristick et al. 2014, 2015, Rome et al. 2013). TA loading induces rapid *opening* motions in Get3 and activates ATP hydrolysis (see Chapter 2; Rome et al. 2013), which drives Get3 to switch its interaction partner from Get4/5 to the Get1/2 receptors at the ER membrane (see Chapter 2; Schuldiner et al. 2005, 2008).

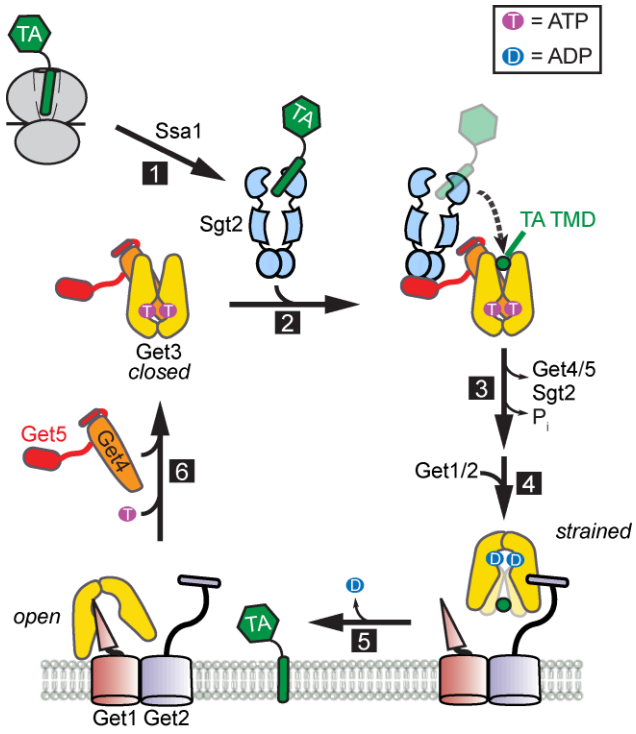

Figure 3.1: Current model of the GET pathway in yeast. Newly synthesized TAs from the ribosome are first captured and chaperoned by Ssa1 and then delivered to the co-chaperone Sgt2 (step 1). Sgt2 next delivers the TA to the ATPase Get3 (step 2), which in the cytosol is ATP-loaded and bound to a scaffolding complex Get4/5 that also interacts with Sgt2. ATP and Get4/5 pre-organize Get3 in a closed conformation, and Get4/5 further inhibits Get3's ATPase activity to prime Get3 for TA capture. TA loading onto Get3 induces Get3 to sample more open conformations that drives Get4/5 dissociation and activates Get3 to hydrolyze ATP (step 3). The resulting Get3•TA complex is in a strained conformation primed to interact with the Get1/2 membrane receptors (step 4). Get1/2 disassembles the Get3•TA complex and facilitates TA insertion into the ER (step 5), leaving Get3 bound to Get1 in an open conformation. ATP and Get4/5 help release Get3 from Get1 and recycle Get3 for further rounds of targeting (step 6).

The TA-TMD docks into a hydrophobic groove formed by ATP- and Get4/5-bound Get3 (Mateja et al. 2009, 2015). Moreover, the transfer of TA from SGTA to TRC40 was not perturbed by excess calmodulin (CaM), an external chaperone (Shao and Hegde, 2011) that also binds TAs, indicating that TAs are protected from off-pathway chaperones during their transfer (Shao et al. 2017). Nevertheless, as hydrophobic interactions are short-ranged, it is unclear how TAs are loaded into the deep TMD-binding groove of Get3, nor how they are shielded from solvent and external chaperones during and after loading. Intriguingly, a conserved helix 8 (α8; Figure 3.2) lines the substrate-binding groove of Get3 (Mateja et al. 2009, 2015). Although α8 is unresolved in most Get3 structures (Figure 3.2B) (Gristick et al. 2014, 2015, Hu et al. 2009, Mateja et al. 2009, 2015), it can be crosslinked to TAs (Mateja et al. 2015). Mutation of conserved α8 residues resulted in yeast growth defects under stress conditions (Mateja et al. 2009) and impaired Get3-dependent TA targeting in yeast lysate (Rome et al. 2013). It was hypothesized that α8 acts as a dynamic lid to enclose the TA binding groove and prevent TAs from aggregation (Mateja et al. 2015). In other chaperones or targeting factors, such as Hsp70 (Mayer and Bukau, 2005) and the signal recognition particle (Akopian et al. 2013), a lid motif lining the substrate binding groove could also stabilize substrate binding or mediate substrate-induced conformational changes.

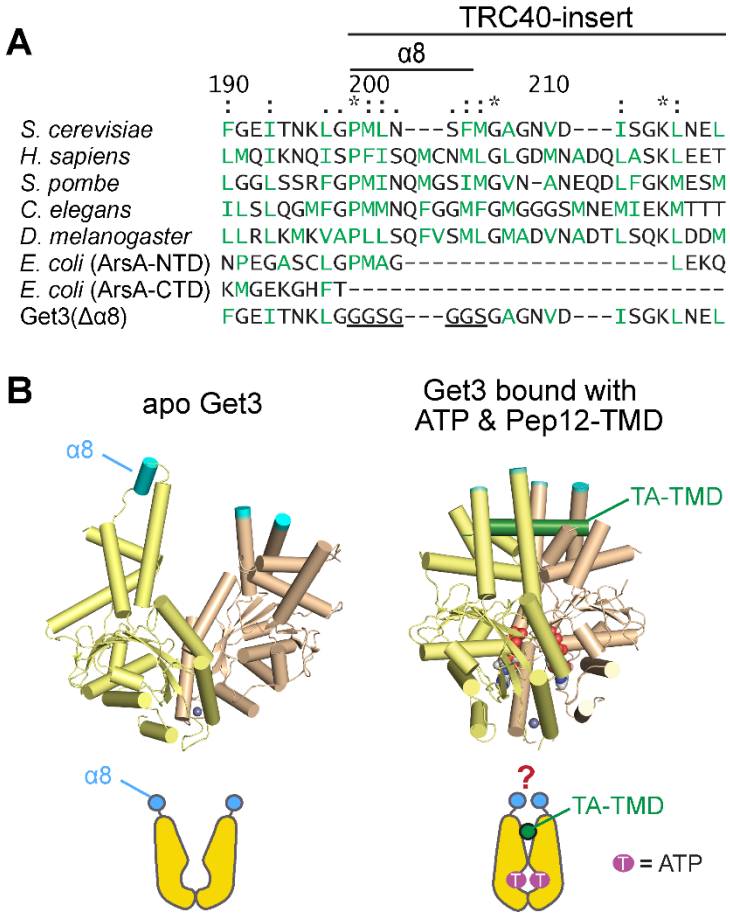

Figure 3.2: A conserved α8 motif lines the substrate binding groove of Get3. (A) Sequence alignment of α8 and its flanking sequences among Get3 homologues. The mutations introduced in Get3(Δα8) are also shown (underlined). Hydrophobic residues are highlighted in green. '.' and ':' denote residues that are modestly or highly conserved in amino acid characteristic, respectively, and '*' denotes residues that are highly conserved in identity. (B) The α8 motif and adjacent residues are highlighted (cyan) in the crystal structures of Get3 in the *open* (left; PDB 3H84) and *closed* (right; PDB 4XTR) conformations. Only one α8 motif is resolved in the *open* structure, while neither α8 motifs are not resolved in the *closed* structure. The question mark ("?") denotes the uncertainty of the positioning of the α8 motifs.

Here, quantitative biochemical and biophysical analyses revealed unexpected roles of α8 in Get3 function. We found that although α8 is not necessary for maintaining a stable Get3•TA complex, it nevertheless prevents TA loss from Get3 to off-pathway chaperones. Most importantly, α8 acts synergistically with Get4/5 to enable rapid TA transfer from Sgt2 to Get3 in a highly protected manner. We propose that α8 forms a molecular conduit for TA transfer to Get3, illustrating a mechanism that chaperones use to ensure client-pathway specificity in a crowded cytosolic environment.

3.2 RESULTS

α8 is necessary for efficient TA targeting

Previously, it was shown that mutation of conserved α8 residues (M200D and L201D) resulted in yeast growth defects under stress conditions, which is characteristic of defects in the GET pathway (Mateja et al. 2009). Different mutations of α8 also impaired Get3-dependent TA targeting to different extents in yeast lysate (Rome et al. 2013). To unambiguously assess the role of α8, we engineered a Get3 mutant in which the highly conserved hydrophobic residues in α8 were replaced by a glycine-serine linker (Figure 3.2A, Get3(Δα8)) (see Chapter 2, Figure 2.14). Four lines of evidence show that the Δα8 mutation did not cause nonspecific structural defects in Get3. First, purified Get3(Δα8) migrated as a well-defined, homogeneous peak on size-exclusion chromatography similarly to wild-type Get3 (Figures 3.3A and 3.3B). Second, Get3(Δα8) adopted the same global fold as wild-type Get3 as determined by circular dichroism (Figure 3.3C). Third, Get3(Δα8) hydrolyzed ATP at rates similar to those of wild-type Get3 (Figure 3.3D). Fourth, Get3(Δα8) displayed ATP-dependent high affinity binding to Get4/5 similar to wild-type Get3 (Figures 3.3E and 3.3F). Finally, Get3(Δα8) displayed a similar conformational distribution and underwent conformational regulations by nucleotides, Get1, and Get4/5 similarly to wild-type Get3 (Figure 3.4), as determined by a previously established single-molecule FRET assay for monitoring global Get3 conformations (see Chapter 2).

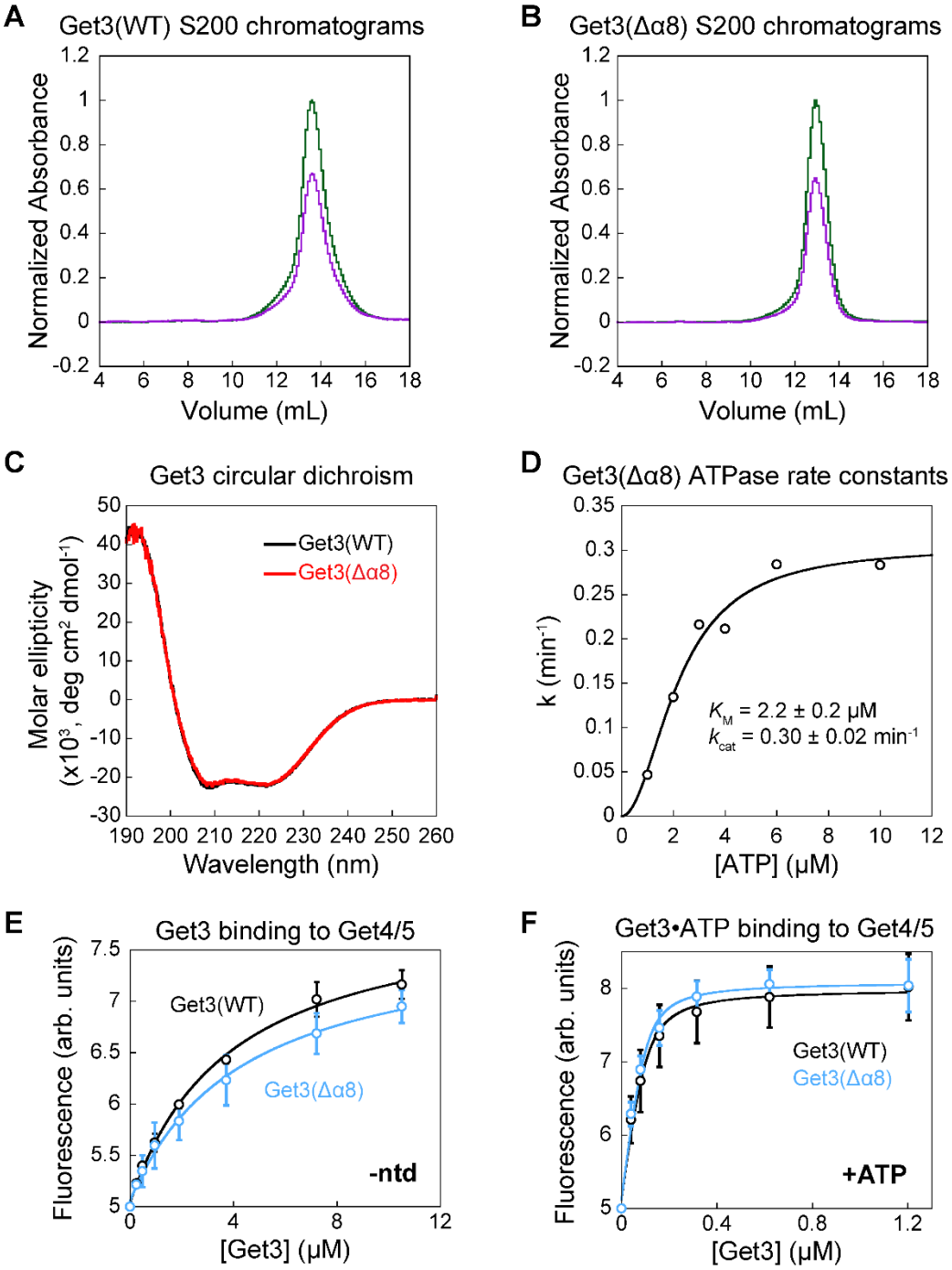
A
Get3(WT) S200 chromatograms
Normalized Absorbance
Volume (mL)
B
Get3(Δα8) S200 chromatograms
Normalized Absorbance
Volume (mL)
C
Get3 circular dichroism
Molar ellipticity (x10³, deg cm² dmol⁻¹)
Get3(WT)
Get3(Δα8)
Wavelength (nm)
D
Get3(Δα8) ATPase rate constants
k (min⁻¹)
K_M = 2.2 ± 0.2 μM
k_cat = 0.30 ± 0.02 min⁻¹
[ATP] (μM)
E
Get3 binding to Get4/5
Fluorescence (arb. units)
Get3(WT)
Get3(Δα8)
-ntd
[Get3] (μM)
F
Get3•ATP binding to Get4/5
Fluorescence (arb. units)
Get3(WT)
Get3(Δα8)
+ATP
[Get3] (μM)

Figure 3.3: Get3(Δα8) exhibits the same global structure, basal ATPase activity, and ATP-dependent binding to Get4/5 as wild-type Get3. (A and B) Size-exclusion chromatogram of purified wild-type Get3 (A) and mutant Get3(Δα8) (B). The green and purple lines denote A_{280} and A_{260}, respectively. (C) Circular dichroism spectra of 5 μM Get3(WT) (black) and 5 μM Get3(Δα8) (red). (D) Multi-turnover ATPase rate constants were determined with 0.5 μM mutant Get3(Δα8). The line was a fit of the data to Equation 3.9, which gave K_M and k_{cat} values of 2.2 ± 0.2 μM and 0.30 ± 0.02 min^{-1}, respectively. These values are within 2-fold to those previously reported for wild-type Get3 (K_M = 3.6 ± 1.0 μM and k_{cat} = 0.33 ± 0.03 min^{-1} at 0.5 μM Get3) (Rome et al. 2013). (E and F) Deletion of α8 does not affect the binding of Get4/5 to Get3, nor the allosteric regulation of Get3 by ATP for Get4/5 binding. Equilibrium titrations were carried out to measure the binding of Get4/5 to wild-type (black) and mutant Get3(Δα8) (blue) in the *apo* (E) and ATP-bound (F) states. 0.5 μM of acrylodan-labeled Get4/5 was used in all experiments, and 2 mM ATP was present in experiments in (F). The lines are fits of the data to Equation 3.10, and gave K_d values of 3.8 ± 0.2 μM and 4.8 ± 3 μM for *apo*-Get3(WT) and Get3(Δα8), respectively, and 0.020 ± 0.008 μM and 0.015 ± 0.0003 μM for ATP-loaded Get3(WT) and Get3(Δα8), respectively. Values are reported as mean ± SD, with n = 2.

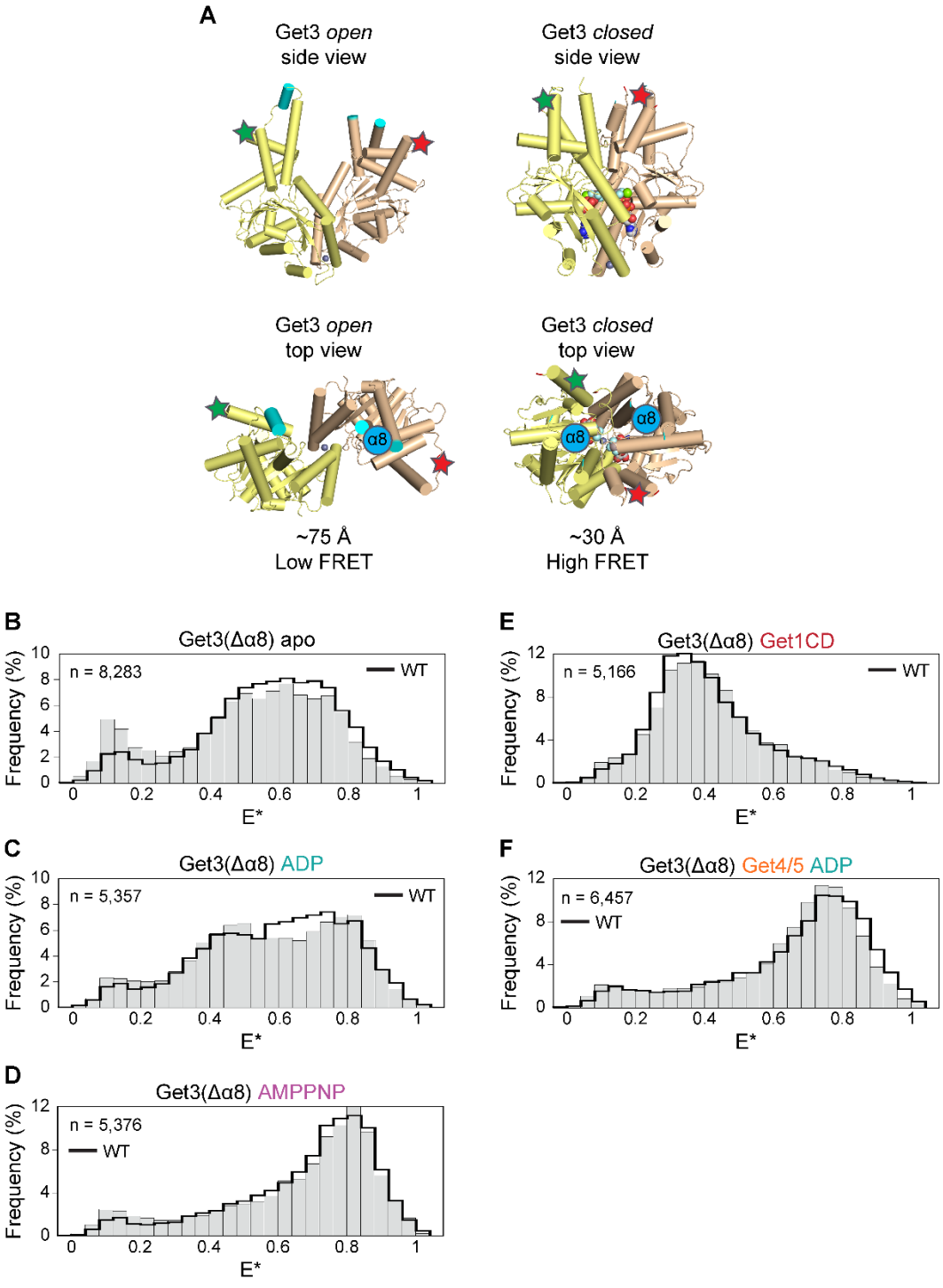
A
Get3 open
side view
Get3 closed
side view
Get3 open
top view
Get3 closed
top view
α8
α8
α8
~75 Å
Low FRET
~30 Å
High FRET
B
Get3(Δα8) apo
n = 8,283
WT
Frequency (%)
E*
C
Get3(Δα8) ADP
n = 5,357
WT
D
Get3(Δα8) AMPPNP
n = 5,376
WT
E
Get3(Δα8) Get1CD
n = 5,166
WT
F
Get3(Δα8) Get4/5 ADP
n = 6,457
WT

Figure 3.4: Get3(Δα8) displays a similar conformational distribution and undergoes conformational regulations by nucleotides, Get1, and Get4/5 similarly to wild-type Get3. (A) Approximate positions of donor and acceptor dyes (green and red stars, respectively) on Get3 in the *open* (left; PDB 3H84) and *closed* (right; PDB 2WOJ) conformations. The estimated distances between the dye pair are ~75 Å in the *open* conformation and ~30 Å in the *closed* conformation. The Förster radius of the Cy3B-ATTO 647N dye pair used in this work is ~55 Å. The approximate positions of α8 that were not resolved in the structures are highlighted as *cyan* circles in the bottom panels. (B–F) FRET histograms illustrating conformational distributions for Get3(Δα8) in the *apo* (A), ADP-bound (B), AMPPNP-bound (C), Get1CD-bound (D), and Get4/5 and ADP-bound (E) states. The FRET histogram of Get3(Δα8) under each condition (grey bars) was similar to those displayed by wild-type Get3 (black lines, see Chapter 2, Figures 2.4 and 2.12). Importantly, Get3(Δα8) was specifically *closed* upon binding of AMPPNP (C) or binding with Get4/5 in the presence of ADP (E), and was *opened* by binding of Get1CD (D).

We first measured the ability of purified Get3(Δα8) to target and translocate *in vitro* translated TAs into yeast rough microsomes (yRMs) in a *Δget3* yeast lysate (Rome et al. 2013, Wang et al. 2010), assessed by glycosylation of an engineered opsin tag on the model TA upon successful insertion into the ER. Get3(Δα8) exhibited a strong defect in this reconstituted targeting reaction (Figure 3.5A), indicating that α8 is necessary for Get3 function. To test if Get3(Δα8) compromised TA targeting *in vivo*, we replaced genomic *GET3* in *S. cerevisiae* with *GET3-FLAG* or *GET3(Δα8)-FLAG* and measured Get3 function *in vivo* using two independent assays. First, we measured the secretion of Kar2p, which is retained in the ER by retrograde trafficking in wild-type cells but is secreted into media from *Δget3* cells due to defective biogenesis of SNARE proteins (a large class of TAs) (Schuldiner et al. 2005, 2008). *GET3(Δα8)-FLAG* yeast displayed increased levels of Kar2p secretion compared to *Get3-FLAG* yeast, consistent with compromised GET

pathway function (Figure 3.5B). Second, pulse-chase experiments showed that the insertion of a newly-synthesized model TA, BirA-Bos1-opsin (Cho and Shan, 2018), into the ER was significantly impaired in *GET3(Δα8)-FLAG* compared to *GET3-FLAG* cells (Figure 3.5C). The defects of *GET3(Δα8)-FLAG* cells cannot be explained by a lower expression level of Get3(Δα8)-FLAG than Get3-FLAG (Figure 3.5D). These results indicate that the α8 element is also necessary for GET-dependent targeting *in vivo*.

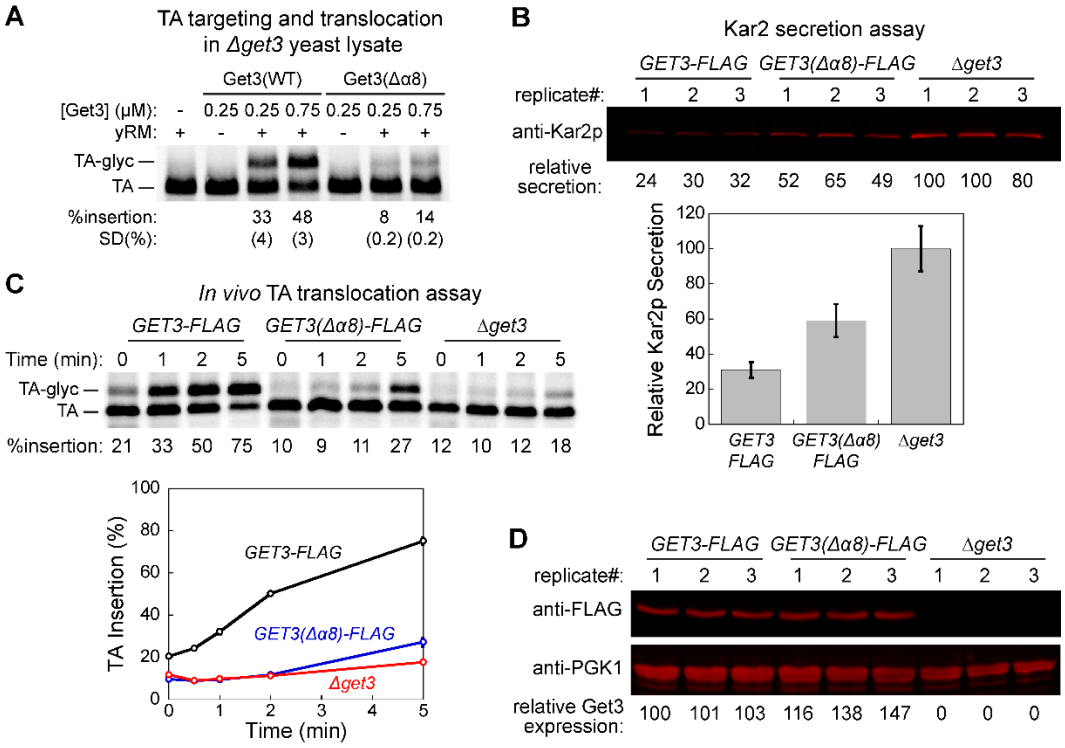

Figure 3.5: The α8 motif in Get3 is important for TA targeting to the ER. (A) TA targeting and translocation by wild-type Get3 or mutant Get3(Δα8) in the *Δget3* yeast lysate. 10 μL translation reactions for the model TA Bos1 were carried out in *Δget3* lysate in the presence of 10 μCi [^{35}S]-methionine and purified Get3 or Get3(Δα8) at indicated concentrations. After 30 min at 26°C, cyclohexamide was added to stop translation. *Δget3* microsomes were added where indicated, and the reactions were incubated for 40 min at 26°C and quenched by SDS sample buffer. Samples were analyzed by SDS-PAGE and autoradiography. Insertion efficiency

was calculated using Equation 3.2. (B) Kar2p secretion by *GET3-FLAG*, *GET3(Δα8)-FLAG*, and *Δget3* yeast cells, measured as described (Schuldiner et al. 2005). Yeast cultures were grown to saturation in YPD at 30°C overnight and diluted to an OD_{600} of 0.1 in fresh YPD. Cultures were grown at 30 °C to mid-log phase (OD_{600} ~ 1) and harvested. Cells were resuspended in fresh YPD to an OD_{600} of 0.5 and incubated at 30 °C for 2 hours. Cells were harvested, and proteins from 1.35 mL of the supernatant (media) was precipitated by 10% TCA, washed with acetone, resuspended in 35 µL of SDS sample buffer, and neutralized by titrating 1M Tris-HCl pH 9.5. Samples were analyzed by Western blot using an anti-Kar2p antibody (gift from P. Walter) at 1:3000 dilution. IRDye® 800CW Goat anti-Rabbit secondary antibody (LI-COR Biosciences) at 1:20,000 dilution was used for visualization using an Odyssey infrared imaging system. The top panel shows a representative western blot. The bottom panel shows quantification of the relative amount of secreted Kar2p from three biological replicates. Values are reported as mean ± SD. (C) Pulse-chase analysis to monitor the translocation of newly synthesized TA *in vivo*, carried out as described in Chapter 3.4 (Cho and Shan, 2018). Insertion into the ER results in glycosylation of the opsin tag on the TA, which allows untranslocated TA and glycosylated TA (TA-glyc) to be resolved on SDS-PAGE (top panel). The bottom panel shows the quantification of three independent experiments. The values represent mean ± SD (3 biological replicates). Error bars are shown but may be too small to be visible. (D) Clarified lysates of the cells from the same cultures in (B) were diluted with SDS sample buffer and immunoblotted against an anti-FLAG antibody (GenScript; top) to determine the steady-state Get3 levels in the different yeast strains. An anti-PGK1 (Abcam) blot served as a control for normalization (bottom). IRDye® 800CW Goat anti-Mouse secondary antibody (LI-COR Biosciences) was used for visualization using an Odyssey imaging system. Get3(Δα8)-FLAG is slightly overexpressed in *GET3(Δα8)-FLAG* cells compared to *GET3-FLAG* cells.

α8 shields TAs from off-pathway chaperones

To test whether α8 helps maintain a stable Get3•TA complex, we measured the kinetic stability of the Get3(Δα8)•TA complex using a FRET assay based on a donor dye incorporated near the TA-TMD and an acceptor dye labeled on Get3 near the substrate binding groove (Rao et al. 2016). We chased a preformed, purified Get3•TA complex with unrelated chaperones that can also effectively bind TAs and monitored TA release from Get3 as a loss of FRET (Figure 3.6A) (see Chapter 2, Figure 2.11). We used two independent chase molecules: a superactive variant of cpSRP43, a membrane protein chaperone in the chloroplast of green plants (Jaru-Ampornpan et al. 2010, Schuenemann et al. 1998) and was shown to bind TAs (Cho and Shan, 2018) (Figures 3.6B and 3.7); and CaM, another TA-binding protein unrelated to the GET pathway (Shao and Hegde, 2011, Shao et al. 2017) (Figure 3.6D). When the observed dissociation kinetics were extrapolated to zero chase concentrations to obtain the intrinsic Get3•TA dissociation rate constants ($k_{dissociation}$; Figures 3.6C and 3.6E), wild-type Get3•TA and mutant Get3(Δα8)•TA exhibited $k_{dissociation}$ values that are within 2-fold of one another (Figure 3.6F). Thus, α8 is not required to maintain a kinetically stable Get3•TA complex.

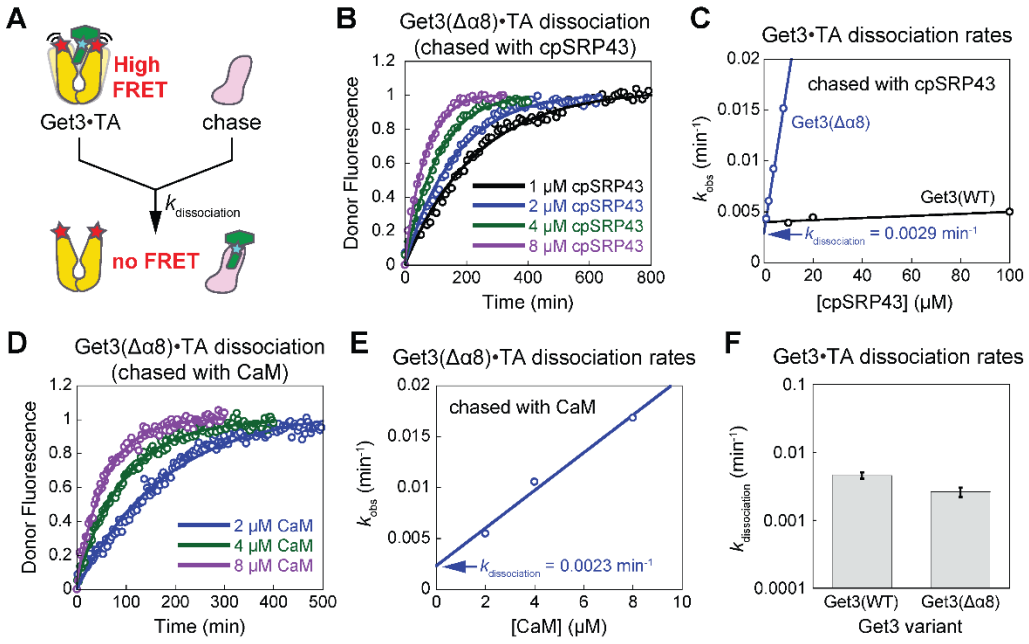

Figure 3.6: α8 prevents promiscuous TA handoff from Get3 to off-pathway chaperones. (A) Schematic for measurement of Get3•TA dissociation kinetics. TA was labeled with a donor dye (cyan star), and Get3 was labeled with acceptor dyes (red stars). Addition of a chase drives irreversible Get3•TA dissociation, which can be monitored as a loss of FRET over time. (B), (D) Time courses for change in the fluorescence of TA^{CM} to monitor TA loss from Get3(Δα8) (50 nM initial complex) using indicated concentrations of intein-cpSRP43 (B) or CaM (D) as chase. Fluorescence was normalized such that the fit of each trace starts at 0 and ends at 1. (C), (E) Increasing concentrations of intein-cpSRP43 (C) or CaM (E) accelerated the observed rate of TA loss from Get3(Δα8), but not from wild-type Get3. (F) Summary of the dissociation rate constants for Get3•TA and Get3(Δα8)•TA complexes (0.0044 ± 0.0006 and 0.0026 ± 0.0004 min^{-1}, respectively). Error bars denote SD, with n = 2-3.

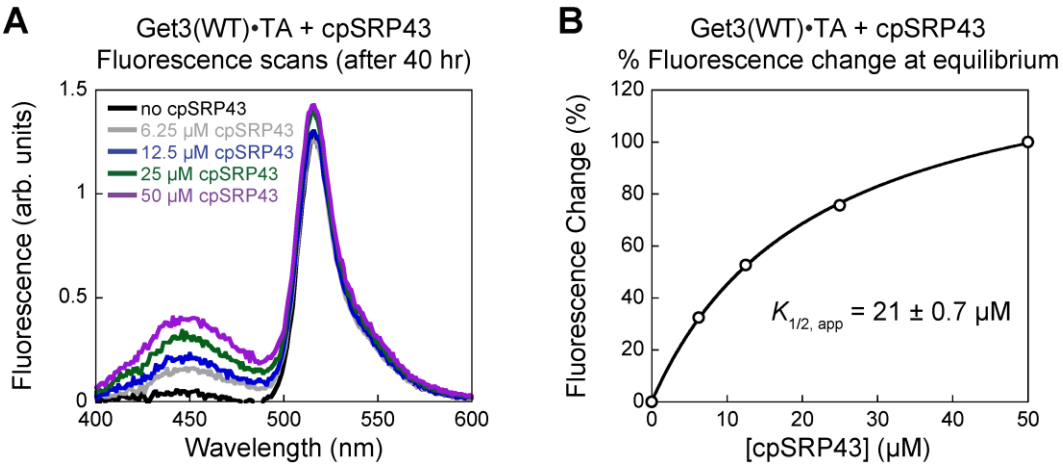

Figure 3.7: cpSRP43 can bind TA proteins. (A) Fluorescence emission spectra were recorded using an excitation wavelength of 370 nm and an emission wavelength of 450 nm 40 hours after 50 nM wild-type $Get3^{BDP}$•TA^{Cm} was chased with indicated concentrations of cpSRP43. (B) The TA^{Cm} fluorescence change at equilibrium based on the data in (A) was plotted against cpSRP43 concentration. The data was fit to Equation 3.6, which gave a $K_{1/2,app}$ value of 21 ± 0.7 μM in the presence of 50 nM

Get3. This suggests that TA is bound to Get3 by ~400-fold more strongly than to cpSRP43.

During these measurements, we noticed that the observed kinetics of TA loss from Get3(Δα8) was strongly accelerated by increasing chase concentration (Figure 3.6B–E), regardless of whether cpSRP43 or CaM was used as the chase. This kinetic behavior cannot be explained by a model in which the chase molecules acted as an inert TA-trap that simply binds dissociated TAs and prevents their rebinding to Get3(Δα8), as the observed reaction kinetics would be rate-limited by TA dissociation and independent of chase concentration in this model (Figures 3.8 and 3.9). Rather, this observation indicates that external chaperones actively stimulate TA release from Get3(Δα8) (Figure 3.8B, top pathway). In contrast to Get3(Δα8), the observed TA release kinetics of wild-type Get3 was independent of chase concentration (Figure 3.6C) (see Chapter 2, Figure 2.11), indicating that the external chaperones act solely as passive TA-traps for wild-type Get3. Thus, although α8 is unnecessary for maintaining a stable Get3•TA complex, it helps Get3 to protect its bound substrate from access by and loss to other chaperones.

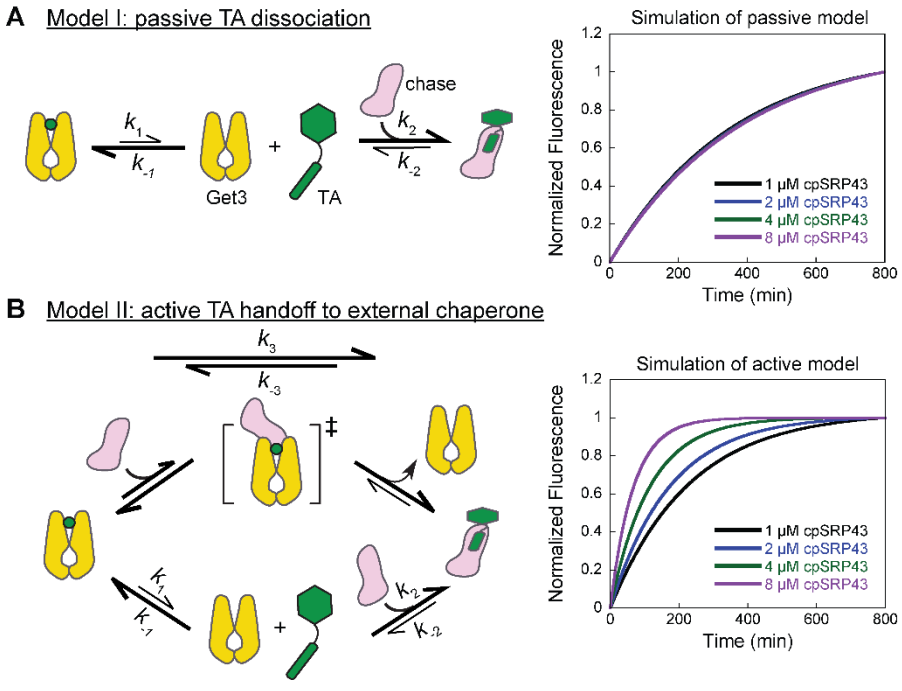

Figure 3.8: Kinetic simulations of TA release from Get3(Δα8). (A) Kinetic simulations (right) based on the passive model (left schematic), in which TA is first released from Get3(Δα8) before binding the chase. (B) Kinetic simulations (right) based on the active model (left schematic), in which Get3(Δα8) can directly handoff TAs to the chase molecule (upper pathway). Spontaneous TA dissociation from Get3 and binding by the chase (lower pathway) was included in the model for completion.

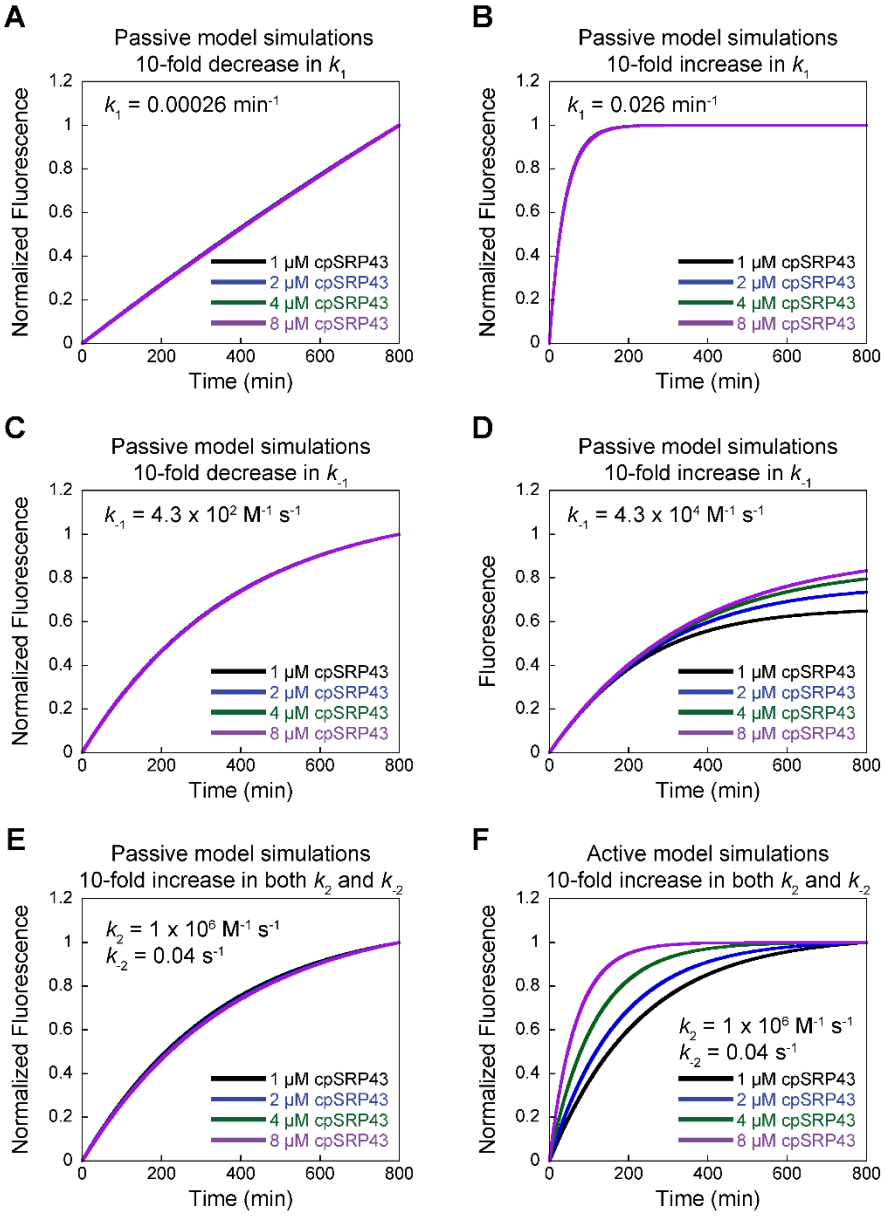

Figure 3.9: Additional kinetic simulations of TA release from Get3(Δα8). (A–D) Changes in Get3•TA dissociation and association kinetics do not qualitatively affect the conclusion that the passive model cannot explain the experimentally observed rate dependence on chase concentration in Figure 3.6B. (E–F) Changes in the rate constants of cpSRP43•TA association and dissociation (the K_d value for cpSRP43•TA was held constant) do not affect the kinetic simulations for both the passive (E) and active (F) models.

α8 and Get4/5 synergistically enable rapid and privileged TA transfer from Sgt2 to Get3

The results above and from previous work (Chapter 2) showed that the Get3(Δα8)•TA complex displays high kinetic stability. Moreover, purified Get3(Δα8)•TA was insertion-competent (see Chapter 2, Figure 2.10). We further showed that Get3(Δα8)•TA can mediate TA targeting and insertion into yRMs with the same efficiency as wild-type Get3 even with Get4/5 present (Figure 3.10), indicating that the Δα8 mutation does not disrupt TA-induced conformational changes that allows Get3 to exchange its binding partner from Get4/5 to the Get1/2 receptors (Figure 3.1, steps 3-4) (see Chapter 2). These observations contrast with the strong defect of Get3(Δα8) in mediating TA targeting in yeast lysate and *in vivo* (Figure 3.5). Although Get3(Δα8) has a higher tendency to hand off the TA to external chaperones than wild-type Get3, the rate of TA loss from Get3(Δα8) ($k \geq 0.015$ min^{-1}) is slow compared to that of TA insertion ($k = 0.14$ min^{-1}; Figure 3.10) and unlikely to account for the observed targeting defect of this mutant. As the experiments in yeast lysate and *in vivo* include all the molecular steps in the GET pathway, we hypothesized that Get3(Δα8) has additional defects in steps prior to the formation of the Get3•TA complex.

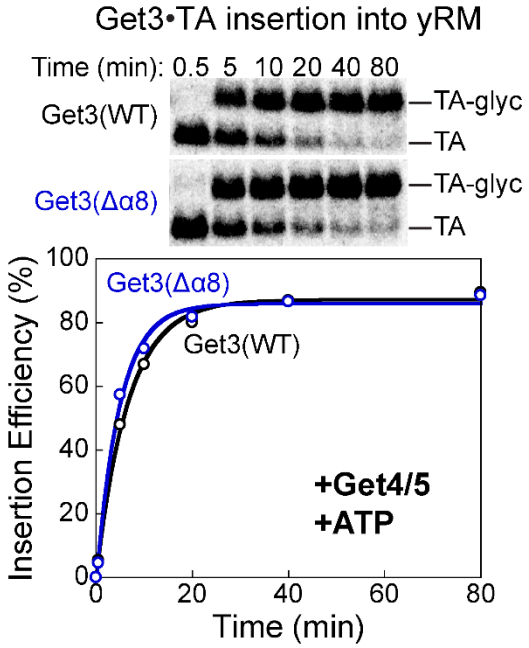

Figure 3.10: TA targeting and insertion assays starting with preformed Get3•TA and Get3(Δα8)•TA complexes. All reactions contained 0.5 μM Get4/5 and 2 mM ATP. Get3(Δα8) can still undergo TA-induced conformational changes to dissociate from Get4/5 to mediate membrane targeting (compare to mutants in Chapter 2, Figure 2.18B).

The only major upstream step involving Get3 is the transfer of TA from Sgt2 to Get3. To test if α8 is important for this transfer event, we used an established FRET-based assay (Rao et al. 2016) in which acceptor-labeled Get3 is presented to a preformed Sgt2•TA complex in which the TA is labeled with a donor dye (Figure 3.11A). Successful TA transfer and loading onto Get3 give rise to efficient FRET between the dye pair (Rao et al. 2016). While we observed rapid TA transfer from Sgt2 to wild-type Get3 in the presence of Get4/5 (see also (Rao et al. 2016)), TA transfer to Get3(Δα8) under the same conditions was ~100-fold slower (Figure 3.11B). Therefore, α8 plays an important role in ensuring rapid TA transfer from Sgt2 to Get3.

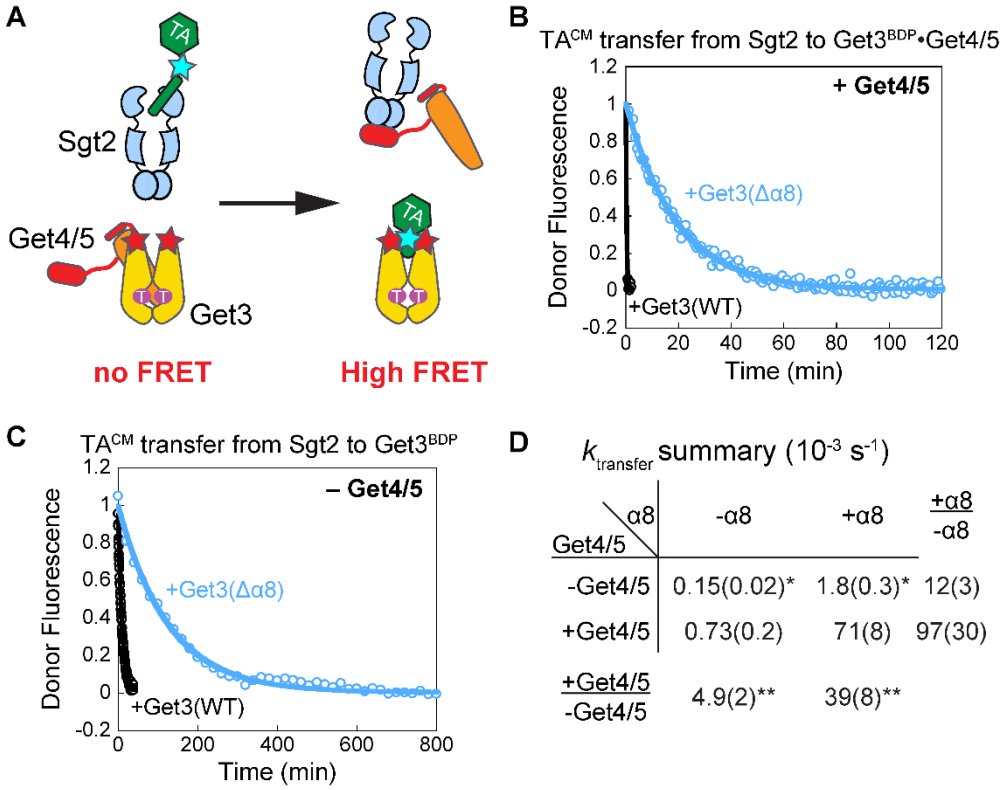

Figure 3.11: α8 and Get4/5 synergistically enable rapid TA transfer from Sgt2 to Get3. (A) Schematic of the FRET assay to measure TA transfer from Sgt2 to Get3. The cyan and red stars denote the donor and acceptor fluorophores on TA and Get3, respectively. (B, C) Donor fluorescence time courses of TA transfer from Sgt2 (25 nM initial Sgt2•TA complex) to 0.3 μM Get3 or Get3(Δα8) with 75 nM Get4/5 present (B), and to 3 μM Get3 or Get3(Δα8) without Get4/5 present (C). Fluorescence was normalized such that the fit of each trace starts at 1 and ends at 0. (D) Summary of observed TA transfer rate constants from the data in (B) and (C). Values are reported as mean (SD), with n = 2. Note that the Get4/5-independent TA transfer was measured at a 10-fold higher Get3 concentration than the Get4/5-dependent transfer (indicated by '*'), such that the reported ratios are lower limits for the stimulatory effect of Get4/5 (indicated by '**').

Since the Get4/5 complex also stimulates TA transfer from Sgt2 to Get3 (Mateja et al. 2015, Rao et al. 2016, Wang et al. 2010), we asked whether Get4/5 and

α8 work synergistically or independently of one another. We therefore measured and compared the rate of TA transfer from Sgt2 to Get3 and Get3(Δα8) without Get4/5 present. Without Get4/5, deletion of α8 has a less deleterious effect, slowing TA transfer kinetics 12-fold (Figures 3.11C and 3.11D). Reciprocally, Get4/5 exerts a smaller stimulatory effect on the Sgt2-to-Get3 TA transfer with mutant Get3(Δα8) compared to wild-type Get3 (Figure 3.11D, last row). In control experiments, Get3(Δα8) binds Get4/5 and undergoes Get4/5-induced conformational changes similarly to wild-type Get3 (Figures 3.3E-F and 3.4), ruling out the possibility that the defect of Get3(Δα8) in Get4/5-dependent TA transfer is due to its defective binding or regulation by Get4/5. Together, these results show that α8 and Get4/5 synergistically enhance TA transfer from Sgt2 to Get3.

Previously, it was shown that TA transfer from SGTA to TRC40, the respective mammalian homologs of Sgt2 and Get3, was impervious to the presence of excess CaM (Shao et al. 2017). We asked if α8 is important for maintaining this 'privileged' transfer. To this end, we repeated the FRET-based TA transfer assay in the presence of excess CaM (Figure 3.12). TA transfer from Sgt2 to wild-type Get3•Get4/5 was not affected by excess CaM (Figure 3.12B), consistent with observations with their mammalian homologues. In contrast, the presence of CaM completely abolished FRET between TA and Get3 in transfer reactions without Get4/5 present (Figure 3.12C), or with mutant Get3(Δα8) even in the presence of Get4/5 (Figure 3.12D). Thus, TA transfer to Get3 becomes susceptible to interference by external chaperones in the absence of either Get4/5 or the α8 motif.

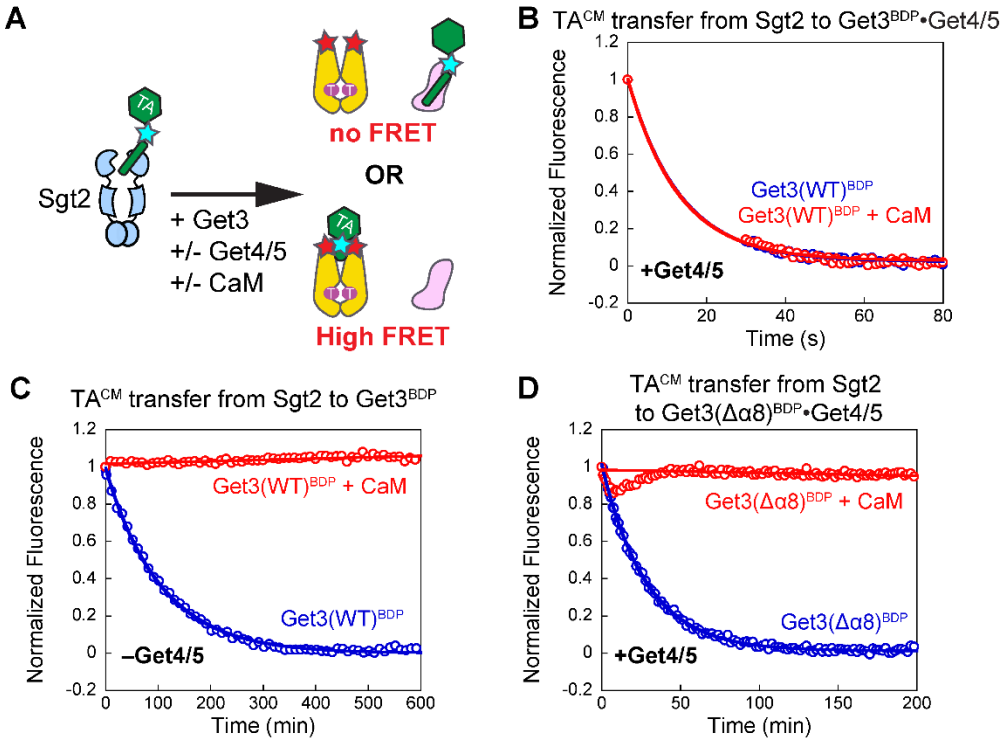

Figure 3.12: Both α8 and Get4/5 are required for privileged TA transfer to Get3 in the GET pathway. (A) Schematic of the Sgt2-to-Get3 TA transfer assay in the presence of excess CaM. (B–D) In the fluorescence-based transfer assay, CaM did not affect TA transfer from Sgt2 to wild-type Get3•Get4/5 (B), but abolished the changes in donor fluorescence during Get4/5-independent TA transfer from Sgt2 (C) or during transfer from Sgt2 to Get3(Δα8)•Get4/5 (D). Where indicated, reactions contained 25 nM Sgt2•TA, 0.3 μM Get3 or Get3(Δα8), 75 nM Get4/5, and 20 μM CaM.

To independently test this model, we monitored the Sgt2-to-Get3 TA transfer using a crosslinking assay. Instead of a fluorescent dye, the photocrosslinker p-benzoyl-l-phenylalanine (Bpa) was incorporated into the TA-TMD via amber suppression (Young et al. 2010). UV-induced crosslinking to Bpa allows direct visualization of the interaction of TA with different chaperones via SDS-PAGE and autoradiography (Figure 3.13A). In the absence of Get3, TA was rapidly lost from Sgt2 and transferred to CaM (Figure 3.13C), as was observed with the SGTA•TA

complex (Shao et al. 2017). Addition of Get3•Get4/5 resulted in rapid transfer of TA to Get3 without any TA loss to CaM (Figure 3.13B), consistent with observations for the homologous mammalian transfer complex (Shao et al. 2017) and with results of the FRET measurements (Figure 3.12B). In contrast, TA transfer to Get3(Δα8)•Get4/5 was almost completely abolished by the presence of CaM, and most of the TA crosslinked to CaM instead (Figure 3.13D). Together, the FRET and crosslinking experiments demonstrate that the α8 motif plays an essential role in enabling privileged TA transfer between Sgt2 and Get3.

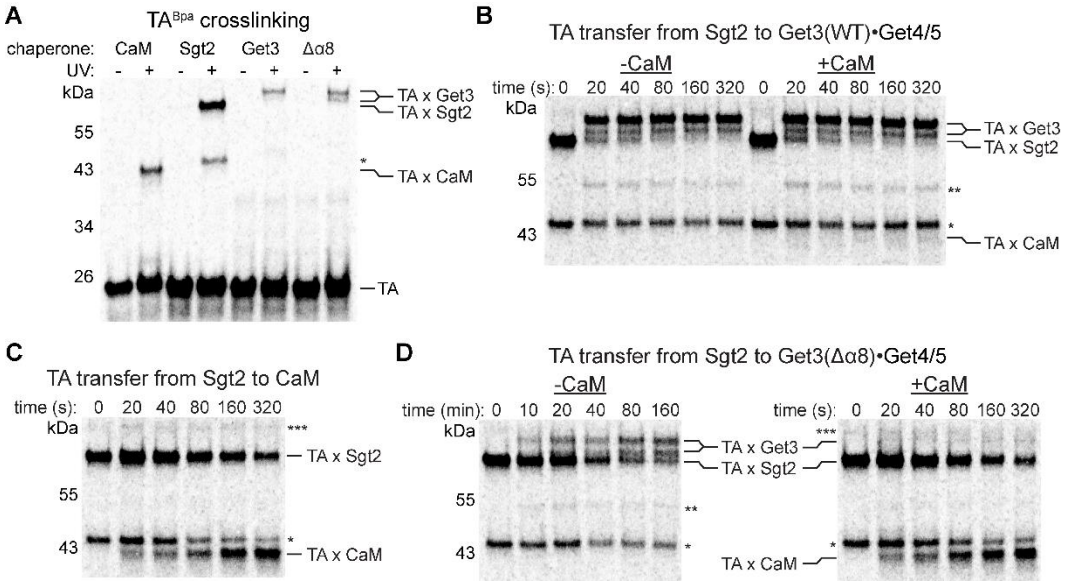

Figure 3.13: Independent verification that α8 is required for privileged TA transfer to Get3 in the GET pathway. (A) SDS-PAGE gel showing TA(Bpa) and its crosslink to different chaperones. '*' denotes a minor crosslinked species in the presence of Sgt2 that was not interpreted. (B–D) Representative SDS-PAGE-autoradiography analyses of the time courses of TA(Bpa) transfer from Sgt2 to 20 μM CaM (C), and to 0.75 μM Get3•Get4/5 (B) or 0.75 μM Get3(Δα8)•Get4/5 (D) with or without 20 μM CaM present. '*', '**', and '***' denote minor crosslinked species that were not interpreted.

Lastly, we tested whether the role of α8 in the Sgt2-to-Get3 TA transfer explains the defect of Get3(Δα8) in the overall targeting reaction (Figure 3.5A). To this end, we initiated TA targeting by mixing a preformed Sgt2•TA complex with Get3, Get4/5, and yRM (Figure 3.14), such that the observed insertion reaction includes the TA transfer step. Addition of wild-type Get3 led to robust TA insertion within 5 min, whereas negligible insertion was observed with Get3(Δα8) (Figure 3.14). This contrasts with the absence of a targeting defect with the preformed Get3(Δα8) complex (Figure 3.10) and indicates that the defect of Get3(Δα8) can be attributed to the loss of efficient TA transfer from Sgt2 to Get3.

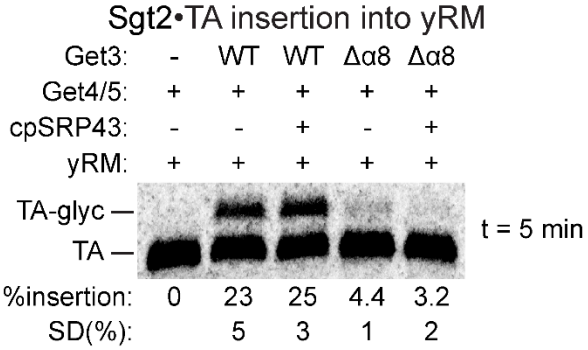

Figure 3.14: TA targeting and insertion assays starting with a preformed Sgt2•TA complex. Values indicate the quantified insertion efficiencies from the representative gel and replicates and are reported as mean ± SD, with $n = 3$.

3.3 DISCUSSION

Molecular chaperones play key roles in membrane protein biogenesis. While guiding client proteins to the target membrane, these chaperones must effectively secure hydrophobic TMDs on client proteins to prevent both aggregation and client loss to off-pathway chaperones. These challenges are especially acute for pathways in which client proteins undergo molecular handovers between chaperones. In this work, biochemical and biophysical analyses shed light on how a conserved α8 lid motif lining the substrate binding groove enables the Get3 ATPase to fulfill these requirements during TA targeting to the ER.

The importance of the α8 element is supported by its evolutionary conservation among Get3 homologues (Figure 3.2) (Mateja et al. 2009, Suloway et al. 2009), yeast growth defects under stress conditions upon mutation of α8 (Mateja et al. 2009), and the defects of mutant Get3(Δα8) in TA targeting *in vitro* and *in vivo* (this work). However, the precise roles of α8 remained enigmatic. Mechanistic dissections in this work show that the major roles of α8 are to accelerate TA transfer to Get3 from the upstream co-chaperone Sgt2 and to confer upon Get3 the privilege to receive TAs over competing chaperones. Deletion of hydrophobic residues in α8 slowed Get4/5-dependent TA transfer from Sgt2 to Get3 by ~100-fold (Figures 3.11B and 3.11E). Moreover, Get3 lost its privilege in capturing TAs from Sgt2 upon mutation of α8, and the TA substrate can be rapidly lost to an external chaperone (Figures 3.12 and 3.13). This explains the previous observation that mutations in α8 reduced the amount of Get3-bound TAs in pulldown assays in rabbit reticulocyte lysate (Mateja et al. 2009). The cooperative effects of Get4/5 and α8 in promoting rapid and privileged TA transfer further suggest that they both stabilize the transition state or a transient intermediate during the transfer reaction. Coupled with the observation that α8 can crosslink to the TA (Mateja et al. 2015), the simplest model to explain all the data is that α8 provides the first structural element in Get3 to contact the TA during its handover from Sgt2, guiding the TA into the hydrophobic substrate binding groove of Get3 and protecting the TA from off-pathway chaperones during this process (Figure 3.15, bracket).

Once the TA is loaded onto Get3, deletion of α8 also renders the TA more susceptible to challenges by external TMD-binding chaperones (Figure 3.15). Whether TAs could be analogously lost from Get3(Δα8) to other chaperones in the yeast cytosol remains to be determined. Nevertheless, the observation here that two unrelated membrane protein chaperones, cpSRP43 and CaM, can both invade the TA binding groove and capture TAs from Get3(Δα8) suggest that loss of substrates to off-pathway chaperones presents a probable mechanistic challenge during membrane

protein biogenesis, and that some chaperones such as Get3 have evolved mechanisms to actively retain substrates within the dedicated targeting pathway.

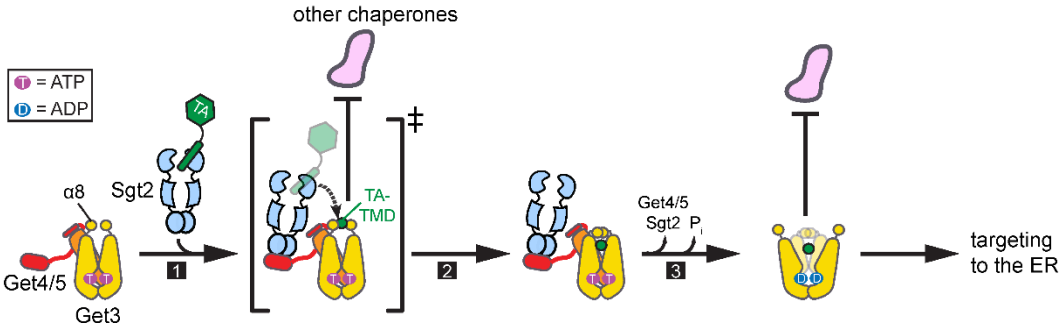

Figure 3.15: Model for the dual roles of α8 as a substrate conduit and as a chaperone lid in the GET pathway. Upon interaction of Sgt2•TA with ATP- and Get4/5-bound Get3 (step 1), Get4/5 and the α8 element on Get3 cooperate to enable the formation of a transient transfer intermediate that provides a protected path for TA handover from Sgt2 to Get3. α8 mediates initial contacts with the TA and guides it into the substrate-binding groove on Get3, while also preventing external chaperones from accessing the substrate during the transfer (species in bracket). Get4/5 increases the local concentrations of Sgt2 and Get3 to enable the action of the α8 element. TA loading then induces conformational changes in Get3 that drive its dissociation from Get4/5 and stimulate ATP hydrolysis (step 3). Once the Get3•TA complex is formed and en route to the ER, α8 also acts as a lid to prevent substrate loss to off-pathway chaperones.

The role of the α8 lid motif in facilitating rapid and privileged TA loading onto the chaperone is unprecedented, and highlights new mechanistic challenges as well as solutions for molecular chaperones. A dual-function lid described here provides an effective and elegant mechanism for a chaperone to capture and retain client proteins within the correct biogenesis pathway during and after substrate handover. This function may be particularly relevant for chaperones that interact with client proteins via degenerate interactions and face competition from other chaperones in the crowded cytosolic environment.

3.4 MATERIALS AND METHODS

S. cerevisiae strain construction

Genomic *GET3* in the BY4741 strain was replaced with *GET3-FLAG* and *GET3(Δα8)-FLAG* using CRISPR-Cas9 mediated genome editing (Ryan et al. 2016). The pCAS plasmid encoding *S. pyogenes* Cas9 and sgRNA was modified to encode a guide sequence (5'-GAATATAACCCTATTACTGA-3') that targets Cas9 to cut the codon for Get3(T342). This pCAS plasmid was co-transformed into BY4741 yeast cells with a double-stranded linear repair DNA, which encodes Get3-FLAG harboring synonymous codon substitutions within the guide sequence and 50 bp homology downstream of the C-terminal FLAG tag for homologous recombination. The *GET3(Δα8)-FLAG* strain was then generated using a modified pCAS plasmid encoding a guide sequence (5'-GTTGTAGAAATCTTAATGTG-3') that targets Cas9 to cut the codon for Get3(T173). The modified pCAS was co-transformed with a double-stranded linear repair DNA that encodes Get3(Δα8)-FLAG with synonymous codon substitutions within the guide sequence into *GET3-FLAG* yeast cells. Following each co-transformation, colonies from the YPD+G418 plate were cultured in YPD, streaked onto YPD, and cultured again in YPD to ensure loss of the pCAS plasmid. The final strains were verified by PCR and sequencing.

Plasmids and recombinant proteins

All plasmids and recombinant proteins used in this study are listed in Tables 3.1 and 3.2. All proteins and protein complexes were ultracentrifuged (TLA100, Beckman Coulter Inc.) at 100,000 rpm for 30 min at 4°C to remove potential aggregates prior to use in *in vitro* assays.

Plasmid name	Shan Lab Catalog No.
pCAS Get3 T173	pSOS3593
pCAS Get3 T342	pSOS3594
pET33b His_6-Get3	pSOS1289
pET33b His_6-Get3(Δα8)	pSOS3365
pET28a His_6-SUMO-Get3 ybbR	pSOS2252
pET28a His_6-SUMO-Get3(Δα8) ybbR	pSOS3051
pET33b His_6-Sgt2	pSOS1723
pET33b Get4-His_6/Get5	pSOS1401
pET33b Get4(C177T/S48C)-His_6/Get5	pSOS1706
pET33b His_6-Get1CD	pSOS1439
pQE His_6-cpSRP43(intein)	pSOS1975
pRSET-A Calmodulin-His_6	pSOS3361
pET29 Sfp-His_6	pSOS2068
pK7 3xStrep-SUMOnc-Bos1-opsin	pSOS2101
pK7 3xStrep-SUMOnc-amberBos1-opsin	pSOS2353
pK7 3xStrep-SUMOnc-Bos1(A228TAG)-opsin	pSOS3410
pRS316 GPD 3HA-BirA-Bos1-opsin	pSOS2910

Table 3.1: List of plasmids used in this study.

Protein name	Reference
His_6-Get3	Suloway et al. 2009
His_6-Get3(Δα8)	Chapter 2; Suloway et al. 2009
Get3 ybbR	Rao et al. 2016
Get3(Δα8) ybbR	Chapter 2; Rao et al. 2016
His_6-Sgt2	Rao et al. 2016
Get4/5	Chartron et al. 2010
Get4(C177T/S48C)/5	Rome et al. 2014
His_6-Get1CD	Rome et al. 2014
Intein-cpSRP43	Liang et al. 2016
Calmodulin-His_6	Shao and Hegde 2011
Sfp-His_6	Yin et al. 2006
His_6-T7 RNA polymerase	Saraogi et al. 2011
Tagless T7 RNA polymerase	Rao et al. 2016

Table 3.2: List of recombinant proteins used in this study.

Protein labeling

Get3 and Get3(Δα8) with a ybbR tag (DSLEFIASKLA) inserted between residues S110 and D111 were labeled with BODIPY-FL (Thermo Fisher Scientific) or a 1:1 mix of Cy3B (GE Healthcare) and ATTO 647N (ATTO-TEC) via Sfp-catalyzed incorporation of dye-CoA conjugates (Rao et al. 2016). 30 µM ybbR-Get3 was mixed with 60 µM dye-CoA and 12 µM Sfp-His_6 in Sfp labeling buffer (50 mM K-HEPES (pH 7.4), 10 mM $MgCl_2$) in a total volume of 800 µL. The reaction mixture was rotated at room temperature for 1 hr. 10 µL 2 M imidazole (pH 8.0) was added before passing the reaction through Ni-NTA agarose (Qiagen) to remove Sfp-His_6. Gel filtration through a Sephadex G-25 (Sigma-Aldrich) column was used to remove excess dye-CoA and exchange dye-labeled Get3 into GET storage buffer (50 mM K-HEPES (pH 7.5), 150 mM KOAc, 5 mM $Mg(OAc)_2$, 20% glycerol, 1 mM DTT).

Get4(C177T/S48C)/5 was labeled with thiol-reactive acrylodan (Thermo Fisher Scientific) (Rome et al. 2014). Protein was dialyzed into labeling buffer (50 mM K-HEPES (pH 7.4), 200 mM NaCl, 10% glycerol) and treated with 2 mM TCEP to reduce disulfide bonds. A 10-fold excess of acrylodan was added and the reaction was incubated overnight at 4°C. The reaction was quenched with 1 mM DTT and excess dye was removed using a Sephadex G-25 column while exchanging acrylodan-labeled Get4/5 into GET storage buffer.

TA substrate was labeled either four residues upstream of the TMD with 7-hydroxycoumarin or replacing Ala 228 in Bos1 TMD with p-benzoyl-l-phenylalanine (Bpa) using amber suppression in *E. coli* S30 lysate (Rao et al. 2016, Young et al. 2010).

Model TA substrates

The model TA used in all *in vitro* assays was the previously described 3xStrep-SUMOnc-Bos1-opsin (Rao et al. 2016), composed of three tandem Strep tags at the N-terminus, a mutant yeast Smt3 with the Ulp1 cut site removed (Pro inserted between residues G98 and A99), the C-terminal residues 207-244 of the TA Bos1 encompassing its TMD, and an opsin tag at the extreme C-terminus (GSMRMNGTEGPNMYMPMSNKTVD) to monitor ER translocation via glycosylation. The model TA for *in vivo* pulse chase experiments was 3xHA-BirA-Bos1TMD-opsin (Cho and Shan, 2018), composed of an N-terminal 3xHA-BirA for HA immunoprecipitation, the C-terminal residues 203-244 of the TA Bos1 encompassing its TMD, a GS linker (GSGGSGS), and an opsin tag at the extreme C-terminus.

Get3•TA and Sgt2•TA complex preparation

For fluorescence measurements, $Get3^{BDP}$•TA^{CM} complexes were generated by *in vitro* translating 3xStrep-tagged TA^{CM} for 2 hrs at 30°C in 10 mL amber suppression reactions with *E. coli* S30 lysate in the presence of 0.5 µM BODIPY-

FL-labeled Get3 variants. For insertion assays, 3xStrep-tagged TA was *in vitro* translated for 2 hrs at 30°C in a 100 µL reaction with *E. coli* S30 lysate in the presence of 2 µM Get3 variants. The resulting Get3•TA complexes were then purified using Strep-Tactin Sepharose (IBA Life Sciences).

Sgt2•TA complexes for transfer and insertion assays were generated by *in vitro* translation of TA^{CM}, TA(Bpa), or TA for 2 hrs at 30°C in 10 mL or 100 µL amber suppression reactions with *E. coli* S30 lysate in the presence of 1 µM His_6-tagged Sgt2. The Sgt2•TA complex was then purified using Ni-NTA (Qiagen).

Fluorescence measurements of Get3•TA dissociation

All fluorescence measurements were carried out on a Fluorolog 3-22 spectrophotometer (HORIBA Instruments) at 25°C in GET assay buffer (50 mM K-HEPES (pH 7.4), 150 mM KOAc, 5 mM $Mg(OAc)_2$, 10% glycerol, 1 mM DTT).

Get3•TA dissociation rates were measured by chasing 20-50 nM of preformed $Get3^{BDP}$•TA^{CM} complexes with indicated concentrations of intein-cpSRP43 or CaM. Loss of FRET over time was monitored by following the fluorescence of TA^{CM} using an excitation wavelength of 370 nm and emission wavelength of 450 nm. Observed time courses were fit to Equation 3.1:

$$F = F_e + (F_0 - F_e)e^{-k_{obsd}t}, \qquad [3.1]$$

where F is the observed donor fluorescence at a particular time, F_0 is the donor fluorescence at t=0, F_e is the donor fluorescence when the reaction is complete, and k_{obsd} is the observed rate constant of TA loss from Get3.

Kinetic simulations of Get3•TA dissociation

Kinetic simulations for the different models of Bos1-TA release from Get3(Δα8) were performed with Berkeley Madonna, version 8.3.18 (R. I. Macey, G.

F. Oster, University of California at Berkeley). For the passive model (Figure 3.8A), the following equations were used:

$$\text{Get3}(\Delta\alpha8)\bullet\text{TA} \underset{k_{-1}}{\overset{k_1}{\rightleftharpoons}} \text{Get3}(\Delta\alpha8) + \text{TA} \qquad [3.2]$$

$$\text{TA} + \text{cpSRP43} \underset{k_{-2}}{\overset{k_2}{\rightleftharpoons}} \text{cpSRP43}\bullet\text{TA} \qquad [3.3]$$

For the active model (Figure 3.8B), the following chemical equations were used:

$$\text{Get3}(\Delta\alpha8)\bullet\text{TA} \underset{k_{-1}}{\overset{k_1}{\rightleftharpoons}} \text{Get3}(\Delta\alpha8) + \text{TA} \qquad [3.2]$$

$$\text{TA} + \text{cpSRP43} \underset{k_{-2}}{\overset{k_2}{\rightleftharpoons}} \text{cpSRP43}\bullet\text{TA} \qquad [3.3]$$

$$\text{Get3}(\Delta\alpha8)\bullet\text{TA} + \text{cpSRP43} \underset{k_{-3}}{\overset{k_3}{\rightleftharpoons}} \text{Get3}(\Delta\alpha8) + \text{cpSRP43}\bullet\text{TA} \qquad [3.4]$$

The rate constant k_1 was experimentally determined to be 0.0026 min^{-1}, or 4.3 x 10^{-5} s^{-1} (Figure 3.6F). The K_d value of wild-type Get3•Bos1-TA was estimated to be 0.1 nM based on the coupled equilibria of TA loading and transfer through the Ssa1-Sgt2-Get3 cascade (Cho and Shan, 2018, Rao et al. 2016) shown in Equation 3.5:

$$\text{Ssa1} + \text{TA} \underset{K_{app}}{\rightleftharpoons} \text{Ssa1}\bullet\text{TA} \overset{K^{rel,\,1}\ \text{Sgt2}}{\underset{\text{Ssa1}}{\rightleftharpoons}} \text{Sgt2}\bullet\text{TA} \overset{K^{rel,\,2}\ \text{Get3}}{\underset{\text{Sgt2}}{\rightleftharpoons}} \text{Get3}\bullet\text{TA} \qquad [3.5]$$

The Ssa1 concentration required for half-maximal solubilization of Bos1-TA (K_{app}) was previously determined to be 0.37 ± 0.07 μM (Cho and Shan, 2018). Equilibrium titrations of Bos1-TA transfer from Ssa1 to Sgt2 indicated that this first transfer reaction is ~100-fold in favor of Sgt2 ($K^{rel,1}$ ~ 100) (Cho and Shan, 2018).

Equilibrium titrations of Bos1-TA transfer from Sgt2 to Get3 suggested that this second transfer reaction is ~30-fold in favor of Get3 ($K^{rel,2}$ ~ 30) (Rao et al. 2016). These data provide estimated K_d values of Sgt2•Bos1-TA and Get3•Bos1-TA of approximately 3.7 nM and 0.1 nM, respectively. This K_d and the measured k_1 value yield a calculated k_{-1} of approximately 4.3 x 10^5 $M^{-1}s^{-1}$ for wild-type Get3•TA. Given the 100-fold slower $k_{transfer}$ of Get3(Δα8) than wild-type Get3 (Figure 3.11), we estimated a 100-fold lower value of k_{-1}, 4.3 x 10^3 M^{-1} s^{-1}, for Bos1-TA binding to Get3(Δα8). Variations in the value of k_{-1} did not change the qualitative conclusion that the observed rate constant of Bos1-TA loss from Get3(Δα8) is independent of chase concentration in the passive model (Figures 3.9C and 3.9D).

From chase experiments of wild-type Get3•Bos1-TA with cpSRP43, we found that a cpSRP43 concentration of 21 ± 0.7 μM was necessary for half-maximal Bos1-TA transfer in the presence of 50 nM Get3 after fitting the data in Figure S4B to

$$F = F_{max} \times \frac{[\text{cpSRP43}]}{K_{1/2,app} + [\text{cpSRP43}]} \quad . \qquad [3.6]$$

This strongly suggests that intein-cpSRP43 binds TA with an ~400-fold weaker affinity than Get3. We estimated a K_d of ~40 nM for the cpSRP43-TA interaction. We assigned a lower limit for k_2 of 1 x 10^5 M^{-1} s^{-1}, given the observation that TA aggregation occurs within the mixing dead-time of ~15 s and that intein-cpSRP43 effectively competes with TA aggregation (Cho and Shan, 2018). k_{-2} was calculated to be 0.004 s^{-1} from the estimated K_d and k_2 values. Increasing the values of k_2 and k_{-2} (holding a constant K_d value) does not change the results of the simulation (Figures 3.9E and 3.9F).

Normalized fluorescence change is proportional to the loss of the Get3(Δα8)•Bos1-TA complex and was calculated as

$$F = 1 - \frac{[\text{Get3}(\Delta\alpha 8) \bullet \text{TA}]}{[\text{Get3}(\Delta\alpha 8) \bullet \text{TA}]_0}, \qquad [3.7]$$

where $[Get3(\Delta\alpha8)\bullet TA]_0$ is the initial Get3(Δα8)•TA concentration and was set to 20 nM. The rate constants k_3 and k_{-3} in Equation 3.4 were determined to be 1.54 x 10^3 M^{-1} min^{-1} and 5.11 x 10^{-4} min^{-1}, respectively, by allowing the software to fit the simulated time courses to the experimental results. The obtained value of k_3 was equal to that obtained from manual fitting of the data in Figure 3.6B, which was also 1.54 x 10^3 M^{-1} min^{-1}.

Monitoring TA transfer from Sgt2 to Get3

TA^{CM} transfer from Sgt2 to $Get3^{BDP}$ was monitored by mixing 120 µL of ~50 nM Sgt2• TA^{CM} with 120 µL of a solution containing 0.6 µM or 6 µM $Get3^{BDP}$. 2 mM ATP was present in all reactions. Where indicated, transfer reactions also contained 0.15 µM Get4/5 with and without 40 µM CaM (supplemented with 1 mM Ca^{2+}). To correct for photobleaching and possible environmental effects on the donor fluorophore, transfer reactions to unlabeled Get3 were also performed in parallel under the same conditions. Time courses of fluorescence changes were recorded for TA^{CM}, corrected for photobleaching and possible environmental effects, and fit to Equation 3.1, where k_{obsd} is the observed rate constant for TA transfer from Sgt2 to Get3.

To monitor TA transfer from Sgt2 to Get3 via crosslinking, Sgt2•TA(Bpa), containing 300 nM Sgt2 and sub-stoichiometric levels of [^{35}S]-methionine-labeled TA(Bpa), was added to 750 nM Get3 and 750 nM Get4/5. Where indicated, CaM was present at 20 µM. All reactions contained 2 mM ATP, 1 mM Ca^{2+} and were incubated at 26°C. At indicated time points, aliquots were removed from the reaction, flash frozen, and subsequently crosslinked on dry ice ~4 cm away from a UVP B-100AP lamp (UVP LLC) for 90 minutes. Aliquots were then thawed and processed for SDS-PAGE and autoradiography.

TA targeting assays

To monitor TA targeting and translocation from preformed Get3•TA or Get3(Δα8)•TA complexes, 50 µL reactions were initiated by adding 10 µL *Δget3* microsomes to purified Get3•TA complexes in the presence of 0.5 µM Get4/5 and 2 mM ATP. [^{35}S]-methionine-labeled TA was normalized to 40,000 dpm for each reaction. Reactions were incubated at 26°C; at indicated time points, 6 µL samples were removed and quenched by addition of SDS sample buffer and flash-freezing in liquid nitrogen. Samples were analyzed by SDS-PAGE and autoradiography. Insertion efficiencies were calculated using Equation 3.8:

$$Insertion\ efficiency = \frac{I_{glycosylated}}{I_{unglycosylated} + I_{glycosylated}} \times 100, \qquad [3.8]$$

where *I* denotes the intensity of the band of interest.

TA targeting and insertion assays starting with a preformed Sgt2•TA complex were measured using purified Sgt2•TA complexes, in which TA is ^{35}S-methionine labeled and normalized to 40,000 dpm. Sgt2•TA was first mixed with other components except for microsomes to 8 µL, and then after 15s, 2 µL *Δget3* microsomes were added to initiate reactions. Reactions contained 75 nM Get4/5, 2 mM ATP, 0.5 µM wild-type Get3 or Get3(Δα8), and 20 µM cpSRP43 where indicated. Initiated reactions were incubated at 26°C for 5 minutes before quenching with SDS sample buffer and flash freezing with liquid nitrogen. Samples were analyzed by SDS-PAGE and autoradiography. Insertion efficiencies were calculated using Equation 3.8.

Pulse-chase analysis of TA insertion in vivo

GET3-FLAG, *GET3(Δα8)-FLAG*, and *Δget3* yeast cells were first transformed with a pRS316 vector containing a GPD promoter and the 3xHA-BirA-Bos1TMD-opsin TA substrate (Cho and Shan, 2018). Transformed yeast cells were

grown in SD-Ura to mid-log phase (OD_{600} ~ 0.6), washed with SD-Ura-Met-Cys media, and resuspended in 1 mL SD-Ura-Met-Cys media to a final OD_{600} of 6. Cells were incubated at 30°C for 25 min and then incubated at 26°C for an additional 10 min. Cells were pulse-labeled with 100 μCi/mL EasyTag™ EXPRESS35S Protein Labeling Mix (Perkin Elmer) for 2 min and chased with 1 mL SD-Ura supplemented with 20 mM cold methionine and 2 mM cysteine. 450 μL aliquots of cells were flash frozen in liquid nitrogen at indicated times during chase. Individual cell aliquots were subsequently thawed and harvested.

Cells were treated with 0.3 M NaOH for 3 min at room temperature, washed with water, resuspended in Lysis buffer (20 mM Tris-HCl (pH 7.6), 150 mM NaCl, 2% SDS), incubated at 70°C for 10 min, and then spun down at 14,000 rpm (16,873 g) for 2 min. Clarified lysate was diluted over 20-fold with HA IP buffer (20 mM Tris-HCl (pH 7.6), 150 mM NaCl, 1% Triton X-100) and incubated with anti-HA magnetic beads (Thermo Fisher Scientific) equilibrated with HA IP buffer containing 0.4 mg/mL BSA. After incubation at 25°C for 10 min, the beads were sequentially washed with: W1 buffer (20 mM Tris-HCl (pH 7.6), 150 mM NaCl, 1% Triton X-100, 2M urea), W2 buffer (20 mM Tris-HCl (pH 7.6), 500 mM NaCl, 1% Triton X-100), W3 buffer (20 mM Tris-HCl (pH 7.6), 150 mM NaCl, 0.1% SDS), and W4 buffer (20 mM Tris-HCl (pH 7.6), 150 mM NaCl). The final wash with W4 buffer was performed twice. Immunoprecipitated proteins were eluted with SDS sample buffer, boiled for 5 min, and analyzed by SDS-PAGE and autoradiography. Insertion efficiencies were calculated using Equation 3.8.

Circular dichroism

Circular dichroism spectra of wild-type Get3 or Get3(Δα8) at 5 μM in 20 mM sodium phosphate pH 7.5 were recorded using an Aviv Model 430 circular dichroism spectrometer at 25 °C. For each sample, 8 scans from 190 nm to 260 nm were collected, averaged, and background subtracted.

ATPase measurements

Multi-site, multi-turnover ATPase rate constants were measured for 0.5 μM Get3(Δα8) and indicated ATP concentrations in GET assay buffer at 25°C (Rome et al. 2013). The ATP concentration dependence of observed rate constants were fit to an allosteric sigmoidal curve with a Hill coefficient of 2 (Equation 3.9):

$$k_{obsd} = \frac{k_{cat} \times [ATP]^2}{K_M^2 + [ATP]^2}, \qquad [3.9]$$

where k_{cat} is the rate constant at saturating ATP concentrations, and K_M^2 is the product of ATP binding affinities for the first and second active site.

Measurements of Get3-Get4/5 binding

Equilibrium binding affinities between Get3 variants and acrylodan-labeled Get4/5 were measured by titrating 250 μL of 0.5 μM acrylodan-labeled Get4/5 with increasing Get3 concentration in the absence (Figure 3.3E) or presence (Figure 3.3F) of 2 mM ATP. Binding of Get3 results in fluorescence enhancement of acrylodan-labeled Get4/5 and was recorded using an excitation wavelength of 370 nm and emission wavelength of 490 nm. Fluorescence was plotted against Get3 concentration and fit to Equation 3.10:

$$F = F_0 + F_{max} \times \frac{K_d + [Get4/5] + [Get3] - \sqrt{(K_d + [Get3] + [Get4/5])^2 - 4[Get3][Get4/5]}}{2[Get4/5]}, \qquad [3.10]$$

where F is the observed fluorescence, F_0 is the initial fluorescence value, F_{max} is the maximum fluorescence change at saturating Get3 concentration, and K_d is the equilibrium dissociation constant of the complex.

µs-ALEX measurements

All proteins were ultracentrifuged in a TLA 100 rotor (Beckman Coulter) at 100,000 rpm for 1 hr at 4°C to remove aggregates before all measurements. Get3 samples were diluted to ~100 pM in GET assay buffer containing 0.3 mg/mL BSA and indicated interaction partners. 2 mM AMPPNP, 4 mM ADP, 10 µM Get1CD, and 4 µM Get4/5 were included where indicated. Samples were placed in a closed chamber made by sandwiching a perforated silicone sheet (Grace Bio-Labs) with two coverslips to prevent evaporation. Data were collected over 30 min using an alternating-laser excitation fluorescence-aided molecule sorting setup (Kapanidis et al. 2004) with two single-photon Avalanche photodiodes (PerkinElmer) and 532-nm and 638-nm continuous wave lasers (Coherent) operating at 135 µW and 80 µW, respectively.

Statistical parameters

All statistical parameters (n and SD) for assays in this study are reported in the corresponding figure legends.

µs-ALEX data analysis

For the collected µs-ALEX data, a dual-channel burst search (Nir et al. 2006) was performed using FRETBursts (Ingargiola et al. 2016) to isolate the photon streams from species containing FRET pairs versus background noise and species containing donor or acceptor only. Each burst was identified as a minimum of 10 consecutive detected photons with a photon count rate at least 15-fold higher than the background photon count rate during both donor and acceptor excitation periods. Since the background rate can fluctuate within a measurement, the background rate was computed for every 50 second interval according to maximum likelihood fitting of the interphoton delay distribution. The identified bursts were further selected according to the following criteria: (i) $n_{DD} + n_{DA} \geq 25$ and (ii) $n_{AA} \geq 25$, where n_{DD} is the number of photons detected from donor during donor excitation, n_{DA} is the

number of photons detected from acceptor during donor excitation, and n_{AA} is the number of photons detected from acceptor during acceptor excitation.

BIBLIOGRAPHY

Akopian D, Shen K, Zhang X, Shan SO. 2013. Signal recognition particle: an essential protein-targeting machine. *Annu. Rev. Biochem.* 82: 693–721

Borgese N, Fasana E. 2011. Targeting pathways of C-tail-anchored proteins. *Biochim. Biophys. Acta* 1808(3): 937–946.

Bozkurt G, Stjepanovic G, Vilardi F, Amlacher S, Wild K, et al. 2009. Structural insights into tail-anchored protein binding and membrane insertion by Get3. *Proc. Natl. Acad. Sci. U. S. A.* 106(50): 21131–21136

Bozkurt G, Wild K, Amlacher S, Hurt E, Dobberstein B, Sinning I. 2010. The structure of Get4 reveals an alpha-solenoid fold adapted for multiple interactions in tail-anchored protein biogenesis. *FEBS Lett*. 584(8): 1509–1514

Burmann BM, Wang C, Hiller S. 2013. Conformation and dynamics of the periplasmic membrane-protein-chaperone complexes OmpX-Skp and tOmpA-Skp. *Nat. Struct. Mol. Biol.* 20(11): 1265–1272.

Chang YW, Chuang YC, Ho YC, Cheng MY, Sun YJ, et al. 2010. Crystal structure of Get4-Get5 complex and its interactions with Sgt2, Get3, and Ydj1. *J. Biol. Chem.* 285(13): 9962–9970

Chartron JW, Clemons WM Jr., Suloway CJ. 2012a. The complex process of GETting tail-anchored membrane proteins to the ER. *Curr. Opin. Struct. Biol.* 22(2): 217–224

Chartron JW, Gonzalez GM, Clemons WM Jr. 2011. A structural model of the Sgt2 protein and its interactions with chaperones and the Get4/Get5 complex. *J. Biol. Chem.* 286(39): 34325–34334

Chartron JW, Suloway CJ, Zaslaver M, Clemons WM Jr. 2010. Structural characterization of the Get4/Get5 complex and its interaction with Get3. *Proc. Natl. Acad. Sci. U. S. A.* 107(27): 12127–12132

Chartron JW, VanderVelde DG, Clemons WM Jr. 2012b. Structures of the Sgt2/SGTA dimerization domain with the Get5/UBL4A UBL domain reveal an interaction that forms a conserved dynamic interface. *Cell Rep*. 2(6): 1620–1632

Chartron JW, VanderVelde DG, Rao M, Clemons WM Jr. 2012c. Get5 carboxyl-terminal domain is a novel dimerization motif that tethers an extended Get4/Get5 complex. *J. Biol. Chem*. 287(11): 8310–8317

Cho H, Shan SO. 2018. Substrate relay in an Hsp70-cochaperone cascade safeguards tail-anchored membrane protein targeting. *EMBO J*. 37(16): e99264

Colombo SF, Cardani S, Maroli A, Vitiello A, Soffientini P, et al. 2016. Tail-anchored protein insertion in mammals: function and reciprocal interactions of the two subunits of the TRC40 receptor. *J. Biol. Chem.* 291(36): 15292–15306

Cox C, Reeder JE, Robinson RD, Suppes SB, Wheeless LL. 1988. Comparison of frequency distributions in flow cytometry. *Cytometry* 9(4): 291–298

Denic V, Dötsch V, Sinning I. 2013. Endoplasmic reticulum targeting and insertion of tail-anchored membrane proteins by the GET pathway. *Cold Spring Harb. Perspect. Biol.* 5(8): a013334.

Favaloro V, Spasic M, Schwappach B, Dobberstein B. 2008. Distinct targeting pathways for the membrane insertion of tail-anchored (TA) proteins. *J. Cell Sci.* 121(11): 1832–1840

Favaloro V, Vilardi F, Schlecht R, Mayer MP, Dobberstein B. 2010. Asna1/TRC40-mediated membrane insertion of tail-anchored proteins. *J. Cell Sci.* 123(9): 1522–1530

Feller W. 1948. On the Kolmogorov-Smirnov limit theorems for empirical distributions. *Ann. Math Stat.* 19(2): 177–189

Ferbitz L, Maier T, Patzelt H, Bukau B, Deuerling E, et al. 2004. Trigger factor in complex with the ribosome forms a molecular cradle for nascent proteins. *Nature* 431(7008): 590–596

Ghaemmaghami S, Huh WK, Bower K, Howson RW, Belle A, et al. 2003. Global analysis of protein expression in yeast. *Nature* 425(6959): 737–741

Gristick HB, Rao M, Chartron JW, Rome ME, Shan SO, Clemons WM Jr. 2014. Crystal structure of ATP-bound Get3-Get4-Get5 complex reveals regulation of Get3 by Get4. *Nat. Struct. Mol. Biol.* 21(5): 437–442

Gristick HB, Rome ME, Chartron JW, Rao M, Hess S, et al. 2015. Mechanism of assembly of a substrate transfer complex during tail-anchored protein targeting. *J. Biol. Chem.* 290(50): 30006–30017

He L, Sharpe T, Mazur A, Hiller S. 2016. A molecular mechanism of chaperone-client recognition. *Sci. Adv.* 2(11): e1601625.

Hegde RS, Keenan RJ. 2011. Tail-anchored membrane protein insertion into the endoplasmic reticulum. *Nat. Rev. Mol. Cell Biol.* 12(12): 787–798

Hu J, Li J, Qian X, Denic V, Sha B. 2009. The crystal structures of yeast Get3 suggest a mechanism for tail-anchored protein membrane insertion. *PLOS ONE* 4(11): e8061

Huang C, Rossi P, Saio T, Kalodimos CG. 2016. Structural basis for the antifolding activity of a molecular chaperone. *Nature* 537(7619): 202–206

Ingargiola A, Lerner E, Chung S, Weiss S, Michalet X. 2016. FRETBursts: An open source toolkit for analysis of freely-diffusing single-molecule FRET. *PLOS ONE* 11(8): e0160716

Janda CY, Li J, Oubridge C, Hernández H, Robinson CV, et al. 2010. Recognition of a signal peptide by the signal recognition particle. *Nature* 465(7297): 507–510

Jaru-Ampornpan P, Shen K, Lam VQ, Ali M, Doniach S, et al. 2010. ATP-independent reversal of a membrane protein aggregate by a chloroplast SRP subunit. *Nat. Struct. Mol. Biol.* 17(6): 696–702.

Jonikas MC, Collins SR, Denic V, Oh E, Quan EM, et al. 2009. Comprehensive characterization of genes required for protein folding in the endoplasmic reticulum. *Science* 323(5922): 1693–1697

Kapanidis AN, Laurence TA, Lee NK, Margeat E, Kong X, et al. 2005. Alternating-laser excitation of single molecules. *Acc. Chem. Res.* 38(7): 523–533.

Kapanidis AN, Lee NK, Laurence TA, Doose S, Margeat E, et al. 2004. Fluorescence-aided molecule sorting: analysis of structure and interactions by alternating-laser excitation of single molecules. *Proc. Natl. Acad. Sci. U. S. A.* 101(24): 8936–8941

Keenan RJ, Freymann DM, Walter P, Stroud RM. 1998. Crystal structure of the signal sequence binding subunit of the signal recognition particle. *Cell* 94(2): 181–191

Kim YE, Hipp MS, Bracher A, Hayer-Hartl M, Hartl FU. 2013. Molecular chaperone functions in protein folding and proteostasis. *Annu. Rev. Biochem.* 82: 323–355

Kubota K, Yamagata A, Sato Y, Goto-Ito S, Fukai S. 2012. Get1 stabilizes an open dimer conformation of Get3 ATPase by binding two distinct interfaces. *J. Mol. Biol.* 422(3): 366–375

Kutay U, Ahnert-Hilger G, Hartmann E, Wiedenmann B, Rapoport TA. 1995. Transport route for synaptobrevin via a novel pathway of insertion into the endoplasmic reticulum membrane. *EMBO J.* 14(2): 217–223

Kutay U, Hartmann E, Rapoport TA. 1993. A class of membrane proteins with a C-terminal anchor. *Trends Cell Biol*. 3(3): 72–75

Lampariello F. 2000. On the use of the Kolmogorov-Smirnov statistical test for immunofluorescence histogram comparison. *Cytometry* 39(3): 179–188

Lee NK, Kapanidis AN, Wang Y, Michalet X, Mukhopadhyay J, et al. 2005. Accurate FRET measurements within single diffusing biomolecules using alternating-laser excitation. *Biophys. J.* 88(4): 2939–2953

Li C, Wen A, Shen B, Lu J, Huang Y, et al. 2011. FastCloning: a highly simplified, purification-free, sequence- and ligation-independent PCR cloning method. *BMC Biotechnol.* 11: 92

Liang FC, Kroon G, McAvoy CZ, Chi C, Wright PE, et al. 2016. Conformational dynamics of a membrane protein chaperone enables spatially regulated substrate capture and release. *Proc. Natl. Acad. Sci. U. S. A.* 113(12): E1615–E1624

Liou ST, Cheng MY, Wang C. 2007. SGT2 and MDY2 interact with molecular chaperone YDJ1 in *Saccharomyces cerevisiae. Cell Stress Chaperones* 12(1): 59–70

Mariappan M, Mateja A, Dobosz M, Bove E, Hegde RS, Keenan RJ. 2011. The mechanism of membrane-associated steps in tail-anchored protein insertion. *Nature* 477(7362): 61–66

Mateja A, Paduch M, Chang HY, Szydlowska A, Kossiakoff AA, et al. 2015. Protein targeting. Structure of the Get3 targeting factor in complex with its membrane protein cargo. *Science* 347(6226): 1152–1155

Mateja A, Szlachcic A, Downing ME, Dobosz M, Mariappan M, et al. 2009. The structural basis of tail-anchored membrane protein recognition by Get3. *Nature* 461(7262): 361–366

Mayer MP and Bukau B. 2005. Hsp70 chaperones: cellular functions and molecular mechanism. *Cell. Mol. Life Sci.* 62(6): 670–684

Merz F, Boehringer D, Schaffitzel C, Preissler S, Hoffmann A, et al. 2008. Molecular mechanism and structure of Trigger Factor bound to the translating ribosome. *EMBO J.* 27(11): 1622–1632.

Mock J-Y, Chartron JW, Zaslaver MA, Xu Y, Ye Y, Clemons WM. 2015. Bag6 complex contains a minimal tail-anchor–targeting module and a mock BAG domain. *Proc. Natl. Acad. Sci. U. S. A.* 112(1): 106–111

Nir E, Michalet X, Hamadani KM, Laurence TA, Neuhauser D, et al. 2006. Shot-noise limited single-molecule FRET histograms: comparison between theory and experiments. *J. Phys. Chem. B* 110(44): 22103–22124

Rao M, Okreglak V, Chio US, Cho H, Walter P, Shan SO. 2016. Multiple selection filters ensure accurate tail-anchored membrane protein targeting. *eLife* 5: e21301

Rome ME, Chio US, Rao M, Gristick H, Shan SO. 2014. Differential gradients of interaction affinities drive efficient targeting and recycling in the GET pathway. *Proc. Natl. Acad. Sci. U. S. A.* 111(46): E4929–E4935

Rome ME, Rao M, Clemons WM, Shan SO. 2013. Precise timing of ATPase activation drives targeting of tail-anchored proteins. *Proc. Natl. Acad. Sci. U. S. A.* 110(19): 7666–7671

Rothblatt JA, Meyer DI. 1986. Secretion in yeast: reconstitution of the translocation and glycosylation of α-factor and invertase in a homologous cell-free system. *Cell* 44(4): 619–628

Ryan OW, Poddar S, Cate JH. 2016. CRISPR-Cas9 genome engineering in *Saccharomyces cerevisiae* cells. *Cold Spring Harb. Protoc.* 2016(6): pdb.prot086827

Saraogi I, Zhang D, Chandrasekaran S, Shan SO. 2011. Site-specific fluorescent labeling of nascent proteins on the translating ribosome. *J. Am. Chem. Soc.* 133(38): 14936–14939

Schuenemann D, Gupta S, Persello-Cartieaux F, Klimyuk VI, Jones JD, et al. 1998. A novel signal recognition particle targets light-harvesting proteins to the thylakoid membranes. *Proc. Natl. Acad. Sci. U. S. A.* 95(17): 10312–10316

Schuldiner M, Collins SR, Thompson NJ, Denic V, Bhamidipati A, et al. 2005. Exploration of the function and organization of the yeast early secretory pathway through an epistatic miniarray profile. *Cell* 123(3): 507–519

Schuldiner M, Metz J, Schmid V, Denic V, Rakwalska M, et al. 2008. The GET complex mediates insertion of tail-anchored proteins into the ER membrane. *Cell* 134(4): 634–645

Shan SO. 2016. ATPase and GTPase tangos drive intracellular protein transport. *Trends Biochem. Sci.* 41(12): 1050–1060

Shao S, Hegde RS. 2011. A calmodulin-dependent translocation pathway for small secretory proteins. *Cell* 147(7): 1576–1588

Shao S, Rodrigo-Brenni MC, Kivlen MH, Hegde RS. 2017. Mechanistic basis for a molecular triage reaction. *Science* 355(6322): 298–302

Simon AC, Simpson PJ, Goldstone RM, Krysztofinska EM, Murray JW, et al. 2013. Structure of the Sgt2/Get5 complex provides insights into GET-mediated targeting of tail-anchored membrane proteins. *Proc. Natl. Acad. Sci. U. S. A.* 110(4): 1327–1332

Stefanovic S, Hegde RS. 2007. Identification of a targeting factor for posttranslational membrane protein insertion into the ER. *Cell* 128(6): 1147–1159

Stefer S, Reitz S, Wang F, Wild K, Pang YY, et al. 2011. Structural basis for tail-anchored membrane protein biogenesis by the Get3-receptor complex. *Science* 333(6043): 758–762

Suloway CJ, Chartron JW, Zaslaver M, Clemons WM Jr. 2009. Model for eukaryotic tail-anchored protein binding based on the structure of Get3. *Proc. Natl. Acad. Sci. U. S. A.* 106(35): 14849–14854

Thoma J, Burmann BM, Hiller S, Müller DJ. 2015. Impact of holdase chaperones Skp and SurA on the folding of β-barrel outer-membrane proteins. *Nat. Struct. Mol. Biol.* 22(10): 795–802.

Torella JP, Holden SJ, Santoso Y, Hohlbein J, Kapanidis AN. 2011. Identifying molecular dynamics in single-molecule FRET experiments with burst variance analysis. *Biophys. J.* 100(6): 1568–1577.

Tsirigotaki A, De Geyter J, Šoštaric N, Economou A, Karamanou S. 2017. Protein export through the bacterial Sec pathway. *Nat. Rev. Microbiol.* 15(1): 21–36

Tung JY, Li YC, Lin TW, Hsiao CD. 2013. Structure of the Sgt2 dimerization domain complexed with the Get5 UBL domain involved in the targeting of tail-anchored membrane proteins to the endoplasmic reticulum. *Acta Crystallogr. D Biol. Crystallogr.* 69(10): 2081–2090

Vilardi F, Lorenz H, Dobberstein B. 2011. WRB is the receptor for TRC40/Asna1-mediated insertion of tail-anchored proteins into the ER membrane. *J. Cell Sci.* 124(8): 1301–1307

Vilardi F, Stephan M, Clancy A, Janshoff A, Schwappach B. 2014. WRB and CAML are necessary and sufficient to mediate tail-anchored protein targeting to the ER membrane. *PLOS ONE* 9(1): e85033

Wang F, Brown EC, Mak G, Zhuang J, Denic V. 2010. A chaperone cascade sorts proteins for posttranslational membrane insertion into the endoplasmic reticulum. *Mol. Cell* 40(1): 159–171

Wang F, Chan C, Weir NR, Denic V. 2014. The Get1/2 transmembrane complex is an endoplasmic-reticulum membrane protein insertase. *Nature* 512(7515): 441–444

Wang F, Whynot A, Tung M, Denic V. 2011. The mechanism of tail-anchored protein insertion into the ER membrane. *Mol. Cell* 43(5): 738–750

Wereszczynski J, McCammon JA. 2012. Nucleotide-dependent mechanism of Get3 as elucidated from free energy calculations. *Proc. Natl. Acad. Sci. U. S. A.* 109(20): 7759–7764

Xu Y, Cai M, Yang Y, Huang L, Ye Y. 2012. SGTA recognizes a noncanonical ubiquitin-like domain in the Bag6-Ubl4A-Trc35 complex to promote endoplasmic reticulum–associated degradation. *Cell Rep*. 2(6): 1633–1644

Xu Z, Horwich AL, Sigler PB. 1997. The crystal structure of the asymmetric GroEL-GroES-$(ADP)_7$ chaperonin complex. *Nature* 388(6644): 741–750

Yamagata A, Mimura H, Sato Y, Yamashita M, Yoshikawa A, et al. 2010. Structural insight into the membrane insertion of tail-anchored proteins by Get3. *Genes Cells* 15(1): 29–41

Yamamoto Y, Sakisaka T. 2012. Molecular machinery for insertion of tail-anchored membrane proteins into the endoplasmic reticulum membrane in mammalian cells. *Mol. Cell* 48(3): 387–397

Yin J, Lin AJ, Golan DE, Walsh CT. 2006. Site-specific protein labeling by Sfp phosphopantetheinyl transferase. *Nat. Protoc.* 1(1): 280–285

Young IT. 1977. Proof without prejudice: use of the Kolmogorov-Smirnov test for the analysis of histograms from flow systems and other sources. *J. Histochem. Cytochem.* 25(7): 935–941

Young TS, Ahmad I, Yin JA, Schultz PG. 2010. An enhanced system for unnatural amino acid mutagenesis in *E. coli*. *J. Mol. Biol.* 395(2): 361–374